UNIVERSIDADE DE SÃO PAULO
INSTITUTO DE FÍSICA DE SÃO CARLOS

LORGIO VICTOR BAUTISTA SAMANIEGO

Study of CAZymes from *Thermothelomyces thermophilus* M77 as antibiofilm agents: an oxidative and hydrolytic approach

LORGIO VICTOR BAUTISTA SAMANIEGO

Study of CAZymes from *Thermothelomyces thermophilus* M77 as antibiofilm agents: an oxidative and hydrolytic approach

Dissertation presented to the Graduate Program in Physics at the Instituto de Física de São Carlos, Universidade de São Paulo to obtain the degree of Master of Science.

Concentration area: Applied Physics
Option: Biomolecular Physics
Advisor: Prof. Dr. Igor Polikarpov

Corrected Version
(original version available on the Program Unit)

São Carlos
2024

Samaniego, Lorgio Victor Bautista
Study of CAZymes from *Thermothelomyces thermophilus* M77 as antibiofilm agents: an oxidative and hydrolytic approach / Lorgio Victor Bautista Samaniego; advisor Igor Polikarpov - corrected version -- São Carlos 2024.
113 p.

Dissertation (Master's degree - Graduate Program in Biomolecular Physics) -- Instituto de Física de São Carlos, Universidade de São Paulo - Brasil , 2024.

1. Cellobiose dehydrogenase. 2. Cellobiohydrolase. 3. Endoglucanase. 4. Microbial biofilms. 5. Simplex-lattice design. I. Polikarpov, Igor, advisor. II. Title.

Dedicado a todos mis seres queridos
Especialmente a mi madre y hermano.

ACKNOWLEDGMENT

Academic and scientific life, at first glance, is not rewarded as it should be due to difficulties in almost all aspects, from financial struggles to personal fulfillment. However, with the help of a caring family and great people, all of whom desire the best for you, it is possible to go further and take a little piece of precious knowledge.

I want to express my gratitude to my mother, Isabel, and my brother, Pedro, for their unconditional love and trust in me. Thank you for your support; you provide the motivation and energy that I need to move forward.

I extend my thanks to Juliana for being my pillar of support during both challenging and positive times.

I am grateful to my professor, Igor Polikarpov, for opening the doors to his remarkable laboratory and providing everything necessary for my research. Thank you for your insightful advice and questions that have helped refine my work and knowledge.

My appreciation goes out to all my colleagues from the lab who have taught me how to conduct good science. Despite occasional difficulties, they have shown that perseverance and hard work are the keys to success. I want to acknowledge this hard-working team, including Anelyse, Nicoli, Paula, Milena, Caio, Samuel, Maria, and all the members of the Group of Molecular Biotechnology. Thank you all!

I'd also like to express my thanks to all my Brazilian and Peruvian friends who have made life outside the lab much more interesting. Thank you for sharing your culture and the many experiences we've had.

Lastly, I want to thank the São Carlos Institute of Physics for being an excellent place to conduct scientific research and for challenging existing paradigms. It demonstrates that outstanding biotechnological and biological research can indeed be conducted in this institution.

This study was financed in part by the Coordenação de Aperfeiçoamento de Pessoal de Nível Superior - Brasil (CAPES) - 88887.612480/2021-00

ABSTRACT

SAMANIEGO, L. V. B. **Study of CAZymes from *Thermothelomyces thermophilus* M77 as antibiofilm agents:** an oxidative and hydrolytic approach. 2024. 113 p. Dissertation (Master in Science) - Instituto de Física de São Carlos, Universidade de São Paulo, São Carlos 2024

This work presents the biochemical characterization of relevant CAZymes from *Thermothelomyces thermophilus* M77, which includes a cellobiose dehydrogenase (*Tth*CDHIIa), an endoglucanase (*Tth*Cel7B), and cellobiohydrolases (*Tth*Cel7A and *Tth*Cel6A). Furthermore, it explores their application as antimicrobial and antibiofilm agents. In the first part of this study, it was demonstrated that *Tth*CDHIIa is thermostable in different ionic solutions and is capable of oxidizing multiple mono and oligosaccharide substrates and to continuously produce H_2O_2. Kinetics measurements depict the enzyme catalytic characteristics consistent with an Ascomycota class II CDH. Our structural analyses show that *Tth*CDHIIa substrate binding pocket is spacious enough to accommodate larger cello and xylooligosaccharides. We also reveal that *Tth*CDHIIa supplemented with cellobiose reduces the viability of *Staphylococcus. aureus* ATCC 25923 up to 32% in a planktonic growth model and inhibits its biofilm growth on 62.5%. Furthermore, *Tth*CDHIIa eradicates preformed *S. aureus* biofilms via H_2O_2 oxidative degradation of the biofilm matrix, making these bacteria considerably more susceptible to gentamicin and tetracycline. In the second part of this study, the investigated cellulases exhibited a preference for acidic conditions and high temperatures in the hydrolysis of substrates. Additionally, we described the functionality of the carbohydrate-binding module. The structural characteristics of cellobiohydrolases and endoglucanases, such as the loop arrangement, aligned with the type of recognized substrate. The optimization of the mixture of *Tth*Cel7A, *Tth*Cel7B, and *Tth*Cel6A using a Simplex-lattice design model revealed that for a higher degradation of *Gluconoacetobacter hansenii* BC, a 49.3% *Tth*Cel7A and 50.7% *Tth*Cel6A enzymatic load is required. To achieve optimal degradation of a pathogenic model and a clinical *Escherichia coli* biofilm, binary mixtures comprising 56.5% *Tth*Cel7B + 43.5% *Tth*Cel6A and 59.6% *Tth*Cel7A + 40.4% *Tth*Cel7B were found to be effective, respectively. This optimization resulted in a reduction in the quantity of enzymes required for biofilm eradication, with EC_{50} values of 0.086 μM and 0.63 μM for the hydrolysis of clinical and pathogenic *E. coli*, respectively. Confocal laser scanning microscopy demonstrated changes in protein and carbohydrate content under cellulase treatment. Notably, *Tth*Cel7B played a key role as a potent eradication agent, particularly since extracted cellulose from *E. coli* biofilms is amorphous. These findings provide valuable insights for the prospective use of endoglucanase

enzymes in the treatment of biofilm-associated diseases. In summary, *T. thermophilus* emerges as a promising source of antibiofilm enzymes.

Keywords: Cellobiose dehydrogenase. Cellobiohydrolase. Endoglucanase. Microbial biofilms. Simplex-lattice design.

RESUMO

SAMANIEGO, L. V. B. **Estudo das CAZymes de *Thermothelomyces thermophilus* M77 como agentes antibiofilme:** uma abordagem oxidativa e hidrolítica**.** 2024. 113 p. Dissertação (Mestrado em Ciências) - Instituto de Física de São Carlos, Universidade de São Paulo, São Carlos 2024

Este trabalho apresenta a caracterização bioquímica das CAZymes relevantes de *Thermothelomyces thermophilus* M77, que inclui uma celobiose desidrogenase (*Tth*CDHIIa), uma endoglucanase (*Tth*Cel7B) e celobiohidrolases (*Tth*Cel7A e *Tth*Cel6A). Além disso, explora a sua aplicação como agentes antimicrobianos e antibiofilme. Na primeira parte deste estudo, foi demonstrado que a *Tth*CDHIIa é termoestável em diferentes soluções iônicas e capaz de oxidar múltiplos mono e oligossacarídeos, produzindo continuamente H_2O_2. Medidas cinéticas retratam as características catalíticas da enzima consistentes com um CDH classe II de origem Ascomycota. Nossas análises estruturais revelam que o sítio de ligação do substrato do *Tth*CDHIIa é espaçoso o suficiente para acomodar celooligossacarídeos e xilooligossacarídeos maiores. Também descobrimos que o *Tth*CDHIIa suplementado com celobiose reduz a viabilidade do *Staphylococcus aureus* ATCC 25923 em até 32% em um modelo de crescimento planctônico e inibe o crescimento do seu biofilme em 62.5%. Além disso, o *Tth*CDHIIa erradica biofilmes pré-formados do *S. aureus* por meio da degradação oxidativa da matriz do biofilme via H_2O_2, tornando essas bactérias consideravelmente mais suscetíveis à gentamicina e tetraciclina. Na segunda parte deste estudo, as celulases investigadas demonstraram preferência por condições ácidas e altas temperaturas na hidrólise dos substratos. Além disso, descrevemos a funcionalidade do módulo de ligação a carboidratos. As características estruturais das celobiohidrolases e endoglucanases, como a disposição dos loops, estão alinhadas com o tipo de substrato reconhecido. A otimização da mistura de *Tth*Cel7A, *Tth*Cel7B e *Tth*Cel6A usando o planejamento em rede Simplex revelou que, para uma maior degradação do *Gluconoacetobacter hansenii* cellulose, é necessária uma carga enzimática de 49.3% de *Tth*Cel7A e 50.7% de *Tth*Cel6A. Para atingir uma degradação ótima dos biofilmes de *Escherichia coli* patogênicos e clínicos, foram encontradas misturas binárias de 56.5% de *Tth*Cel7B + 43.5% de *Tth*Cel6A e 59.6% de *Tth*Cel7A + 40.4% de *Tth*Cel7B, respectivamente. Essa otimização resultou em uma redução na quantidade de enzimas necessárias para a erradicação de biofilmes, com valores de EC_{50} de 0.086 μM e 0.63 μM para a hidrólise de *E. coli* clínica e patogênica, respectivamente. A microscopia confocal de varredura a laser demonstrou alterações no conteúdo de proteínas e carboidratos sob tratamento com celulase.

Notavelmente, a *Tth*Cel7B desempenhou um papel fundamental como agente de erradicação potente, especialmente considerando que a celulose extraída dos biofilmes de *E. coli* é amorfa. Essas descobertas fornecem informações valiosas para o uso prospectivo de enzimas endoglucanase no tratamento de doenças associadas a biofilmes. Em resumo, *T. thermophilus* emerge como uma fonte promissora de enzimas antibiofilme.

Palavras-chave: Celobiose desidrogenase. Celobiohidrolase. Endoglucanase. Biofilmes microbianos. Planejamento em rede Simplex

LIST OF FIGURES

LIST OF TABLES

LIST OF ABREVIATIONS AND ACRONYMS

BC	Bacterial cellulose
BHI	Brain heart infusion
CAZY	Carbohydrate-active enzymes
CBM	Carbohydrate-binding module
CD	Conserved domains
CDH	Cellobiose dehydrogenase
CLBM	Cellobiono-1,5-lactam
CMC	Carboxymethyl cellulose
CSLM	Confocal laser scanning microscopy
CV	Crystal violet
DCPIP	2,6 - Dichlorophenolindophenol
DEAE	Diethylaminoethyl
DET	Direct electron transfer
DH	Dehydrogenase
DNS	Diethylaminoethyl
eDNA	Extracellular DNA
EPS	Extracellular polymeric substance
FAD	flavin adenine dinucleotide
H_2O_2	Hydrogen peroxide
HPAEC	High-performance anion exchange chromatography
IET	Inter-domain electron transfer
Kcat	Catalytic constant
KM	Michaelis constant
KM/kcat	Catalytic efficiency
MBEC	Minimum biofilm eradication concentration
MES	2-(N-morpholino)ethanesulfonic acid
NAG	N-Acetylglucosamine
PASC	Phosphoric acid swollen cellulose
PBS	Phosphate-buffered saline
PCR	Polymerase chain reaction
PIA	Polysaccharide intercellular adhesin

PNAG	Poly-β-1,6-N-acetyl-D-glucosamine
SAXS	Small-angle X-ray scattering
SDS-PAGE	Sodium dodecyl sulphate-polyacrylamide gel electrophoresis
TSB	Tryptic soy broth
UV/VIS	Ultraviolet/visible
Vmax	Maximal enzymatic velocity
XRD	X-Ray diffraction
YPD	Yeast Extract-Peptone-Dextrose

CONTENT

PART I:

Biochemical characterization of the cellobiose dehydrogenase from Thermothelomyces thermophilus and its application as an antibiofilm agent

Chapter 1

Introduction

1.1 Cellobiose dehydrogenase properties

Cellobiose dehydrogenases (CDHs, E.C 1.1.99.18) are oxidative extracellular hemoflavoenzymes produced by a variety of wood-degrading fungi species, including *Trametes* sp.*, Phanerochaete chrysophobia, Humicola insolens, Chaetomium* sp., *Coniophora puteana* and *Neurospora crassa* [1].Typical CDHs are two-domain monomeric enzymes consisting of an electron-transferring cytochrome (Cyt) and a sugar-oxidizing flavodehydrogenase (DH) domains, which are connected by a flexible linker region [2,3]. As a first step of the catalyzed reaction, DH domain mediates the $2e^-/2H^+$ oxidation of the cellobiose anomeric carbon to cellobionolactone, resulting in a reduced FAD molecule ($FADH_2$) [4,5]. Then, an inter-domain electron transfer (IET) occurs from the $FADH_2$ of the DH domain to the heme b group of the Cyt domain, followed by a direct electron transfer (DET) from Cyt to external electron acceptors, such as, for example, lytic polysaccharide monooxygenases (LPMOs) [6–8] (Figure 1).

Although CDH is not an oxidase, because of its poor DET to molecular oxygen (O_2), this enzyme can produce hydrogen peroxide (H_2O_2) as a side product, after O_2 acceptance of the electrons from $FADH_2$ [3].

Cellobiose dehydrogenases are classified in the Carbohydrate-Active enzymes database (CAZy database; http://www.cazy.org) as part of the "Auxiliary Activities" (AA) class. Due to the modular characteristic of CDH, it has been further classified within two different families, the AA3 family (AA3_1 subfamily) covering the DH domain; and the AA8 family, consisting of iron reductases, because of the Cyt domain [9,10].

A further classification of CDH enzymes, based on phylogenetic and domain analysis, suggests dividing them into four clusters or classes (I - IV) [11](Figure 2a). Class I encompasses CDH enzymes of basidiomycota origin, which possess the DH domain alone or in combination with the Cyt domain. The phylum Ascomycota hosts the highest number of CDH enzymes, further divided into classes II, III, and IV. Many of these sequences lack the Cyt domain,

indicating its dispensability for certain catalytic activities that solely depend on the DH domain. Cluster II can also be subclassified into IIA when the CBM domain is present and IIB when it is absent [11](Figure 2b).

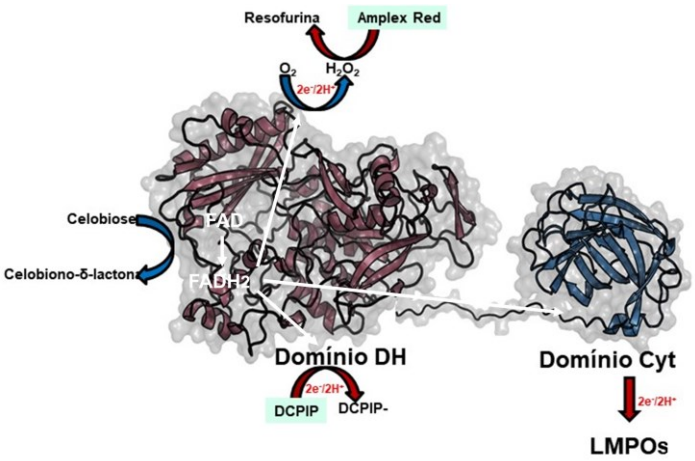

Figure 1 - Cellobiose dehydrogenase chemical reactions and its coupling to different enzymatic essays.
Source: By the author

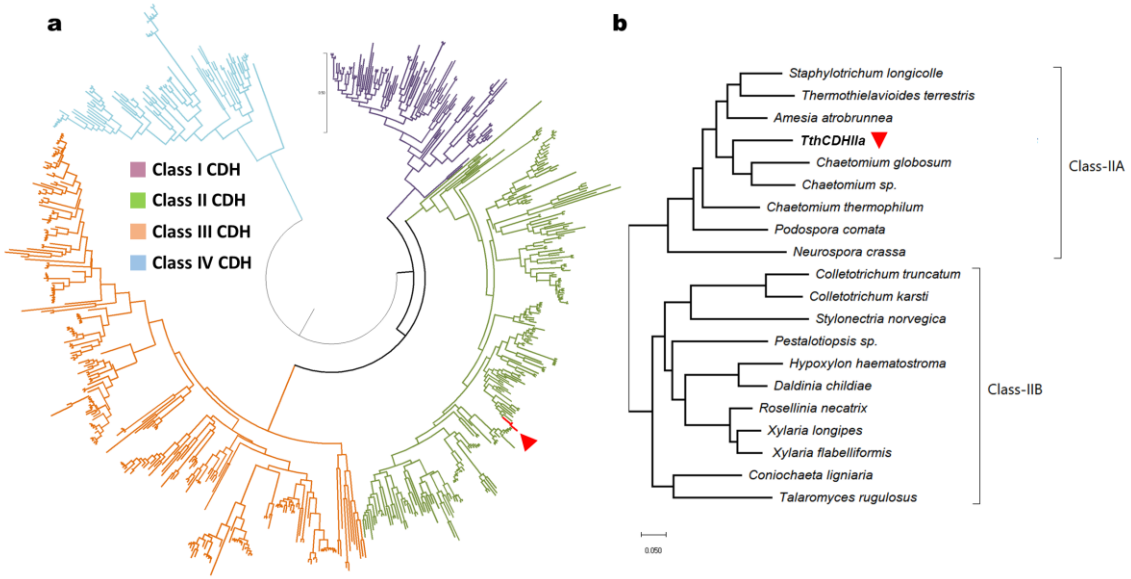

Figure 2 - Phylogenetic analysis of cellobiose dehydrogenase. (a) Phylogenetic tree of cellobiose dehydrogenase from different organism, divided in Class I,II,III and IV. (b) Phylogenetic tree representing the class II subgroups, into IIA and IIB. TthCDHIIa is marked as red triangle.
Source: Adapted from SÜTZL *et al.*[11]

On the other hand, the diversity of biochemical characteristics makes CDH a powerful enzyme to carry out a variety of biotechnological tasks. The use of CDH as biosensor of analytes like cellobiose, lactose, glucose and catecholamines is well known [3,12–14]. Its relevance as

constituent of biofuel cells and bioanodes is very attractive as a potential "green" source of electric energy [15,16]. In addition to the aforementioned bioelectrochemical applications, CDH is also used for production of lactobionic and aldonic acids, [17] and as a component of enzymatic cocktails for plant biomass hydrolysis [18–20].

1.2 Bacterial biofilms

1.2.1 Definition and distribution

From an integral point of view, biofilm is a microbial ecosystem embedded, most of the time, in a self-secreted extracellular polymeric substance (EPS) that show biological, chemical and physical properties that planktonic forms do not have, the so-called emergent properties [21,22].

The biofilm distribution is remarkably higher on oceanic (deep subsurface, upper sediment, open ocean) and continental (soil, deep sediment, ground waters) habitats [23]. These environmental biofilms are too diverse that escape from standard biofilm definitions. On the contrary, human-colonizing biofilm are just a tiny fraction of the number of bacterial cells in biofilms on Earth surface (~ 0.00011%). Most of them are symbiotic association like the ones found in plaque,[24] skin [25] and gut microbiota,[26] that brings beneficial treats. And others, the pathogenic bacteria counterpart, produce biofilms conferring advantages like tolerance to the immune system and antimicrobial agents, and antimicrobial resistance [27].

1.2.2 Bacterial biofilm life cycle

The life cycle of a biofilm is initiated by the planktonic form of bacteria. Under static conditions, there exists a gradient of nutrients concentrated at the bottom of any system. Bacteria will accumulate in this region, through motility and reversible adhesion. Over time, the lack of nutrients, reduced freedom of movement (due to mechanical restrictions on flagellar motion), and other environmental cues will be sensed by the bacteria, promoting the synthesis of cyclic diguanylate (c-di-GMP). C-di-GMP is responsible for activating all metabolic pathways to synthesize EPS [28]. These events mark the beginning of the initial irreversible adhesion phase. As signals intensify and clonal cell growth occurs within the continuously expanding EPS matrix, early biofilm development takes place (Figure 3).

Once the biofilm matures, it provides several advantages to the bacteria compared to its planktonic form. These advantages include improved chances of survival when facing challenges such as nutrient deprivation, dehydration, pH changes, bacteriophages, predators, or the immune system [27]. Simultaneously, biofilm aggregates can disperse and colonize new surfaces, bypassing the need to go through the previous phases (Figure 3).

Finally, the biofilm can enter a dispersion phase triggered by environmental stimuli such as changes in nutrient availability and an increase in nitric oxide, leading to a decrease in c-di-GMP concentration. This molecular change reduces polysaccharide synthesis, activates endogenous enzymes responsible for actively degrading the EPS, and promotes bacterial motility [29,30].

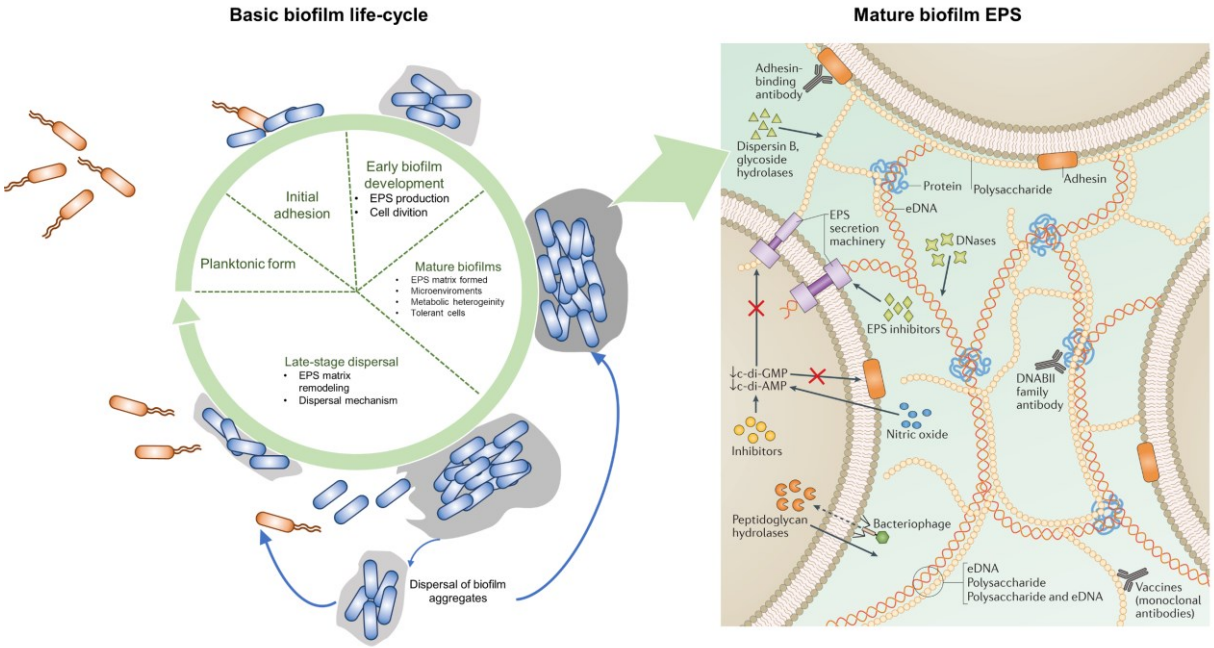

Figure 3 - The biofilm life cycle model and the principal components of the extracellular polymeric substance of mature biofilms.
Source : Adapted from KOO *et al.*[30]

1.2.3 Composition of biofilms

The EPS matrix is mainly composed of polysaccharides, proteins, nucleic acids, and low molecular weight components. The type and proportion of these molecules determine the structure and function of the biofilm. Additionally, the interaction between them is crucial. Activities such as matrix cross-linking, retention of exoenzymes on polysaccharide structures, and stabilization of DNA through proteins and cations are necessary for mechanical resistance and further protection against the host's response [21].

1.2.3.1 Polysaccharides

Polysaccharides are incredibly diverse due to variations in monosaccharides, glycosidic linkages, branching, and non-carbohydrate substitutions, leading to an extensive array of structures with the biofilm structure [21,31](Figure 4).

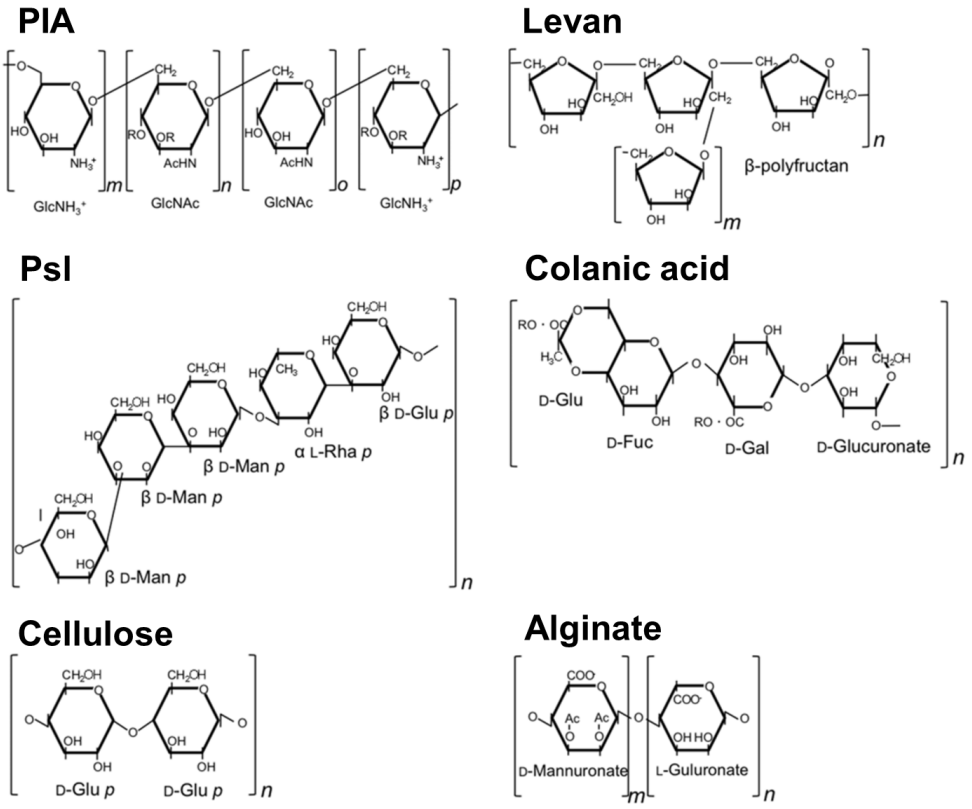

Figure 4 - Schematic representation of the principal polysaccharide components of bacterial biofilms.
Source: Adapted from LIMOLI; JONES; WOZNIAK.[31]

One of the major exopolysaccharides found in the biofilm matrix is PIA (polysaccharide intercellular adhesin), which is associated with many staphylococcal bacteria. Its structure consists of a positively charged polymer of β-1–6-N-acetylglucosamine that is partially deacetylated, typically around 15–20%. PIA plays a crucial role in the construction and maturation of the biofilm, providing mechanical stability in high shear-force environments. Its positive charge facilitates interactions with teichoic acids on the membranes of Staphylococcal cells, serving as a strong intercellular adhesive [31,32].

Other examples of aggregative polysaccharides can be found in *Pseudomonas aeruginosa* biofilms, namely Psl and Pel. Psl which boasts a more intricate structure, is a neutral

pentasaccharide comprised of l-rhamnose, d-glucose, and d-mannose repeats in a 1:1:3 ratio [33]. In contrast, Pel is a linear cationic homopolymer primarily consisting of partially de-N-acetylated α-1,4-N-acetylgalactosamine (GalNAc) with predominant dimeric repeats of N-galactosamine (GalN) and GalNAc [34].

Other important polysaccharides are cellulose, colonic acid, alginates, levan, Vibrio polysaccharide (VPS), β-glucans, γ-PGA (poly-γ-glutamate), epsA-epsO operon-encoded exopolysaccharide and others. All with functions of adhesion , scaffolding and stability of the biofilm matrixome [35].

1.2.3.2 Proteins

The proteic portion of the biofilm matrix is comprised of extracellular enzymes that serve various purposes, including functioning as an external digestion system, providing protection against molecules (such as the degradation of antibiotics), and participating in the modification of other EPS. The remaining fraction consists of amyloids, which are water-insoluble proteins characterized by a highly ordered structure. These amyloids play a role in enhancing the polysaccharide polymers, sharing similar functions within the biofilm matrix [21].

1.2.3.3 Nucleic acids

This macromolecule holds the third most significant position among EPS, primarily contributing to the stabilization of the biofilm matrix. Extracellular DNA (eDNA) has been identified as an agent facilitating horizontal genetic transfer. eDNA can modify the innate immune response, mitigate inflammation, and hinder phagocytosis [36].

1.3 Searching for new antibiofilm agents.

In the last two decades a growth in infections caused by drug-resistant and biofilm-forming bacteria has been consistently reported [37,38]. CDH might play a role as an attractive antimicrobial and antibiofilm agent, due to its ability to continuously produce hydrogen peroxide from oligosaccharides like cellobiose,[39] which are not metabolizable by pathogens [40]. This non-canonical use of CDH and other enzymes in biomedical applications has been growing, as documented by several recent studies [41–45].

So, for all the exposed above, in this study we proposed as a new antibiofilm candidate, a CDH enzyme form *Thermothelomyces thermophilus* (*Tth*CDHIIa)[46]. *T. thermophilus* is a filamentous fungus that grows in soils and high temperature compost (35-48°C) and has an excellent lignocellulose degrading capability [47]. Initial biochemical characterization of a native CDH from this organism has been performed,[48] and independent experiments using it as an accessory enzyme were conducted [19,49]. After the complete genome sequence of *T. thermophilus* became available,[50] two variants of CDH were discovered. However, no thorough characterization or previous investigation into its application as an antibiofilm agent has been conducted.

Chapter 2

Objectives

2.1 Overall objectives

The overall Part I objective is the biochemical characterization of the oxidative enzyme Cellobiose dehydrogenase from *T. thermophilus* (*Tth*CDHIIa) with focus on the substrate recognition and production of hydrogen peroxide with the final aim of its application as and antimicrobial, inhibition and eradication agent of *S. aureus* biofilm model.

2.2 Specific objectives

- Expression of *Tth*CDHIIa on a *P. pastoris* system and purification
- Determination of activity and substrate specificity and steady-state kinetic measurements of *Tth*CDHIIa
- Determination of *Tth*CDHIIa stability by ThermoFluor assay
- Quantification of hydrogen peroxide production
- Structural modeling of *Tth*CDHIIa
- Assessment of *S. aureus* biofilm growth inhibition and eradication by *Tth*CDHIIa
- Planktonic growth inhibition of *S. aureus* by *Tth*CDHIIa
- Determination of minimum biofilm eradication concentration (MBEC) under *Tth*CDHIIa pretreatment conditions
- Analysis of soluble product of *Tth*CDHIIa treated biofilm

Chapter 3

Material and methods

3.1 Cloning, expression and purification of *Tth*CDHIIa

3.1.1 Molecular cloning of *Tth*CDHIIa

The *Tth*CDHIIa coding sequence without its signal peptide (GenBank: AEO58137.1) was cloned between the XbaI and XhoI sites of pPICZαA plasmid (Biomatik, Cambridge, Ontario, Canada). This construct was propagated in *E. coli* DH5α prior to linearization with PmeI. Then, P. pastoris X-33 cells were transformed by electroporation using Gene Pulser Xcell system (Bio-Rad, Hercules, California, USA). Some plate transformants on YPDS medium containing 100 µg/mL Zeocin (Invitrogen, Carlsbad, USA) were isolated for small-scale expression of *Tth*CDHIIa in order to identify the colonies with the highest levels of expression.

3.1.2 Expression and purification of *Tth*CDHIIa

Expression of *Tth*CDHIIa started with a P. pastoris pre-inoculum in YPD medium containing 100 µg/mL of Zeocin (Invitrogen, Carlsbad, USA). Next, P. pastoris biomass production was performed in 2 L Erlenmeyer flasks containing 500 mL buffered glycerol-complex medium (BMGY) until the cellular density reached an OD600 = 4. The cells were collected by centrifugation, resuspended in 100 mL of buffered methanol-complex medium (BMMY) and incubated for 120 h at 200 rpm and 30 °C for the induction period, which was carried out by adding 0.75 % (v/v) of methanol every 24 hours. Then, cells were collected by centrifugation (14 000 x g, 15 min, 4 °C). The supernatant containing the secreted *Tth*CDHIIa was precipitated with ammonium sulfate until the final saturation of 70%, collected by centrifugation (20 000 x g, 20 min, 4 °C) and then resuspended in 20 mM Tris-HCl pH 8. The protein sample was further purified through size exclusion chromatography in an ÄKTA Purifier system (GE Healthcare, Chicago, USA) using a HiLoad 16/60 Superdex 200 column (GE Healthcare, Chicago, USA) equilibrated with 20 mM Tris-HCl pH 8 and 150 mM NaCl buffer. The fractions containing *Tth*CDHIIa were combined and concentrated using 10,000 MWCO Pierce protein concentrator PES (Thermo Scientific, Waltham, USA). The absence of contaminants of the expressed protein sample were assessed by SDS-PAGE. The purified

protein was quantified spectrophotometrically at 280 nm, (theorical mass = 86,58 kDa and ε = 157, 51 M−1 cm−1 as predicted by PROTPARAM) using the NanoDrop 2000 Spectrophotometer (Thermo Scientific, Waltham, USA).

3.2 Biochemical characterization of *Tth*CDHIIa

3.2.1 Spectral characterization

UV/Vis spectra were measured in the spectral region from 250 to 700 nm using 8 µM purified *Tth*CDHIIa, which was cloned and purified as detailed in the Supplementary material, in 20 mM Bis-Tris buffer pH 6 with or without 1 mM cellobiose, rendering the reduced and oxidized spectra, respectively. A blank spectrum consisting of 20 mM Bis-Tris pH 6 was also collected. All the recordings were performed at 30 °C in an Infinite 200M PRO microplate reader (Tecan, Hombrechtikon, Switzerland).

3.2.2 Activity and substrate specificity assays and steady-state kinetic measurements

*Tth*CDHIIa activity was measured spectrophotometrically by following the reduction of the electron acceptor 2,6 dichlorophenolindophenol (DCPIP, ε520 = 6,9 M-1 cm-1) (Sigma-Aldrich, St. Louis, USA) at 520 nm using a Synergy™ HTX Multi-Mode microplate reader (BioTek Instruments, Colmar, France). The standard assay consisted of a mixture of 0.3 mM of DCPIP diluted in 10% (v/v) ethanol, 50 mM Bis-Tris buffer pH 6, and 0.2 µM of *Tth*CDHIIa. Reactions started with addition of 20 mM cellobiose, and the decrease in absorbance was monitored for three minutes.

In order to determine *Tth*CDHIIa optimum temperature, DCPIP assays were performed from 20 °C to 80 °C. Optimal pH was determined using 20 mM acetate/borate/phosphate buffer (ABF) ranging from pH 2.0 to 10.0 using the standard assay conditions described above.

Substrate specificity of *Tth*CDHIIa was tested against different monosaccharides (glucose, mannose, galactose, fructose and N-acetylglucosamine) and disaccharides (cellobiose, lactose and maltose) (all from Sigma-Aldrich, St. Louis, USA) at 40 mM, and cello-oligosaccharides (cellotriose, cellotetraose and cellopentaose - Megazyme, Wicklow, Republic of Ireland) at 1.5 mg/mL, all under the same DCPIP reaction conditions.

*Tth*CDHIIa kinetic parameters were determined using a suitable range of concentrations of the aforementioned substrates and fitted by Michaelis-Menten equation using Origin 2020 (OriginLab Corporation, Northampton, MA, USA). All experiments were carried out in triplicate. Temperature stability of the enzyme was determined by measuring its residual activity after incubation at 37, 50, 60 and 70 °C, for up to 6 h. Aliquots were taken at fixed time points, placed on ice, and had its enzymatic activity determined as described before. The effects of Co+2, Ca+2, Ni+2, Zn+2, Mg+2, Na+1, Sr+2, Mn+2, Cu+2, Li+1 and Fe+3 ions at 10 mM on the enzyme activity were also evaluated.

3.2.3 ThermoFluor assays

The effect of different cations on structural stability of *Tth*CDHIIa was assessed by differential scanning fluorimetry. Each measurement was carried out using a mixture of 5 µL of the enzyme at 17.3 µM, 10 µL of 50 mM Bis-Tris buffer pH 6, 10 mM ion solution (Co+2, Ca+2, Ni+2, Zn+2, Mg+2, Na+1, Sr+2, Mn+2, Cu+2, Li+1 or Fe+3) and 5 µL of 2000 x SYPRO Orange dye (Invitrogen, Carlsbad, USA) diluted 300 times in water. The samples were incubated in an iCycler iQ RealTime PCR Detection System (Bio-Rad, Veenendaal, The Netherlands) with temperature increments of 1 °C per minute. The melting temperatures (Tm) were recorded.

3.2.4 Hydrogen peroxide production

The production of H_2O_2 by the enzyme was quantified by a coupled 2-step reaction. First, 0.2 µM *Tth*CDHIIa, 50 mM Bis-Tris buffer pH 6 and different substrates at a final concentration of 20 mM (mono and disaccharides) or 0.5 mg/mL (cello-oligosaccharides), were incubated at 37 °C. After 30 min, reactions were stopped by heat-inactivation (2 min at 95 °C). Then, 25 µL of the previous reactions were added to a mixture of 200 µM AmplexRed (Invitrogen, Carlsbad, USA), 5 U/mL horseradish peroxidase (Sigma-Aldrich, St. Louis, USA) and 50 mM Bis-Tris buffer pH 6, at a final volume of 100 µL, followed by absorbance measurement at 560 nm and compared to a standard H_2O_2 curve. The amount of H_2O_2 (µM) produced over 24 h was determined using 0.05 (0.58 µM) and 0.1 mg/mL of *Tth*CDHIIa (1.16 µM) under the reaction conditions described above. All the experiments were performed in triplicates and measured at 37 °C in an Infinite 200M PRO (Tecan, Hombrechtikon, Switzerland) microplate reader.

3.2.5 Determination of soluble oxidized cello-oligosaccharides

Oxidation of cello-oligosaccharides (degrees of polymerization, DPn 2-5) and xylo-oligosaccharides (DPn 2-6) by *Tth*CDHIIa was monitored by High-Performance Anion Exchange Chromatography coupled to Pulsed Amperometric Detection (HPAEC-PAD). The enzymatic oxidation assay was performed in 50 mM sodium phosphate buffer pH 6, 1 µM of *Tth*CDHIIa, and oligosaccharides of DP2 at 1 mM, or 0.4 mg/mL for DP3-6. For cellooligosaccharides, the reactions were carried out at 37 °C for 1 h, while for xylooligosaccarides, the conditions were set to 50 °C and 24 h. All the reactions were performed in an Eppendorf ThermoMixer C (Eppendorf Co., Hamburg, Germany) at 800 rpm. The final reactions were stopped by heat-inactivation at 95 °C for 10 min, centrifuged at 13 000 x g for 5 min and filtered through a 0.22 µm membrane.The soluble products were analyzed with a CarboPac PA1 (2 × 250 mm) analytical column (Dionex Co., Sunnyvale, CA, USA) coupled to a 2 x 50 mm guard column in a Dionex ICS 5000 system (Dionex Co., Sunnyvale, CA, USA). Both column and detector compartments were maintained at 30 °C. One microliter of the sample was injected, and solutions of 0.1 M NaOH (A) and 0.1 M NaOH with 1 M NaOAc (B) were the eluents, with a flow rate of 0.3 mL min^{-1}. The gradient of elution has been described elsewhere [5]. For monitoring the total oxidation of C2 (1mM), an incubation at 50°C for 0.25, 0.5, 1 and 2h was tested. Parallel measurements from this reaction using HPAEC and Amplex red assay was performed as described previously.

3.3 Structural modeling of *Tth*CDHIIa

The structure of *Tth*CDHIIa was computationally modeled employing ColabFold AlphaFold 2_advanced (https://colab.research.google.com/github/sokrypton/ColabFold/blob/main/beta/AlphaFold2_advanced.ipynb) that uses MMseqs2 algorithm [51]. Amino acids sequence was submitted to ColabFold and modeled under default settings for genetic databases, filtering, and sampling options. Then, the most robust model (>90 pLDDT) was refined with Amber-Relax option to improve the geometry of the side-chains bonds. In order to incorporate cofactors (FAD and heme b) and substrates in our predicted model, we used the crystallographic structure of a cellobiose dehydrogenase from *Myriococcum thermophilum* (PDB: 4QI6 and 4QI5), *Mt*CDH, as a template, and performed structural alignments using PyMOL (The PyMOL Molecular Graphics System, Version 1.8 Schrodinger, LLC, New York, NY, USA). In order to investigate the interaction of *Tth*CDHIIa with oligosaccharides, cellobiose, cellotetraose and

xylobiose, models were built with GLYCAM-Web (https://glycam.org/cb/) and then pair fitted to cellobiono-1,5-lactam present in crystallographic structure of *Mt*CDH (PDB id: 4QI5). The rank 1 model with 94.34 pLDDT was evaluated with Structural Analysis and Verification Server (SAVES) web tool (https://saves.mbi.ucla.edu/), obtaining a 94.76% overall quality factor using the program ERRAT. In addition, the Ramachandran plot from PROCHECK package showed that our structure has 99.7 % of residues within favored and additionally allowed regions. The protein sequence alignment of *Tth*CDHIIa and MtCDH was performed using MEGAX package program and the ClustalW algorithm. Then alignment figure was generated using ESPript 3.

3.4 Biofilm growth inhibition and eradication

The ability of *Tth*CDHIIa to inhibit Staphylococcus aureus ATCC 25923 biofilm formation and to eradicate its preformed 24 hours-old biofilm was evaluated according to the protocol described in [52]. Briefly, for the inhibition assay, 200 µL of *S. aureus* ATCC 25923 inoculum at OD600 = 0.03 prepared in Brain Heart Infusion (BHI) (Neogen, Lansing, Michigan, USA) broth supplemented with 1% glucose (Sigma-Aldrich, St. Louis, USA), *Tth*CDHIIa (0.1 or 0.3 mg/mL), and 20 mM cellobiose were incubated at 37 °C for 20 h under static conditions in the wells of non-treated 96-well plates (Greiner Bio-One, Nürtingen, Germany). The resulting biofilms were stained using crystal violet (CV) and absorbances were measured at 595 nm in the Multiskan FC Microplate Reader (Thermo Scientific, Waltham, USA) and the percentage of biofilm growth was calculated using the equation (1):

$$\%\, Biofilm = 100 \times (Sample_{A595} - SC_{A595})/(GC_{A595} - SC_{A595}) \quad (1)$$

Where SC_{A595} and GC_{A595} correspond to the measurement of the sterility control and the growth control, respectively. The biofilm viability and distribution were also analyzed by confocal laser scanning microscopy (CLSM) as detailed in the Supplementary material. For the eradication experiments, *S. aureus* biofilms were grown for 24 h, then the supernatant was discarded, the biofilms were washed with PBS, and subjected to an enzymatic treatment with *Tth*CDHIIa (0.1 or 0.3 mg/mL) and 20 mM cellobiose in 5 mM MES (pH 6) at 37 °C for 4 h. Wells treated with the same solution except for the enzyme were considered as controls. Finally,

a CV-staining and absorbance reading was performed using the above-described protocol. The experiments were performed in triplicate.

3.5 Planktonic growth inhibition and viability assay

The planktonic growth inhibition test consisted of an initial inoculum of *S. aureus* ATCC 25923 at OD600= 0.03 plus *Tth*CDHIIa at 0.1 or 0.3 mg/mL incubated in LB broth for 20 h at 37 °C in the wells of a microplate. After that, the percentage of viable cells was determined by adding 40 µL of a 0.15 mg/mL resazurin (Sigma-Aldrich, St. Louis, USA) solution to 200 µL of the culture. This mixture was incubated at 37 °C for 2 h and the fluorescence was measured at the excitation/emission wavelengths of 550/590 nm, respectively, in an Infinite 200M PRO microplate reader (Tecan, Hombrechtikon, Switzerland). The percentage of planktonic live cells was calculated using the equation (2):

$$\%\ \text{Planktonic viable cells} = 100\ (Sample_{550/590} - SC_{550/590})/(GC_{550/590} - SC_{550/590}) \quad (2)$$

where $SC_{550/590}$ and $GC_{550/590}$ correspond to the fluorescence measurement of the sterility control and the growth control, respectively. The experiments were performed in triplicate.

3.6 Confocal laser scanning microscopy (CLSM)

A biofilm inhibition test was performed as described before in a untreated 24-well plate (Corning,New York, NY, USA) at a final volume of 1mL. After 20h of incubation at 37°C, the medium was discarded, and the remaining biofilms were rinsed with ultrapure water. The LIVE/DEAD™ BacLight™ Bacterial Viability Kit for microscopy (Invitrogen, Carlsbad, USA) was employed. A 1000X dilution of both SYTO 9 and propidium iodide in a 0.9% NaCl was performed. 500 µL of this mixture was applied to the biofilms and incubated at room temperature in the dark for 15 min. A 0.9% NaCl wash was performed to eliminate any excess of the dye mixture. These samples were analyzed qualitatively on a Zeiss LSM 780 confocal microscope (Zeiss, Oberkochen, Germany) equipped with a Chameleon Coherent laser (Tisapphire) as two-photons excitation source with Plan-Apochromat objective lenses (10X). The fluorescence detection for SYTO 9 and propidium iodide was measured at the

excitation/emission wavelengths of 480/500 and 490/635 nm respectively. The images were analyzed using the software package ZEISS ZEN 3.6 (Zeiss, Oberkochen, Germany).

3.7 Determination of Minimum Biofilm Eradication Concentration (MBEC) under *Tth*CDHIIa pretreatment conditions

A 24 h-old *S. aureus* ATCC 25923 biofilm was grown in microplates as described in section 3.4. Serial dilutions of gentamicin, tetracycline or chloramphenicol (Sigma-Aldrich, St. Louis, USA) ranging from 64 to 1 µg/mL in BHI broth + 1% glucose were applied to the washed biofilms and incubated overnight at 37 °C. At the next day, the biofilms were washed with PBS and then the wells were filled with 100 µL PBS. Biofilms were sonicated for 10 min to suspend the cells, and then were subjected to a resazurin viability assay as described in section 3.5. A dose-response curve was plotted to obtain the MBEC value, defined as the minimal concentration of antibiotic required to reduce biofilm cell viability below the detection limit of the test [53].

Once the MBEC was determined for all three antibiotics, 24 h-old fresh biofilms were washed and then treated for 4 h at 37 °C with a solution of *Tth*CDHIIa at 0.3 mg/mL plus 20 mM cellobiose in 5 mM MES (pH 6). After the incubation, the remaining biofilms were washed and overnight incubated with BHI broth + 1% glucose and half of the MBEC concentration for each antibiotic, independently. Following this incubation, the viability of cells in the resuspended biofilm was measured with the resazurin test, as described above.

3.8 Analysis of soluble product of *Tth*CDHIIa treated biofilm.

S. aureus ATCC 25923 biofilms were grown in 15 mL conical tubes from an OD600 = 0.03 inoculum in BHI broth supplemented with 1% glucose for 24 h at 37 °C. Then, the Extracellular Polymeric Substance (EPS) was extracted with a 1.5 M NaCl solution according to the protocol described in [54]. Seventy microliters of the EPS solution were subjected to an overnight (37 °C) enzymatic oxidation with 0.3 mg/mL *Tth*CDHIIa in 100 mM sodium phosphate buffer pH 6 (350 µL final volume reaction). The possible soluble products were analyzed by HPAEC as described in the Supplementary material. Controls with 0.65 mM N-acetyl glucosamine (NAG) (Sigma-Aldrich, St. Louis, USA) and 2 mM H_2O_2 were also performed.

3.9 Statistical analysis

The enzymatic activity data were represented as the mean of three independent experiments (n = 3) and its associated standard deviation (S.D.). Statistical analysis has been performed in all the microbiological data using analysis of variance (ANOVA) and Tukey test for mean comparisons in the software Origin 2020 (OriginLab Corporation, Northampton, MA, USA). P-values less than 0.01 ($p < 0.01$) were considered statistically significant.

Chapter 4

Results and discussion

4.1 Production and characterization of *Tth*CDHIIa

After 48 h of methanol induction, the highest activity of the culture supernatant (as assayed using DCPIP test) was achieved (678 U/L) (Figure 5a). Then, the recombinant *Tth*CDHIIa was successfully purified in *P. pastoris* (Figure 5b). The UV/VIS spectral characterization of *Tth*CDHIIa in its oxidized state showed the Soret peak at 420 nm (Figure 5c) [55], indicating the presence of heme b cofactor in the Cyt-domain, while the FAD cofactor can be seen as a broad absorbance lecture between 450 – 500 nm. After reduction with 1 mM cellobiose, the Soret band shifted to 429 nm, and two more peaks appeared at 533 and 564 nm, known as β and α peak, respectively, representing the reduced heme b group [56].

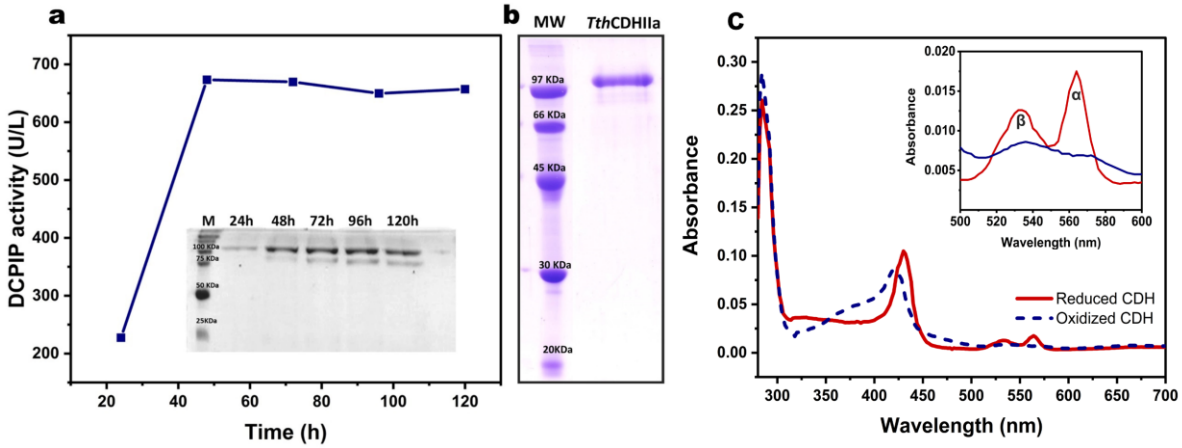

Figure 5 - Production and spectral characterization of *Tth*CDHIIa. (a) Expression in *P. pastoris* described in volumetric activity (DCPIP assay) along time. (b) SDS-PAGE of purified *Tth*CDHIIa. MW: molecular weight ladder. (c) Spectrum showing the oxidized (dashed blue line) and reduced (red line) spectra after application of 1 mM cellobiose. The data were recorded in 20 mM Bis-Tris buffer pH 6 (69 µg loaded).
Source: Adapted from SAMANIEGO *et al.*[46]

*Tth*CDHIIa has a stable suboptimal activity (40% to 60%) under acidic conditions (pH 3 – 5) with an optimum pH of 6. The enzyme loses almost all its oxidative capacity at pH 8 (Figure 6a). Its optimum temperature is 60 °C (Figure 6b). *Tth*CDHIIa activity remains stable for up to 6h at 37 and 50 °C. On the other hand, at 60 °C it progressively loses near 60% of its activity after 3 h of incubation. The enzyme is completely inactivated after 30 min at 70 °C (Figure 6c).

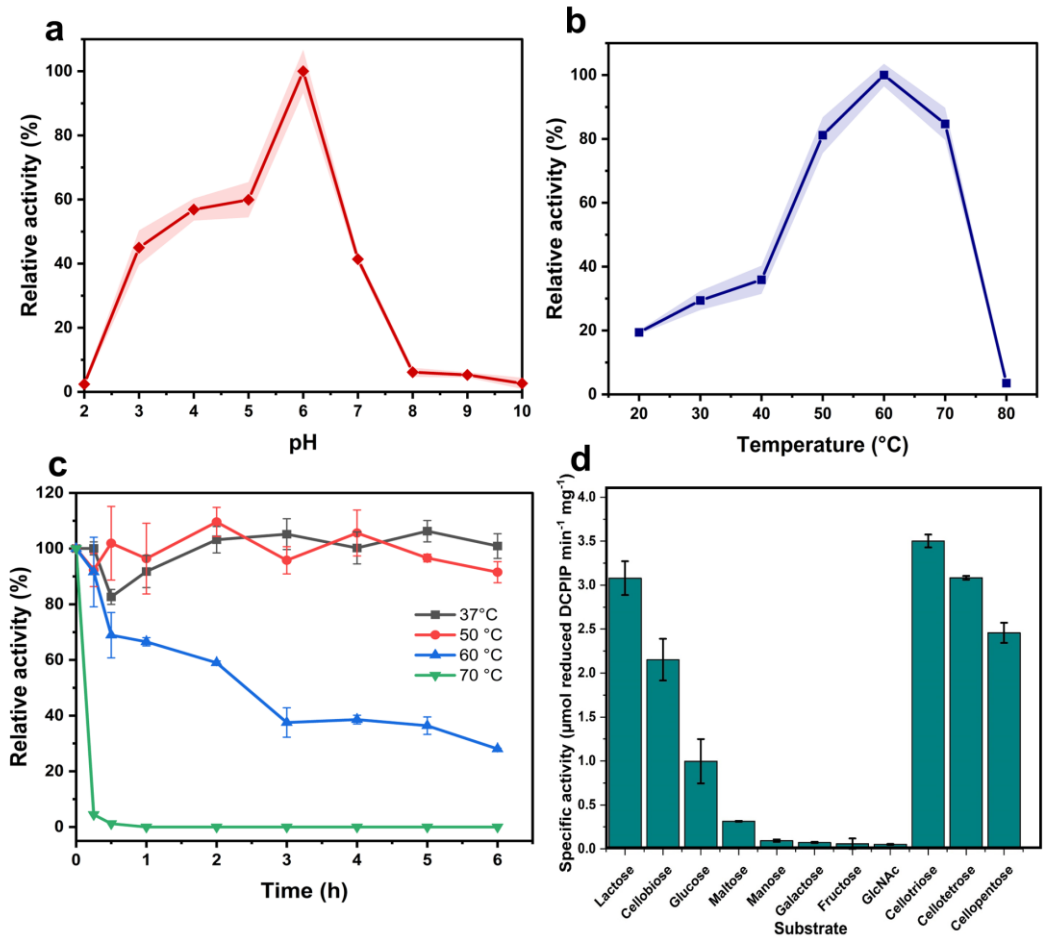

Figure 6 - Biochemical characterization of *Tth*CDHIIa. Effects of temperature and pH on the enzymatic activity are demonstrated in panels (a) and (b), respectively. Standard enzymatic reaction consisted of 50 mM Bis-Tris buffer pH 6 buffer, 0.3 mM DCPIP, 20 mM cellobiose and 0.2 µM of *Tth*CDHIIa. *Tth*CDHIIa was incubated in 20 mM acetate-borate-phosphate buffer to determine the optimum pH at 30 °C. (c) Residual activity of *Tth*CDHIIa. The temperature stability of the enzyme was measured by determining residual activity after incubation at 37, 50, 60 and 70 °C. All activity measurement was performed following for 3 min the DCPIP reduction at the described condition variations. (d) Substrate preference of TthCDHIIa measured using DCPIP as an electron acceptor. Reaction performed with 0.2 µM of *Tth*CDHIIa in 50 mM Bis-Tris buffer pH 6, 40 mM of soluble substrates (mono or disaccharides), or 1.5 mg/mL cello-oligosaccharides and 0.3 mM DCPIP at 30°C for 3 min. Bars and shadows refer to the standard deviation (n = 3).
Source: Adapted from SAMANIEGO *et al.* [46]

An initial screening of substrate preference using the DCPIP test was conducted, and it identified disaccharides like lactose and cellobiose, in combination with cellooligosaccharides, as some of the most favorable substrates (Figure 6d). Also, we evaluated the effect of different ions on *Tth*CDHIIa enzymatic activity and thermal stability. In general, there was a slight boosting effect in the presence of divalent cations, such as Co^{+2} (114%), Ca^{+2} (109%), Zn^{+2} (107%), Ni^{+2} (106%) and Mg^{+2} (104%) at 10 mM concentration (Figure 7a). Divalent cations like Ca^{+2} show an ion bridge effect, that stabilizes and bring together both CDH domains

improving the IET and substrate accommodation [57]. Conversely, Mn^{+2}, Cu^{+2} and Li^{+1} ions decreased the enzymatic activity by an average of 30%, while Fe^{+3} can inhibit more than 90% of the capacity of CDH to reduce DCPIP (Figure 7a). A thermofluor assay was used to determine the melting temperature of *Tth*CDHIIa both in the absence and presence of cations. Without any added ion, the DH domain and the Cyt domain had Tms of 69 °C and 51 °C, respectively (Figure 7b, Table 1). This was maintained in the presence of most ions but copper, for which the Cyt-domain Tm was reduced to 45 °C, and iron, for which unfolding of the entire *Tth*CDHIIa was evident.

Previous studies have reported that Cu^{+2} is able to decrease the activity of the DH-domain of a CDH from *Cerrena unicolor* on 16% and of *Pycnoporus sanguineus* on 20% [58,59]. Our thermofluor assay showed that in addition to DH-domain, the Cyt-domain was also less stable in the presence of these ions.

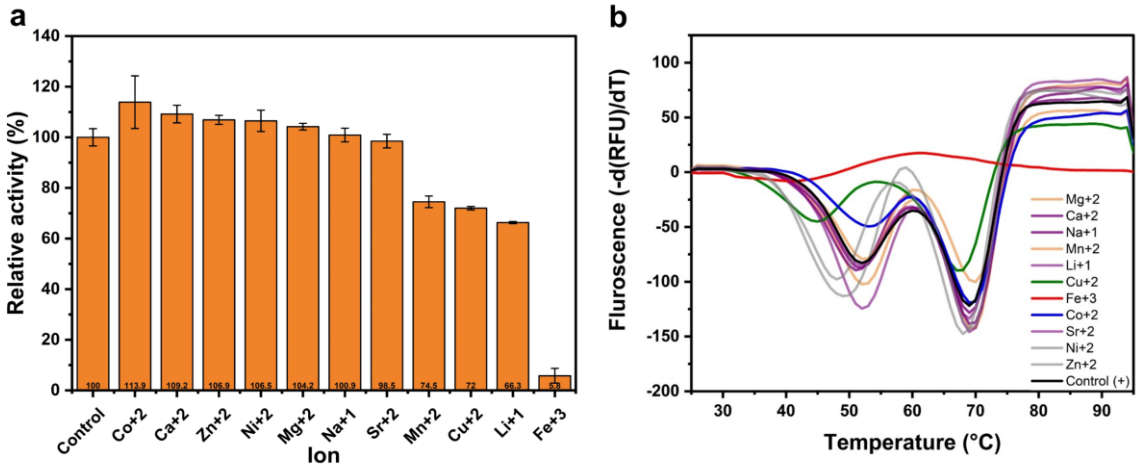

Figure 7 - Ions effect on the enzymatic activity and structural thermal stability. (a) The addition of ions in 10 mM final concentration under the described standard reaction condition was tested. (b) Thermal shift curve in 50 mM Bis-Tris buffer pH 6 and 10 mM ion solution.
Source: Adapted from SAMANIEGO *et al.* [46]

Table 1 - Apparent melting temperature (Tm) of *Tth*CDHIIa

10 mM Ions	Tm (°C)	
	DH domain	Cyt Domain
Co^{+2}	69	53
Mg^{+2}	70	52

(continued)

(continuation)

Table 1 - Apparent melting temperature (Tm) of *Tth*CDHIIa

10 mM Ions	Tm (°C)	
	DH domain	Cyt Domain
Na^{+1}	69	52
Mn^{+2}	70	52
Li^{+1}	69	52
Sr^{+2}	69	52
Ca^{+2}	69	51
Zn^{+2}	69	49
Ni^{+2}	68	48
Cu^{+2}	67	45
Fe^{+3}	41	30
Control	69	51

The monitored fluorescence and the peak temperature in $\Delta\phi/\Delta t$ curve were used to extract the melting temperature (T_m)

Source: Adapted from SAMANIEGO *et al*.[46]

4.2 Hydrogen peroxide production

We measured the production of H_2O_2, using different substrates cited above (Figure 8a). At mild conditions of 37 °C and 30 min of reaction, *Tth*CDHIIa produced 19 µM of H_2O_2 from lactose oxidation. Surprisingly, glucose oxidation produced a very similar concentration of H_2O_2 (18.3 µM), despite much higher K_m (142 mM) and limited catalytic efficiency on this substrate (k_{cat}/K_M =0.034 mM^{-1} s^{-1}) (Table 2, Figure 6d). It is important to note the similar H_2O_2 production from cellobiose (16 µM), cellotriose (16 µM), cellotetraose (14 µM) and cellopentaose (14 µM) oxidation by *Tth*CDHIIa. *Tth*CDHIIa was also able to produce H_2O_2 from the oxidation of other monosaccharides, besides glucose, such as mannose (13 µM) and galactose (8 µM). This wide spectrum of substrates allowing the enzyme to produce H_2O_2 employing monosaccharides, oligosaccharides, carboxymethyl cellulose, crystalline cellulose and cotton was previously reported analyzing a well-characterized ascomycete CDH, *Mt*CDH [60].

We also investigated the time course production of H_2O_2 (Figure 8b). Using 0.1 mg/mL of *Tth*CDHIIa, the H_2O_2 production reaches a plateau (84 µM) after 2 h, and a decay in H_2O_2 molarity becomes evident after 5 h of incubation. After 24 h of enzymatic reaction, a residual production of approximately 20 µM H_2O_2 could be quantified.

In other studies, a group of class I (basidiomycetes) CDHs from *Phlebia lindtneri* (*Pl*CDH), *Phanerodontia (Phanerochaete) chrysosporium* (*Pch*CDH), *Cerrena unicolor* (*Cu*CDH), and *Pycnoporus sanguineus* (*Ps*CDH) revealed variable capacities to produce hydrogen peroxide [41]. In 24h reactions and using cellobiose as a substrate, the maximum production of H_2O_2 by *Cu*CDH reached about 150 μM, both *Pch*CDH and *Ps*CDH produced 80 μM H_2O_2, whereas *Pl*CDH was only capable to deliver about 1 μM H_2O_2 [41]. When lactose was used as a substrate, enzymatically delivered H_2O_2 levels varied between 1.3 and 310 μM H_2O_2 for the same four enzymes [41]. It is important to mention that much higher concentrations of the enzyme (up to 0.6mg/mL) were used in these experiments [41]. The levels of H_2O_2 production were found correlated with the strong variations in antimicrobial activity against growth inhibition *S. aureus* ATCC 25923 planktonic cells (98.7%, 62.6% and 55.2% inhibition of the bacterial growth for *Ps*CDH/cellobiose, *Cu*CDH/cellobiose and *Pch*CDH/cellobiose, respectively). No impacts on *S. aureus* ATCC 25923 bacterial growth was observed when *Pl*CDH/cellobiose was used for hydrogen peroxide production. However, it is not clear why *Cu*CDH/cellobiose combination which generated highest levels of H_2O_2, let to only intermediate inhibition of the bacterial growth, whereas application of *Ps*CDH/cellobiose resulted in almost complete elimination of *S. aureus* ATCC 25923 planktonic cells (98.7%). Furthermore, although *Pch*CDH/cellobiose produced about the same levels of H_2O_2 as *Pl*CDH/cellobiose, the former combination led to only modest 55.2% inhibition of the bacterial growth. Finally, the effects on the microbial biofilm formation and degradation unfortunately have not been investigated in this study [41].

Noteworthy, with exception of *Pl*CDH, the enzymes did not show decay in generated H_2O_2 concentration during 24 h of reaction [41]. It is possible that *Tth*CDHIIa is prone to oxidative inactivation at certain H_2O_2 concentrations, as already observed for *Mt*CDH [60]. It is known that a number of amino acids including histidine, tyrosine, tryptophan, and, in particular, methionine and cysteine are susceptible to oxidation [61]. *Tth*CDHIIa amino acid sequence has 13 cysteines, one of which is not involved in S-S bridges formation (Cys291) (Fig 2a). Considering the high content of methionine in CDHs structures responsible for the coordination of the FAD group, some efforts have been previously done to replace this amino acid residues using site-directed mutagenesis aiming to produce a CDH with higher resistance to H_2O_2 [62]. Similar strategy can also be applied to *Tth*CDHIIa in order to produce more robust mutant enzymes, less prone to oxidation by H_2O_2.

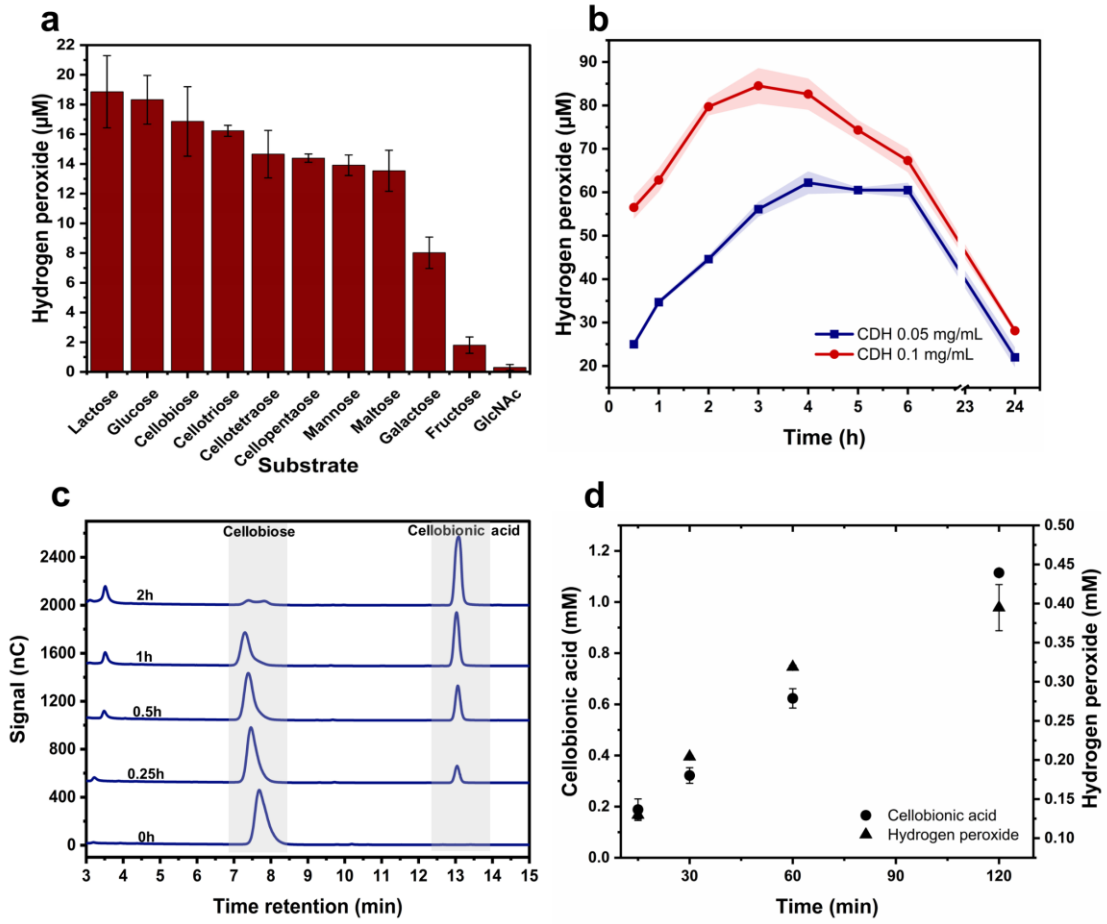

Figure 8 – Hydrogen peroxide production by *Tth*CDHIIa. (a) Production of H_2O_2 by 0.2 µM *Tth*CDHIIa in 50 mM Bis-Tris buffer pH 6 incubated for 30 min at 37 °C with different mono- and oligosaccharides. (b) Time course of H_2O_2 generation from 0.05 mg/mL (0.58 µM) and 0.1 mg/mL (1.16 µM) of *Tth*CDHIIa using cellobiose (20 mM). (c) HPAEC analysis of the complete oxidation of 1 mM cellobiose at 50 °C by 1 µM of *Tth*CDHIIa in 50 mM sodium phosphate buffer pH 6. (d) Correlation in the production of cellobionic acid and hydrogen peroxide over time by 1 µM of *Tth*CDHIIa in 50 mM sodium phosphate buffer pH 6. All H_2O_2 quantification results by Amplex red assay were measured in triplicate and shadows or bars refer to the standard deviation.
Source: Adapted from SAMANIEGO *et al.*[46]

Parallel measurements of H_2O_2 and cellobionic acid (auto hydrolysis product of cellobiono-lactone) production evidence a linear and time-dependent behavior (Figure 8c,d). After 15 min of reaction, 0.19 mM and 0.13 mM of cellobionic acid and H_2O_2 are produced, respectively, which is relatively close to the theorical stoichiometric correspondence between 1:1 cellobiose/H_2O_2. However, as the enzymatic reaction continues, the measured cellobionic acid surpasses the measured H_2O_2; at 2 h of reaction there is approximately 1 mM and 0.4 mM of each product, respectively, indicating concomitant consumption of H_2O_2 (Figure 8d).

4.3 Substrate preference and steady-state kinetics of *Tth*CDHIIa

Aiming to describe in a more quantitative way the use of different substrates by *Tth*CDHIIa, we analyzed the kinetic parameters of the enzyme (Table 2). The lowest K_M (0.024 mM) and highest k_{cat}/K_M of 198 mM^{-1} s^{-1}, was measured for cellobiose. These values are similar to those obtained for other CDHs from Ascomycetes, such as *M. thermophilum* [63], *Chaetomium atrobrunneum*, *Hypoxylon haematostroma*,[1] *Stachybotrys bisbyi*,[64] and *Thielavia terrestris* [65]. Lactose, the epimer of cellobiose, had the second lowest K_M (0.10 mM) and the second highest k_{cat}/K_M of 60.88 mM^{-1} s^{-1}. The capacity of *Tth*CDHIIa to distinguish between lactose and cellobiose can be calculated by the ratio of catalytic efficiencies [k_{cat}/K_M Cellobiose]/[k_{cat}/K_M Lactose], giving a factor of 3.3, revealing relatively low substrate discrimination in comparison to the more selective class I CDHs (basidiomycetes), but within the range observed for class II CDHs [1].

Table 2 - *Tth*CDHIIa kinetic parameters

Substrate	V_{max}	K_M (mM)	k_{cat} (s^{-1})	k_{cat} / K_M (mM^{-1} s^{-1})
Cellobiose	0.94 ± 0.02	0.023 ± 0.003	4.7 ± 0.1	198 ± 30
Lactose	1.16 ± 0.07	0.100 ± 0.03	6.0 ± 0.4	60 ± 1.5
Maltose	0.094 ± 0.002	1.9 ± 0.1	0.49 ± 0.01	0.25 ± 0.01
Glucose	0.89 ± 0.02	142 ± 38	4.6 ± 0.1	0.034 ± 0.008
Cellotriose	1.07 ± 0.04	0.33 ± 0.03	5.6 ± 0.2	17 ± 2
Cellotetrose	1.01 ± 0.02	0.29 ± 0.04	5.24 ± 0.09	18 ± 2
Cellopentose	0.64 ± 0.04	0.155 ± 0.003	3.3 ± 0.2	21 ± 2
Xylobiose	0.71 ± 0.09	11 ±2	3.3 ± 0.4	0.30 ± 0.03

Kinetic parameters are estimated on the basis of DCPIP reduction. The enzymatic activity was determined in 50 mM Bis-Tris buffer pH 6.0 at 30 °C.

Source: Adapted from SAMANIEGO *et al.* [46]

Despite their bigger molecular size, the cellooligosaccharides are recognized and oxidized by the enzyme (Table 2). Apparently, the enzymatic efficiency stays approximately the same and even grows a little as the chain length of substrate increases . A similar behavior was previously observed for CDH from *Neurospora crassa* [66]. Being tested against monosaccharides, only activity on glucose could be detected, with K_M and K_M/k_{cat} estimated as 142 mM and 0.034 mM^{-1} s^{-1}, respectively.

4.4 ColabFold predicted model of *Tth*CDHIIa

A primary sequence alignment of *Tth*CDHIIa with *Mt*CDH (PDB: 4QI6) shows considerable conservation of the amino acid residues, both in Cyt and DH domains as well as in CBM module (Figure 9).

The ColabFold prediction generated a robust model for structural analysis (Supplementary data), revealing that *Tth*CDHIIa exhibits the classic two-domain architecture of CDH family, with the Cyt-domain presenting an immunoglobulin-like beta-sandwich fold connected via a peptide linker to the DH-domain, an α/β structure with a p-hydroxybenzoate hydroxylase (PHBH) fold [4]. Furthermore, at the C-terminal region, the carbohydrate-binding module (CBM), stabilized by two disulfide-bonds, was also modelled. The conformational arrangement of the *Tth*CDHIIa was modeled in a closed state, with the DH-domain making contact with the Cyt-domain in a way that both cofactors, heme b and FAD, are in a proximity (Figure 10a). This conformation was confirmed experimentally in other CDHs with crystallographic, SAXS and atomic force microscopy experiments [5,67].

A structural comparison with *Mt*CDH (PDB:4QI6) revealed the conserved catalytic dyad (Hys701 and Asn748) and substrate binding residues (Tyr619, Arg601, Tyr549, Trp295 and Asn292) (Figure 10b). The position of cellobiono-1,5-lactam (CLBM) showed that catalytic subsite (subsite C) is close enough to His701 and Asn748, similar to what is observed for *Mt*CDH [5]. The binding subsite (subsite B) composed of the non-reducing monomer of cellobiose or CLBM also shows interaction with the corresponding amino acids (Arg601 Asn292 and Trp 295). Close analysis of *Tth*CDHIIa active site shows a prominent cavity towards subsite B (Figure 10c), which is also observed in the *Mt*CDH structure (Figure 10d).

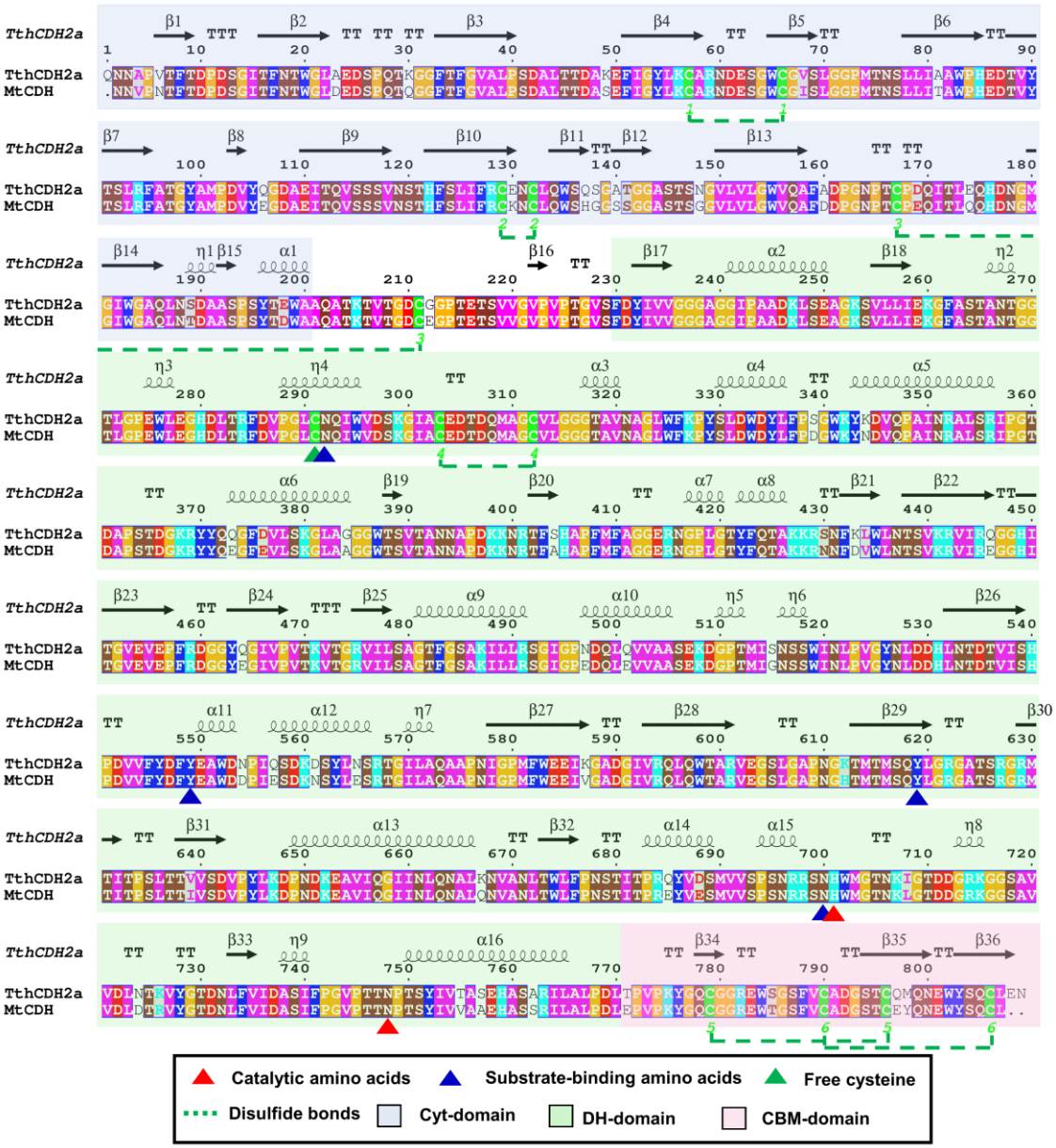

Figure 9 - Alignment of *Tth*CDHIIa with its closest homolog, *Mt*CDH (PDB: 4QI6). Identical or similar amino acids are colored according to their physicochemical properties as follows: negatively charged (red), positively charged (cyan), uncharged polar (maroon), non-polar (pink), aromatic(blue), cysteine (green), proline and glycine (orange). The secondary structure of *Tth*CDHIIa is shown above each residue. The sequences corresponding to the Cyt domain are colored in light-blue shaded box; DH-domain, in green shaded box and CBM-domain in pink shaded box. Disulfide bonds are marked in green dashed lines. The catalytic and substrate-binding residues are marked in red and blue triangles, respectively. The free cysteine is marked in green triangle.

Source: Adapted from SAMANIEGO *et al.*[46]

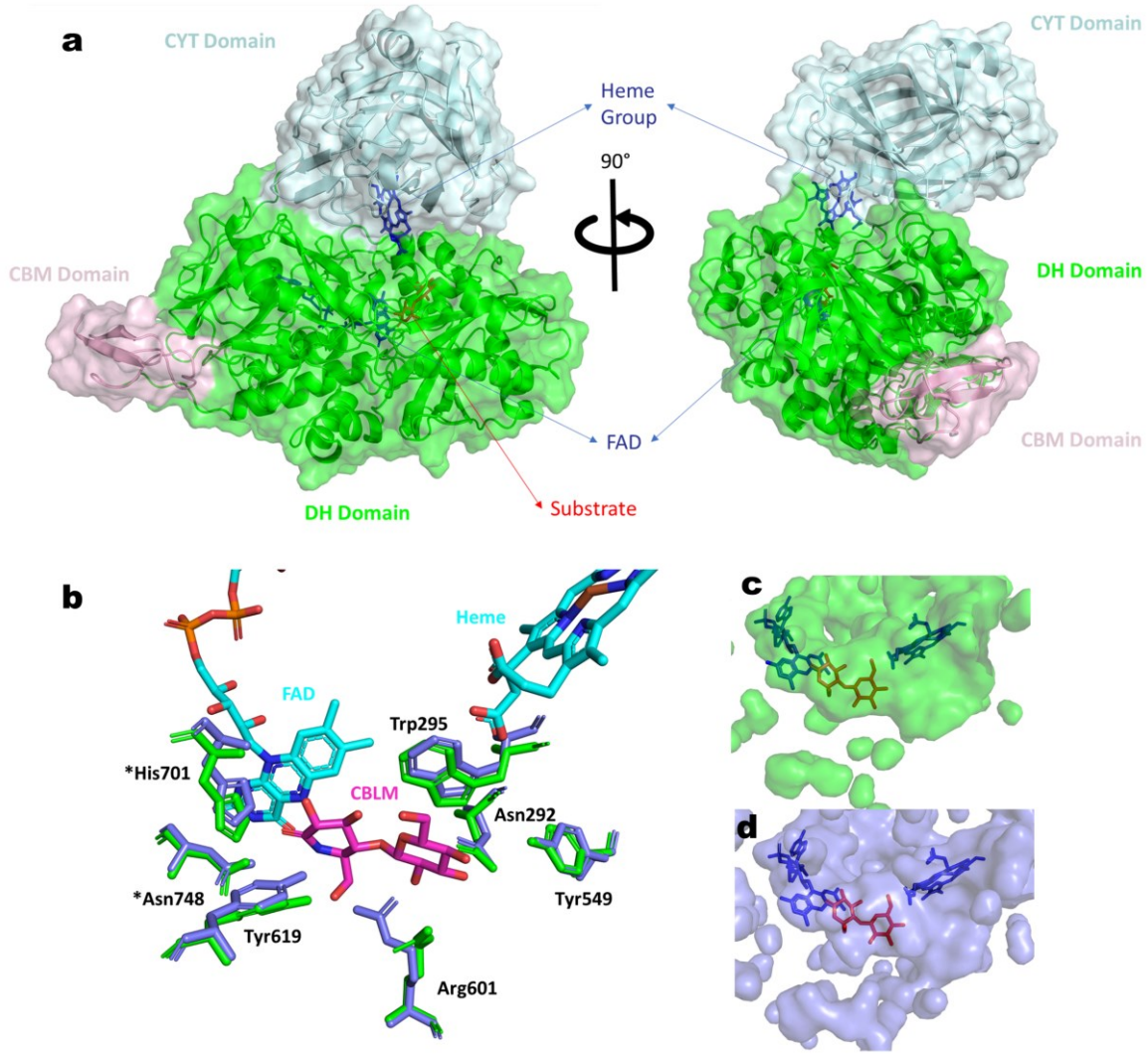

Figure 10 – Structural analysis of *Tth*CDHIIa. (a) ColabFold predicted three-dimensional structure of *Tth*CDHIIa was coupled manually to its substrate and cofactors using Pymol as described previously. The three domains are clearly distinguished, Cyt-domain evidence an all-β folding docked with a Heme group, meanwhile DH-domain a more complex α/β structure and a FAD cofactor. The prediction depicted a closed state of *Tth*CDHIIa, with a proximity between Cyt and DH-domain, producing close contact of FAD and Heme group, and the substrate in between. (b) Superposition of catalytic (His701 and Asn748) and binding residues (Tyr619, Arg601, Tyr549, Trp295 and Asn292) of *Tth*CDHIIa (green sticks) and *Mt*CDH (light blue sticks) (PDB: 4QI6), showing the structural conservation of this region (DH-domain). Similarities in the enzymatic pockets of (c) *Tth*CDHIIa and (d) *Mt*CDH after CLBM binding.

Source: Adapted from SAMANIEGO *et al.*[46]

4.5 Structural basis of oligosaccharides oxidation by *Tth*CDHIIa

The oxidized products of cello and xylooligosaccharides were directly detected by HPAEC-PAD, making use of the differences in their retention times as compared to their reduced counterparts. As expected, the HPAEC chromatogram using cellobiose (C2) as substrate shows a production of oxidized cellobiose (C2ox) after 1 h of incubation at 37 °C (Figure 11a), but in a smaller quantity as compared to 50 °C (Figure 8c). All other cello-oligosaccharides (DP3-6) were partially oxidized (~40%) from the initial concentration applied (0.4 mg/mL), generating respective oxidation products (C3ox, C4ox, C5ox and C6ox) in quantities similar to that of C2ox. It is not surprising that the already characterized native CDH from *T. thermophilus* has a similar magnitude of discrimination between cellobiose/cellotetraose ([k_{cat}/K_M Cellobiose]/ [k_{cat}/K_M cellotetraose]) [48] and the oxidation pattern comparable to our recombinant version of the enzyme (Table 2), that can be extended to other cellooligosaccharide substrates. Furthermore, although the enzyme has a low catalytic efficiency (0.3 $mM^{-1}s^{-1}$) at 30 °C on xylooligosaccharides, these substrates (DP2-6) were completely oxidized after 24 h of incubation at 50 °C (Figure 11b).

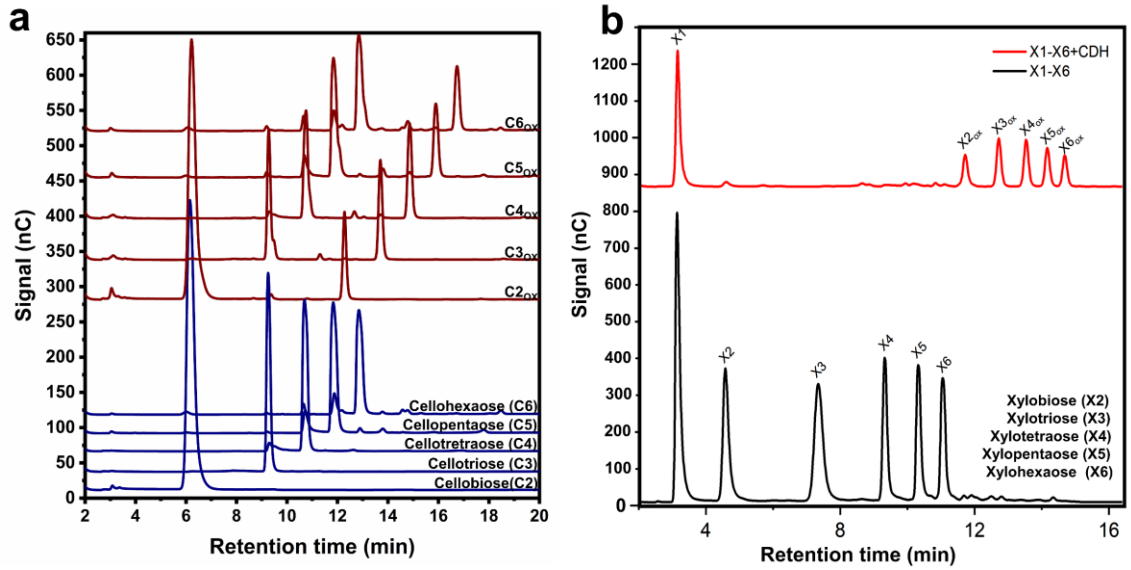

Figure 11 – Oxidation of cello- and xylooligosaccharides by *Tth*CDHIIa. HPAEC chromatograms showing the products released by 1 µM of *Tth*CDHIIa after incubation with (a) cellobiose (C_2, 1mM) and cellooligosaccharides (C_3-C_6, 0.4 mg/mL) and (b) xylobiose (X_2, 1mM) and xylooligosaccharides (X_3-X_6, 0.4 mg/mL) for 24 h at 50 °C in 50 mM sodium phosphate buffer pH 6. Peaks were assigned based on cello and xylooligosaccharide standards shifted retention time in its oxidized state.
Source: Adapted from SAMANIEGO *et al.*[46]

Oxidation of xylooligosaccharides is less common in AA3 class enzymes, only reported for CDH isoforms of *N. crassa* [66,68]. Other CAZymes such as oligosaccharide-oxidizing enzymes (Family AA7) [9] can oxidize xylooligosaccharides more efficiently than *Tth*CDHIIa,[69] but for cellooligosaccharides the level of oxidation is similar. For example, glucooligosaccharide oxidase (GOOX) from *Sarocladium strictum* [70] exhibits oxidation rates comparable to the activities reported here. On the other hand, FgCelDH7C, an oligosaccharide dehydrogenase from *Fusarium graminearum*,[71] also a member of AA7 family, shows lower catalytic efficiencies than that of *Tth*CDHIIa.

To evaluate whether it is sufficient to accommodate the studied oligosaccharides into the substrate pocket of *Tth*CDHIIa, CLBM was computationally extended to cellotetraose. No steric hindrance that could impede the accommodation of this substrate was observed (Figure 12a). Furthermore, Trp295 and Tyr549 act as an aromatic-stacking platform to stabilize the additional subsites. The presence of aromatic amino acids in the binding groove is a requirement for dehydrogenases to be active on oligosaccharides [71].

The same logic can be applied to xylooligosaccharides recognition and oxidation. As expected, similarly to cellobiose, xylobiose (X2) snugly fits the catalytic pocket of *Tth*CDHIIa (Figure 12b). The presence of the reducing end in the anomeric carbon makes X2 an electron donor. However, the lack of the C6-moeity in X2 results in the loss of interactions with Tyr619 and Thr599, which is consistent with an increase of K_M for this substrate (~ 11.2 mM,) in comparison to cellobiose (0.024 mM) or cellotetraose (0.289 mM).

Broad recognition of oligosaccharides is further supported by the conformation of the substrate entrance. Although *Tth*CDHIIa 3D model is in a closed state, the proximity of the domains forms a channel large enough (cross-sectional area 167.4 $Å^2$) (Figure 12c) to permit the entry of cello (34 $Å^2$) or xylooligosaccharides (13.9$Å^2$) (Figure 12d) or, potentially, any other oligosaccharides with larger decorations. The exposed area is directly related to the length of the docked oligosaccharide. As an example, another AA3-family member, pyranose oxidase (POX), exhibits a narrow, almost occluded, substrate channel [72], meanwhile cello and xylo-oligosaccharide oxidases and dehydrogenases have exposed and extended active site [69,71]. This structure-based evidence provides an explanation for experimentally observed broad range of *Tth*CDHIIa specificity toward soluble cello- and xylooligosaccharides.

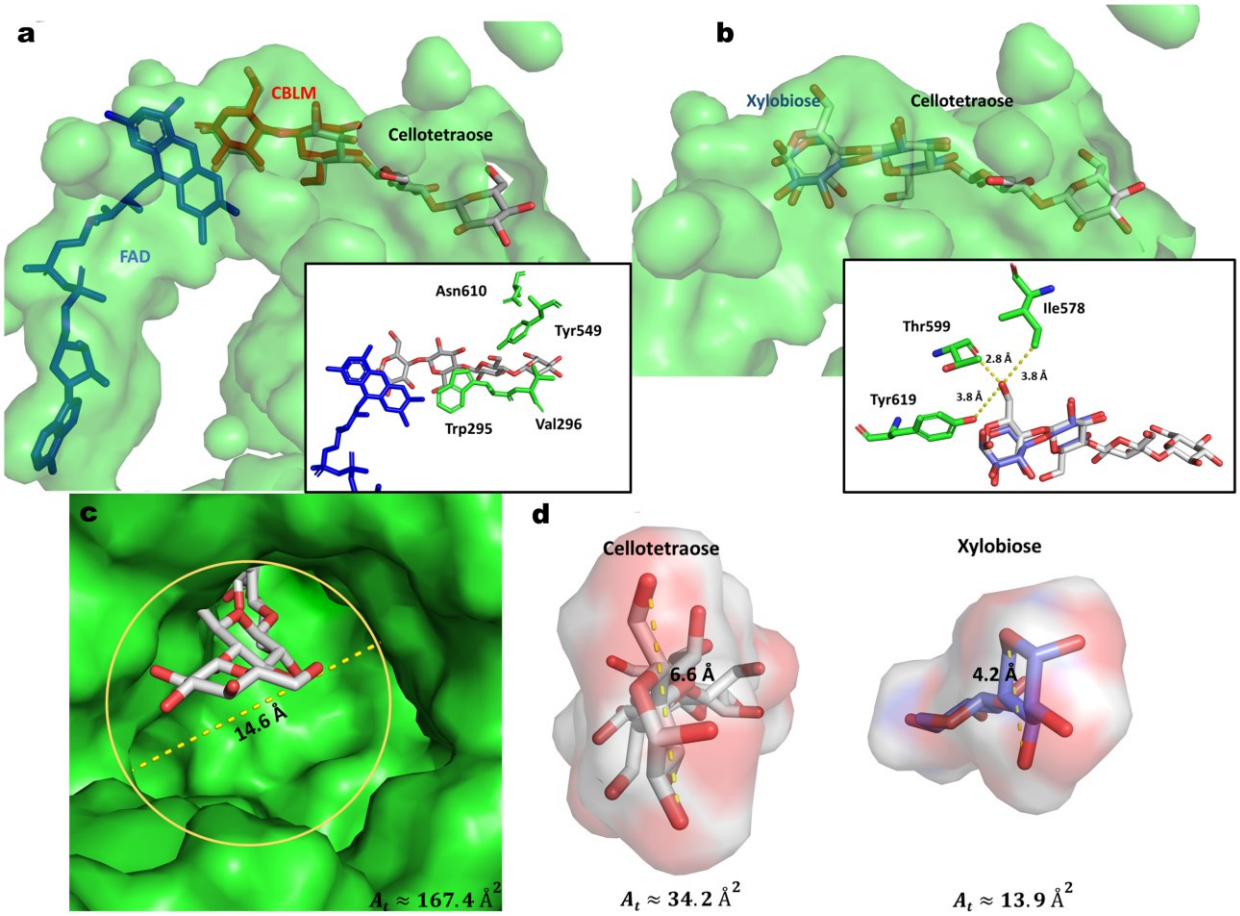

Figure 12 - Structural basis of oligosaccharides oxidation by *Tth*CDHIIa. (a) Cellotetraose molecule bound within *Tth*CDHIIa pocket with no steric hindrance and exhibiting aromatic stacking interactions with Trp295 and Tyr549 (shown in a box). (b) Xylobiose (blue sticks) comfortably bound to *Tth*CDHIIa pocket. As compared with cellobiose (and other cellooligosaccharides), xylobiose lost interactions with Tyr619 and Thr599, because of the lack of the C6-moeity, which explains weaker binding of this substrate to the enzyme.(c) Surface representation of the substrate channel cross-sectional area (167 Å^2) of *Tth*CDHIIa active site, large enough to accept (d) cellotetraose or xylobiose molecule.
Source: Adapted from SAMANIEGO *et al.*[46]

4.6 Antimicrobial and antibiofilm applications of *Tth*CDHIIa

Diseases associated with biofilms represent up to 80% of nosocomial infections, with *S. aureus* being the leading cause [73]. Staphylococcal chronic infections are especially prone to biofilm formation, allowing the bacteria to attach and persist on host tissues like bones, skin, mucosa, heart valves,[74] and medical devices, like artificial implants, pacemakers, prosthetic joints and catheters [75]. Taking advantage of *Tth*CDHIIa's broad substrate specificity and its continuous, mild and *in situ* production of H_2O_2, we applied this redox enzyme on *S. aureus* planktonic cultures and biofilms to evaluate its antimicrobial and antibiofilms effects.

4.6.1 Impact of *Tth*CDHIIa-mediated H_2O_2 production on *S. aureus* planktonic and biofilm growth

An initial screening of the effect of different concentrations of *Tth*CDHIIa on the planktonic growth of *S. aureus* shows an approximate 50% inhibition (IC_{50}) with 2uM (0.17mg/mL) of *Tth*CDHIIa (Figure 13). For the following experiments, a lower (0.1 mg/mL) and a higher concentration (0.3 mg/mL) were considered.

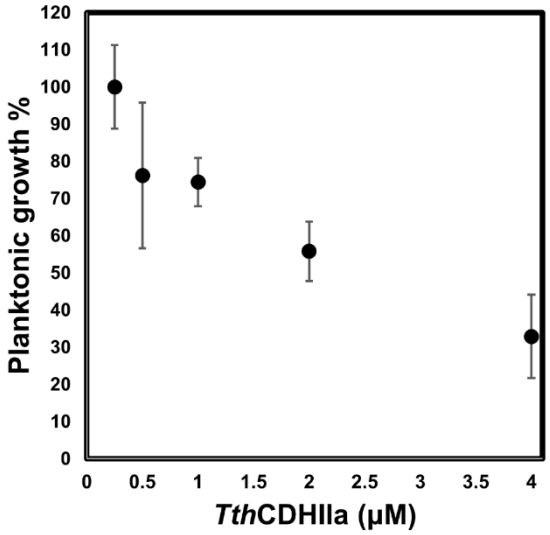

Figure 13 - Initial screening of different concentration of *Tth*CDHIIa (0.25, 0.5, 1, 2 and 4 µM) against *S. aureus* ATCC 25923 grown in liquid culture in the presecense of 20 mM of cellobiose for 20h at 37°C.
Source: Adapted from SAMANIEGO *et al.*[46]

An application of *Tth*CDHIIa in *S. aureus* cultures results in a reduction of cell viability after 20 h of incubation. *Tth*CDHIIa (0.1 mg/mL or 20µg) alone reduces the viability of the initial inoculum by 9.5%, while the simultaneous addition of C2, its preferred substrate, significantly increases its antimicrobial effect to 38.8%. Higher concentrations of the enzyme (0.3 mg/mL or 60 µg) reduce 68% of the *S. aureus* cell viability (Figure 14a). As a consequence of the antimicrobial effect of *Tth*CDHIIa , the formation of biofilm was affected proportionally. To quantify this behavior, an inhibition of biofilm formation test was performed. Using 0.3 mg/mL of *Tth*CDHIIa a reduction of 62.5% in biofilm formation was observed, when compared to the growth control (Figure 14b). Since the standardized optimum condition for growing *S. aureus* biofilms includes supplementation with 1% glucose (BHIG), the application of 0.1 mg/mL (20 µg) *Tth*CDHIIa with or without C2 did not show significant differences, both resulting in ~ 50 % reduction of the biofilm formation. This effect is likely to be due to the

glucose oxidation by *Tth*CDHIIa, which results in H_2O_2 production, as detailed in section 3.2. A CSLM experiment (Figure 15) shows that cellobiose did not interfere with the viability or the biofilm cell structure. Application of *Tth*CDHIIa (0.3 mg/mL) alone results in a different architecture of the biofilm and just a slight decrease in cell viability. On the contrary, supplementation with C2 decreases greatly the viability of the cells, with a heterogeneous impact on the biofilm.

These results are comparable with studies using an engineered version of *Mt*CDH (*M. thermophilus*) with increased oxygen reactivity and immobilized on chitosan particles, which showed growth inhibition of 50% using 97µg of enzyme and 50 mM of C2 [42]. In recent works, the direct application of *Cu*CDH and *Pch*CDH, both at a concentration of 0.6 mg/mL supplemented with 5 mM of C2, produced a growth inhibition of 62.7 and 55.2%, respectively [41]. Is important to acknowledge that in both studies the same strain of *S. aureus* ATCC 25923 was employed as in the present study. The first reported application of CDH as an antimicrobial agent, uses a recombinant *Mt*CDH [45] embedded in hydrogels of gelatin and alginate at 5 U/mL or 1.6 mg/mL of concentration (as derived from the specific activity 3.1 U/mg [63]) with supplementation of 2 mM C2. This high quantity of enzyme achieved a 100% inhibition for *S. aureus* [45]. Peculiarly, in another study of the same enzyme, 0.1 mg/mL (0.33 U/mL) of *Mt*CDH

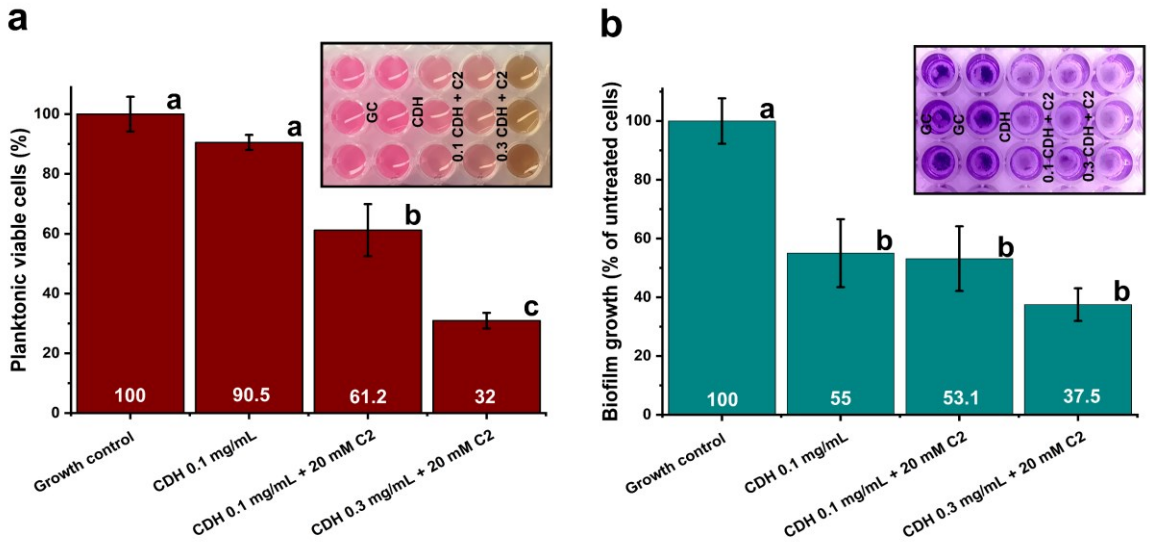

Figure 14 - *Tth*CDHIIa as an antimicrobial and antibiofilm agent. (a**)** Effect of *Tth*CDHIIa on *S. aureus* ATCC 25923 planktonic growth quantified as viable cell (%) using the resazurin fluorescence test. **(b)** Effect of *Tth*CDHIIa on biofilm formation (biofilm inhibition test) of *S. aureus* ATCC 25923 quantified as biofilm growth (% with respect the untreated cells) in a CV staining. Concentration of 0.1 or 0.3 mg/mL of *Tth*CDHIIa was applied in conjunction with 20mM cellobiose and *S. aureus* ATCC 25923 at OD_{600}=0.03. Growth control consisted of the corresponding growth medium supplemented with 20mM cellobiose. Control conditions, using CDH without cellobiose, were also tested. Columns labeled with different letters represent statistically different results ($p < 0.01$) for relative effect, according to ANOVA and Tukey test for mean comparison (n = 3)

Source: Adapted from SAMANIEGO *et al.*[46]

and 1mM C2 was applied directly in a liquid culture of *S. aureus* for growth and biofilm inhibition, also producing 100% of inhibition [43]. Our results can be compared when *Mt*CDH is supplemented with approx. 0.125 mM C2 (~ 60% of planktonic growth or 40% inhibition) .

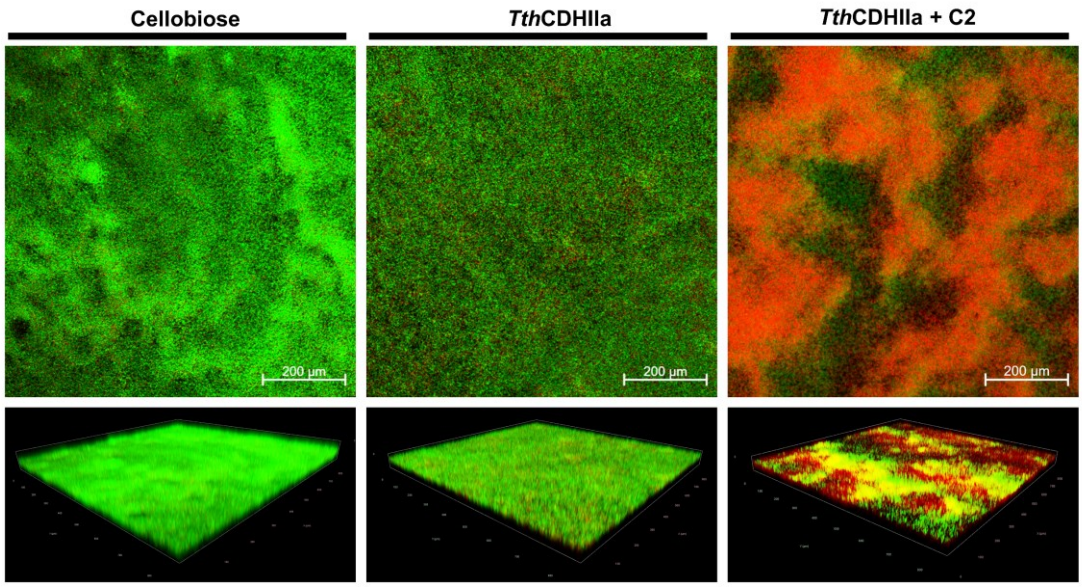

Figure 15 - Confocal laser scanning microscopy (CLSM) images from biofilm inhibition test, showing the viability (upper image) and 3D distribution of the biofilm cells (lower image). SYTO 9 bind viable cells measured at the green fluorescence channel (500 nm); meanwhile propidium iodide detect dead cell at red channel (635 nm)
Source: Adapted from SAMANIEGO *et al.*[46]

The antimicrobial and antibiofilm properties of *Tth*CDHIIa can be also attributed to the production of aldonic acids (cellobionic acid, Figure 8c,d), which leads to a decrease in the pH. Although it has already been demonstrated that in an acidic environment, the growth of *S. aureus* is slowed down [76], further experiments are necessary to confirm this hypothesis. Curiously, this behavior resembles the action of some fermentative bacteria such as, for example, *Lactobacillus hilgardii*, which produce simultaneously lactonic acids and H_2O_2 and can inactivate the growth of other bacteria in mixed cultures [77].

4.6.2 Effect of *Tth*CDHIIa in *S. aureus* biofilm eradication and HPAEC analysis of 24 h-old *S. aureus* biofilm treated with *Tth*CDHIIa

Most of the studies related to the antibiofilm effect of CDHs rely on the biofilm inhibition test, where the enzyme is added at the same time as the freshly bacterial suspension. Here we evaluate for the first time the eradication effect of a CDH. This another antibiofilm

effect is important to assess, because of the recalcitrant nature of established *S. aureus* biofilms. In order to evaluate this parameter, a 24h-old biofilm was grown and treated for 4 hours with 0.3 mg/mL of *Tth*CDHIIa supplemented with its cognate substrate (C2). The results show a 53.8% reduction of the biofilm biomass as compared to the control (Figure 16a). *Tth*CDHIIa biofilm degradation was equivalent to the direct application of 2 mM of H_2O_2 (49.4 % biomass reduction). The oxidative degradation of the Extracellular Polymeric Substance (EPS) using a direct application of H_2O_2 has been reported previously in biofilms of nosocomial isolates of *Staphylococcus sp.*[78] and *Pseudomonas sp.* [79].

Interestingly, the treatment with *Tth*CDHIIa (0.3mg/mL) without the addition of its cognate substrate C2, resulted in a biofilm biomass degradation of 44.6% (Figure 16a). This result might indicate that *Tth*CDHIIa is oxidizing polysaccharides from *S. aureus* EPS to produce H_2O_2. Since poly-β-D-(1→6)-N-acetyl-glucosamine (PNAG) is the predominant polysaccharide of many medically important biofilm-producing bacterial strains of *S. aureus,* [80–82] a PNAG oxidation by *Tth*CDHIIa seems plausible.

HPAEC analysis of *Tth*CDHIIa-treated EPS showed the release of an unknown product after overnight incubation of *S. aureus* ATCC 25923 24 h-old biofilm EPS at 37 °C and *Tth*CDHIIa at 0.3 mg/mL (Figure 16b, asterisk). The presence of this product, in addition to C2ox, is more evident after the addition of C2 to the reaction. The direct application of 2 mM H_2O_2 to the EPS, produced a greater amount of the product. A control employing NAG (N-acetyl-glucosamine) and 2mM H_2O_2, resulted in a product with the same retention time, indicating that the detected substance could be a product of NAG oxidation by hydrogen peroxide (Figure 16c).

The employed protocol for EPS extraction [54] apparently generates long chains of PNAG, that are not resolved in an HPAEC system as evidenced by the experimental controls. Other approaches to extract PNAG from *S. epidermidis*, resulted in short polymeric forms of PNAG that were resolved successfully in a HPAEC-PAD-ESI-MS [83]. Since previous works have demonstrated H_2O_2-mediated degradation of other complex carbohydrates such as polysaccharide A (PSA) from *Bacteroides fragilis* in cellular environments,[84] and the H_2O_2-mediated cleavage of chitosan (β-1,4 linked NAG and glucosamine),[85] it is tempting to speculate that *Tth*CDHIIa-produced H_2O_2 under studied conditions caused oxidation and depolymerization of PNAG.

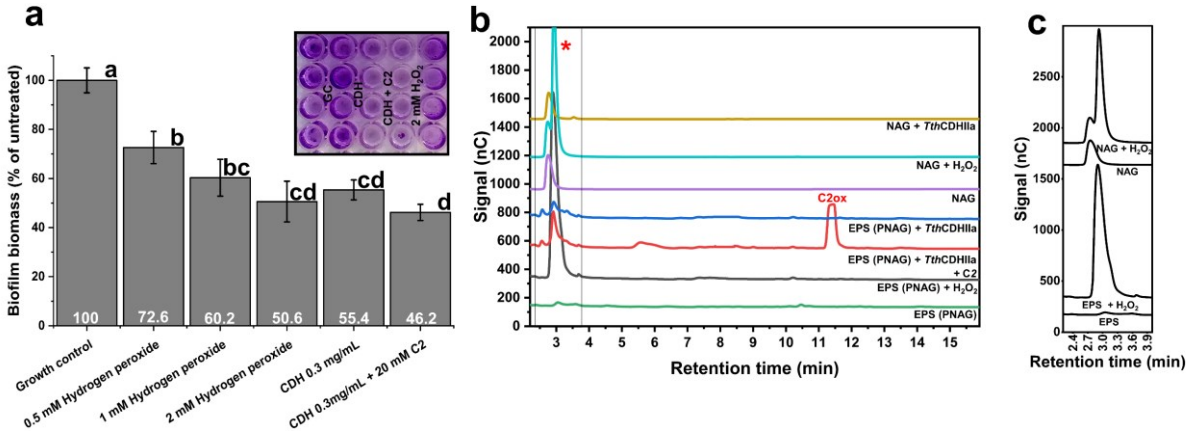

Figure 16 - *Tth*CDHIIa as a biofilm eradication agent. (a) Eradication of 24h-old *S. aureus* ATCC 25923 biofilms after a 4h-treatment with 0.1 or 0.3 mg/mL *Tth*CDHIIa (with or without cellobiose) or hydrogen peroxide (0.5, 1 and 2 mM) All reagents were dissolved in a 5mM MES buffer pH 6 at 37°C. HPAEC chromatogram showing the effect of 0.3 mg/mL *Tth*CDHIIa (with or without cellobiose) or 2mM H_2O_2 applied to (b) extracted EPS (PNAG) of a 24h-old *S. aureus* ATCC 25923 biofilm and to (c) NAG (0.65 mM) after an overnight incubation at 37°C in 100 mM sodium phosphate buffer pH 6. Columns labeled with different letters represent statistically different results ($p < 0.01$) for relative effect, according to ANOVA and Tukey test for mean comparison (n = 3).
Source: Adapted from SAMANIEGO *et al.* [46]

4.6.3 Biofilm viability and synergism with antibiotics

S. aureus biofilm cells viability was not impacted by the 4 h treatment with *Tth*CDHIIa in the eradication tests (data not shown). A short exposition of a 15-day old biofilm of *S. aureus* ATCC 25923 to 15 mM of H_2O_2 has been reported,[86] resulting in only a 50% reduction in the cell viability. It is clear that EPS from *S. aureus* biofilm can be successfully degraded by *Tth*CDHIIa, but in order to fully eliminate the recalcitrant bacteria embedded in the partially destroyed biofilm, supplementation with antibiotics makes itself necessary. To study the impact of the enzymatic treatment on bacterial sensibility to antibiotics, we first determined the MBEC for gentamicin (32 µg/mL), tetracycline (8 µg/mL) and chloramphenicol (2 µg/mL) (Figure 17a), and then applied half of these concentrations in the next series of experiments. The *Tth*CDHIIa pretreatment (0.3 mg/mL and C2) promotes a boosting effect in the activity of gentamicin over biofilm's cells, changing the viability from 97.4% (16 µg/mL gentamicin treatment alone) to 57.7% (16 µg/mL gentamicin after *Tth*CDHIIa pretreatment) (Figure 17b). After tetracycline treatment alone, the biofilm's cell viability drops to 46.7% and further decreases to 24% when *Tth*CDHIIa pretreatment is applied. In the experiments with chloramphenicol and *Tth*CDHIIa, only a slight reduction of viability (from 80 to 75%) was observed.

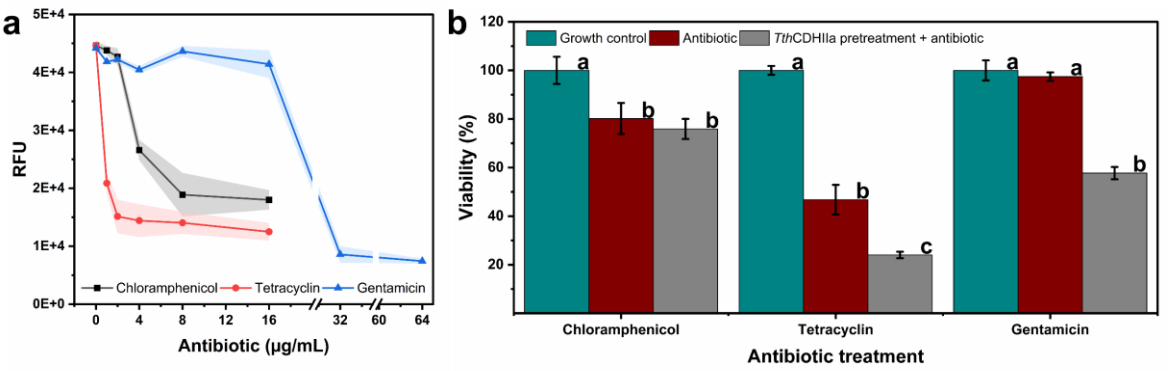

Figure 17 - MBEC determination and synergism of *Tth*CDHIIa with antibiotics. (a) MBEC of chloramphenicol, tetracyclin and gentamicin tested against 24h-old *S. aureus* ATCC 25923 biofilm using a resazurin fluorescence assay. Shadows refer to the standard deviation (n = 3). (b) *Tth*CDHIIa pretreatment effect on half minimum biofilm eradication concentration (MBEC) of chloramphenicol (1µg/mL), tetracycline (4 µg/mL) and gentamicin (16 µg/mL) for *S. aureus* ATCC 25923. A growth control (green bars) and antibiotic at half MBEC concentration (red bars) were employed as controls. Columns labeled with different letters represent statistically different results ($p < 0.01$) for relative effect, according to ANOVA and Tukey test for mean comparison (n = 3).
Source: Adapted from SAMANIEGO *et al.*[46]

The different effects of antibiotics plus *Tth*CDHIIa treatment on the cell viability within biofilm could be impacted by the diffusion of the antibiotics in the remaining EPS. Variables like ionic interaction of antibiotics with PNAG [87] or extra flow restriction imposed by eDNA clusters [88] make antibiotic diffusion a parameter that varies so significantly that even differences between *S. aureus* lineages (e.g., ATCC 6538 and ATCC 27217) can be observed [89]. Others have already performed enzymatic treatments in biofilms, using CDH coupled to deoxyribonuclease I [90], proteinases plus antibiotics [91] or enzymatic mixtures of trypsin, β-glucosidase, and DNase I [92], and this diversity of enzymes with effect on biofilms are proof of the heterogeneity of the biofilm structure.

A compound of interest could be considered active against preformed biofilms if the treatment causes a reduction in CV staining, metabolic activity (resazurin test) or both [52]. *Tth*CDHIIa fulfills the first requirement, making it a dispersal agent capable of significantly improving the efficacy of antibiotics against *S. aureus* biofilm cells.

To sum up the interaction of *Tth*CDHIIa with *S. aureus* bacteria, we can differentiate two states of action. The first one corresponds to the antimicrobial and biofilm inhibition activity by the production of H_2O_2 through C2 oxidation. H_2O_2 produced by *Tth*CDHIIa is not specific to *S. aureus* and theoretically could kill any bacteria at a certain concentration threshold [93]. In the second stage, the biofilm eradication capacity of our enzyme would be specific to biofilms rich in carbohydrates, like the PNAG presented in *S. aureus* ATCC 25923 [82]. We speculate that other *S. aureus* strains with more proteinaceous or PIA-independent phenotypes

might be less sensitive to our treatment [81]. Potentially our enzyme could be effective against pathogenic bacteria with cellulose biofilms like those produced by *E. coli*, *C. difficile*, *P. fluorescens* and *M. tuberculosis* [94].

Chapter 5

Conclusions

In the Part I study, the cellobiose dehydrogenase from *T. thermophilus* (*Tth*CDHIIa) was successfully expressed and characterized. The ability of *Tth*CDHIIa to produce oxidized cello and xylo-oligosaccharides; to reduce synthetic electron acceptors (DCPIP) and generate H_2O_2 from a diversity of saccharides, confirms its catalytic versatility and potential biotechnological and biomedical application. All these features are supported by the two-domain architecture and the large enzymatic pocket of the predicted 3D-closed state conformation. *In vitro* application of *Tth*CDHIIa in *S. aureus* ATCC 25923 culture evidences its antimicrobial action and inhibition of biofilm formation. In preformed biofilms, *Tth*CDHIIa is capable of oxidizing EPS carbohydrates releasing soluble saccharides, reducing the biofilm biomass; and making *S. aureus* ATCC 25923 recalcitrant cells more susceptible to antibiotics gentamicin and tetracycline. This demonstrates a possibility to apply the enzyme for *S. aureus* biofilms inhibition and eradication and to use *Tth*CDHIIa to increase sensibility of *S. aureus* cells toward existing antimicrobial treatments.

PART II :

Biochemical characterization of glucanases (cellobiohydrolases and endoglucanases)from Thermothelomyces thermophilus and its synergistic application as an antibiofilm agent

Chapter 6

Introduction

6. 1 Cellulases

Cellulases are enzymes responsible for breaking down cellulose through the hydrolysis of β-1,4-glycosidic bonds. Fungal cellulases are classified in the CAZY database into several families, including GH1,GH3, GH5, GH6, GH7,GH9, GH12, GH30, GH45 and GH48 [95,96] . Within these families, cellulases exhibit 4 main activities: endo-β-1,4-glucanase (EC 3.2.1.4), reducing end-acting cellobiohydrolase (EC 3.2.1.176), non-reducing end-acting cellobiohydrolase (EC 3.2.1.91) and β-glucosidase (EC 3.2.1.21).

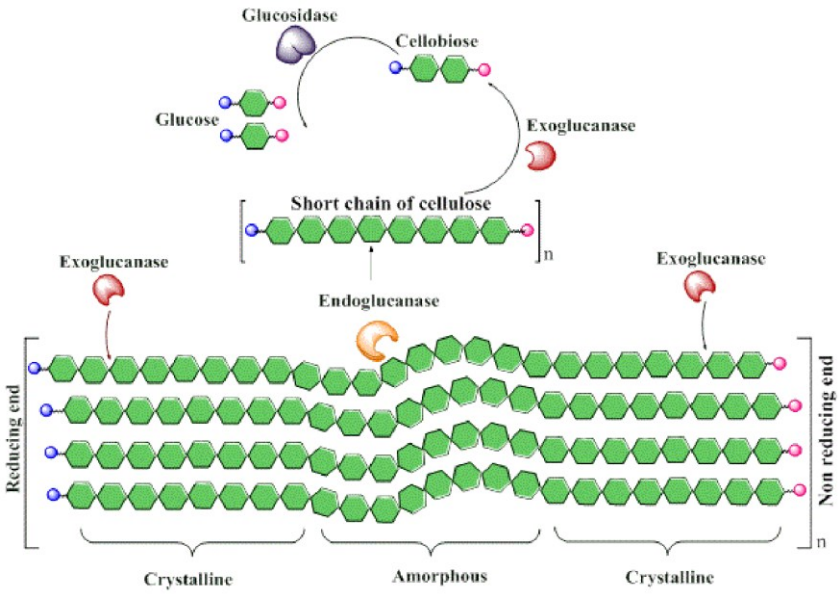

Figure 18 - Schematic representation of synergistic action of cellulase in a cellulose model.
Source: SAJITH *et al.*[95]

Cellulases operate within a synergistic system, wherein endoglucanase cleaves the amorphous region between the cellulose chains, generating fragments of cellulose and creating new ends for cellobiohydrolases to hydrolyze [95]. These cellobiohydrolases can act from either the reducing or non-reducing end of the cellulose molecules, releasing cellobiose. This product will then be further cleaved into glucose by the action of a β-glucosidase, reducing the cellobiose content and, consequently, alleviating the inhibition of the endo- and exoglucanases (Figure 18).

The GH7 family is one of the most studied cellulase, with representants from both functions, cellobiohydrolase (reducing end) and endoglucanase. These enzymes share a retaining mechanism of action that is based in two distinctive steps, where two glutamates residues are involved [97](Figure 19). In the first step (glycosylation step) a proton is transferred from the acid/base residue (Glu 217 of a GH7 from *Hypocrea jecorina*) to the glycosidic oxygen [98]. This process is accompanied by an attack at the anomeric carbon of the carbohydrate in the −1 binding site by a nucleophile (Glu 212), resulting in the formation of a glycosyl-enzyme intermediate. In the second step (deglycosylation step), an incoming water molecule attacks the anomeric carbon. This action breaks the bond between the glycosyl group and the enzyme and transfers a proton to the acid/base residue (Glu 217) [98].

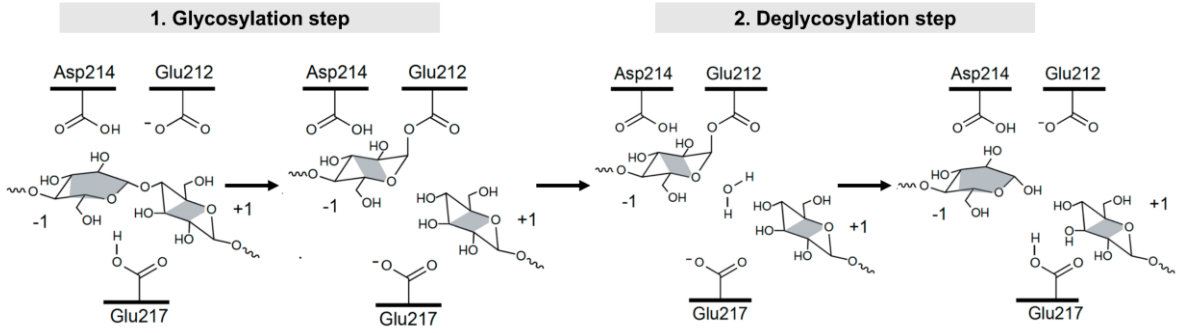

Figure 19 - Schematic representation depicting the action mechanism of GH7 cellulases.
Source: KNOTT *et al.*[98]

The difference in the mechanism of action between endoglucanase and cellobiohydrolase is determined by the arrangement of loops that extend from their core beta-sandwich structure. These loops have a notable impact on substrate recognition, the capacity to bind to crystalline cellulose, processivity, and various other enzymatic characteristics [97].

On the other hand, GH6 enzymes are less studied than the previous GH7 counterpart, but are specifically important as a synergistic enzyme, because of its ability to hydrolyze cellulose chains from the nor-reducing end. The mechanism described for this enzyme, consists of an inverting mechanism of one step, with an aspartic acid as the catalytic residue that is activated in a modified pK_a environment supplied by other surrounding aspartic acid [99].

Cellulases have broad applications in the industrial sector. One example is the bioconversion of cellulosic biomass into ethanol, organic acids, and other solvents. Other important areas of application include fermentation, industrial food production, detergents, textiles, and agriculture [100].

6.2 Bacterial cellulose

Cellulose is the most prominent biological macromolecule on Earth, with terrestrial plants being the major source [101]. However, cellulose is also found in microorganisms. Indeed, evolutionary studies suggest that the bacterial cellulose synthesis and secretion machinery (Bcs) was acquired from ancestral cyanobacteria through horizontal gene transfer [102].

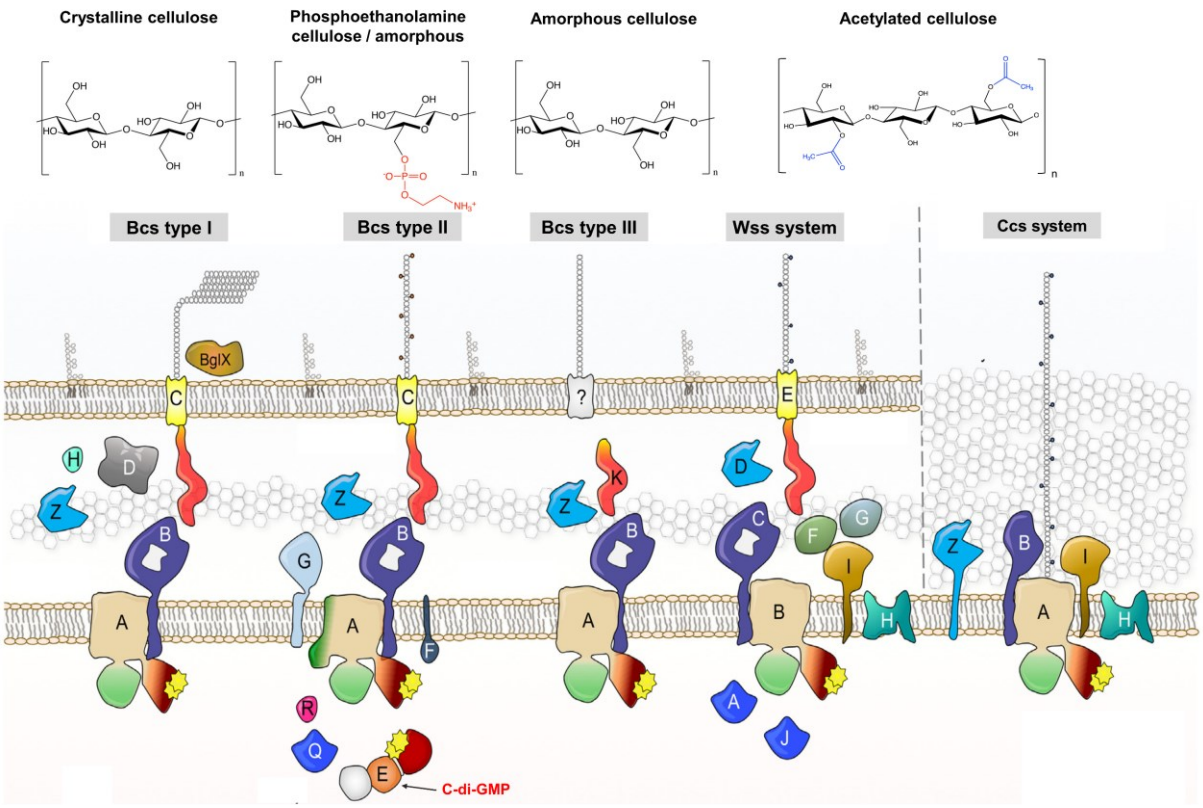

Figure 20 - Representation of the bacterial cellulose secretion systems and the cellulose chemical modifications. Source: Adapted from ABIDI *et al.*[94]

Bcs systems can be classified into different types or categories [94]. The Type I system is characterized by the secretion of cellulose with a crystalline arrangement, due to the expression of unique proteins like BcsD. This system is found in industrially relevant microorganisms such as *Gluconoacetobacter hansenii* or *G. xylinus* . The Bcs Type II system is characterized by the presence of the BcsE protein, which responds to the biofilm signal molecule, C-di-GMP, and a phosphoethanolamine transferase (BcsG). *E. coli* strains belong to this group, having important impact on pathogenic variants. The Type III system produces amorphous cellulose without any of the distinctive proteins mentioned earlier (Figure 20).

Alternative systems of cellulose secretion are described in *P. aeruginosa*, expressed through the operon Wss, which includes an acetylation protein complex. All the previous examples correspond to gram-negative bacteria. Recently, a candidate from the gram-positive group was described and denominated as Clostridial cellulose synthase (Ccs). The key glycosyltransferase CssA from the Ccs system is the only homologous protein found in the Bcs system (BcsA protein). Furthermore, Ccs produces acetylated cellulose similar to the Wss system [103](Figure 20).

Cellulose is a key component in a plethora of pathogenic biofilms. *E. coli* cellulose enhances epithelial adhesion and consequently the invasion and biofilm formation in enteric and intestinal mucosa. Cellulose alone , up to date reports, cannot induce immune response. However, by enmascaring some immunogenic determinant expressed on the surface of bacterial cells, can modulate the immunologic system for biofilm survival [104]. The presence of chemical substitutions on cellulose, like phosphoethanolamine (pEtN), has an impact on biofilm development. Specifically, the pattern of pEtN substitutions on cellulose accelerates the fibrous arrangement of curli proteins,[105] another important EPS on *E. coli* biofilm. The coproduction of these polymers has been relevant to the high adherence of *E. coli* biofilms on bladder cells under high shear conditions [106].

6.3 Fungal cellulases as treatment of cellulosic biofilms

As exposed above, cellulose biofilms are more complex than expected , especially for the discovery of chemical modifications and the characterization of new pathogenic bacteria with this EPS. A critical example is the recent study on *Mycobacterium tuberculosis*, that reveals the presence of cellulose in its biofilm, both in vitro [107] and in vivo [108]. For this reason, is important to search for new treatments that target this EPS. Fungal cellulases are a good option for their high diversity of sources and their easy production on recombinant systems.

Taking advantage of this, we produced a set of cellulases from *T. thermophilus* and applied them into cellulosic biofilms from *G. hansenii*, *E. coli* 042 and an environmental *E. coli* strain, to get insight which are the more impactful through a design mixture experiment.

Chapter 7

Objectives

7.1 Overall objectives

The overall objective of Part II is the study of a cellobiohydrolase I(Cel7A), endoglucanase (Cel7B) and a cellobiohydrolase II (Cel6A) from *T. thermophilus* with focus on their synergistic effect on degradation of cellulose-based biofilms .

7.2 Specific objectives

- Expression and purification of *Tth*Cel7A, *Tth*Cel7B and *Tth*Cel6A from *T. thermophilus* produced on an *Aspergillus nidulans* system.
- Determination of activity, substrate specificity, optimal pH and temperature, and binding kinetics measurements.
- Structural modeling of cellulases
- Bacterial cellulose production
- Optimization of cellulases mixture using a {3, 3} Simplex-Lattice design
- Assessment of biofilm eradication of *E. coli* 1 (clinical) and *E. coli* 042 (pathogenic) strains.
- Determination of minimum biofilm eradication concentration (MBEC) under optimal mixture of cellulases.
- Analysis of biofilm structure and eradication by confocal laser scanning microscopy

Chapter 8

Materials and methods

8.1 Microorganisms strain and culture conditions

Aspergillus nidulans A773 (pyrG89; wA3; pyroA4) were purchased from the Fungal Genetic Stock Center (FGSC, Manhattan, KS, USA). *Gluconacetobacter hasenii, Escherichia coli* 1 and 042, were obtained from laboratory collaborators. *A. nidulans* A773 was cultivated in a Minimum medium agar (composed of Clutterbuck salt solution: 6g/L $NaNO_3$, 0.52g/L KCl, 0.52g/L $MgSO_4$ and 1.52 g/L KH_2PO_4, and trace elements: 22 mg/L $ZnSO_4$, 11 mg/L H_3BO_3, 7.9 mg/L $MnCl_2$. $4H_2O$, 5 mg/L $FeSO_4.7H_2O$ 1.6 mg/L $CoCl_2$. $6H_2O$ 1.6 mg/L $CuSO_4$. $5H_2O$, 1.1 mg/L Na_2MoO_4 .$4H_2O$ and 50 mg/L EDTA salt) supplemented with 1% (w/v) glucose and 0.01 mg/mL pyridoxine. *E. coli* biofilm was cultivated in Tryptic soy broth (TSB) medium at 37°C in static conditions. *G. hasenii* ATCC 2376 was grown in a medium consisting of 2.5% (w/v) mannitol, 0.5% (w/v) yeast extract and 0.3% (w/v) peptone (pH 6) at 30°C for 15 days, without agitation.

8.2 Cloning

All cloned enzymes were kindly provided by the research group of Prof.Dr Fernardo Segato (University of Sao Paulo - Lorena).

From GH7 family it was cloned an endoglucanase(*Tth*Cel7B, Accession number: XP_003663441.1) and a cellobiohydrolase (*Tth*Cel7A, Accession number, XP_003660789). From GH6 family it was cloned an exoglucanase, *Tth*Cel6A (Accession number, XP_003661032).

8.3 Enzyme production and purification

Glycerinated spores from successfully transformed *A. nidulans* were inoculated in Minimum medium agar plates supplemented with 0.01 mg/mL pyridoxine and 1% glucose and incubated at 30 °C for 48 h. For recombinant protein production, the resulting mycelia was inoculated in a Minimum medium broth supplemented with 3% maltose, 1% glucose and 0.01

mg/mL pyridoxine and incubated for 2 days in static conditions at 30 °C. Then, the supernatant was recovered through filtration using a qualitative membrane (Miracloth, Millipore) followed by centrifugation at 10 000 x g for 30 min, to eliminate all cellular debris and mycelia. This solution was concentrated and buffer-exchanged (50 mM Tris-HCl pH 8) by tangential flow filtration using a 5 kDa cut-off HollowFiber cartridge (GE Healthcare Life Sciences).Then, an ion exchange chromatography in gravity flow was performed using a DEAE-Sephadex resin (Sigma) equilibrated with 50 mM Tris-HCl pH 8. The proteins of interest were eluted with a NaCl gradient (0.1, 0.2, 0.3, 0.4 and 0.5 M). All three proteins were further purified employing size exclusion chromatography in a HiLoad 16/60 Superdex 200 column (GE Healthcare, Chicago, USA) equilibrated with 20 mM Tris-HCl pH 8 and 150 mM NaCl buffer. Fractions corresponding to the proteins were pooled and concentrated. The purity of the proteins was evaluated by 12% SDS-PAGE and they were quantified using a NanoDrop 2000 Spectrophotometer (Thermo Scientific, Waltham, USA) at 280 nm (*Tth*Cel7A , theoretical mass = 54 kDa, ε = 91.8 $M^{-1}cm^{-1}$; *Tth*Cel6A, theoretical mass = 48.62 kDa, ε = 90.93 $M^{-1}cm^{-1}$; *Tth*Cel7B, theoretical mass = 46.63 kDa, ε = 83.07 $M^{-1}cm^{-1}$, as predicted by ProtParam). The enzymes were sterilized through syringe membrane filtration (0.22 μm).

8.4 Bacterial cellulose production

Bacterial cellulose (BC) was produced by *G. hasenii* ATCC 2376 in a mannitol-rich medium, as previously described[109]. The production was placed in 200 mL of medium in a 500 mL Erlenmeyer flask. After 15 days, the cellulose discs were harvested, and the attached bacteria were removed by incubating them in 100mM NaOH at 80°C for 2 hours. Subsequently, the discs were thoroughly rinsed with water until a neutral pH was achieved. Smaller discs, each with a diameter of 6mm, were manually cut using a paper punch. Finally, the BC discs were sterilized via autoclaving. Additionally, a BC suspension was prepared with a concentration of 0.36% (w/v) using a homogenizer.

8.5 Biochemical characterization and molecular modelling

8.5.1 Substrate preference, temperature, and pH response

The standard enzymatic reaction was conducted in a 100 mM buffer with 0.1 μM of cellulase and a suitable substrate at the optimal temperature, and then incubated for 30 minutes. Reducing sugars were quantified using the DNS method,[110] with one enzymatic unit (U) defined as the amount of enzyme that produces 1 μmol of reducing sugar per minute as a product. Optimal pH was determined by employing a citrate-phosphate-glycine buffer system, spanning from pH 2 to 10, while utilizing 0.5% (w/v) PASC as the substrate at 60°C. Optimal temperature was tested in a sodium acetate buffer at pH 5 with 0.5% (w/v) PASC as the substrate, over a temperature range of 20 to 80°C.

The screening of different cellulose substrates involved a mixture of 0.1 μM of cellulase, a 100 mM sodium acetate buffer at pH 5, and 0.5% (w/v) of commercial substrates (Avicel PH-101, CMC low viscosity, or PASC) or 0.2% (w/v) BC suspension, followed by incubation at 50°C for 30 minutes.

8.5.2 HPAEC-PAD analysis

The degradation of BC discs and the detection of the types of soluble sugars released were assessed using High-Performance Anion Exchange Chromatography coupled with Pulsed Amperometric Detection (HPAEC-PAD). The reaction involved a mixture of 1 μM of cellulase, a 100 mM sodium phosphate buffer at pH 6, and a BC disc in a final volume of 350 μL. This mixture was incubated at 37°C for 24 hours. Subsequently, the reaction was stopped by incubating it at 95°C for 5 minutes, and the soluble fraction was filtered through a 22 μm filter membrane before analysis. The products were analyzed with a CarboPac PA1 (2 × 250 mm) analytical column (Dionex Co., Sunnyvale, CA, USA) in a Dionex ICS 5000 system (Dionex Co., Sunnyvale, CA, USA). Both column and detector compartments were maintained at 30 °C. One microliter of the sample was injected, and solutions of 0.1 M NaOH (A) and 0.1 M NaOH with 1 M NaOAc (B) were the eluents. The flow was set to 0.3 mL min^{-1} and the gradient was as follows: from 0 to 10% B in 10 min, 10 to 30 % B in 15 min, 30 to 100 % B in 5 min, 100 % B for 8 min, 100 to 0% B in 1 min, followed by column reequilibration for 15 min.

8.5.3 Adsorption kinetic

An initial concentration of 0.5 mg/mL of cellulases or BSA (theorical mass = 66.4 kDa, ε = 43.8 $M^{-1}cm^{-1}$) were independently incubated with BC discs in a final volume of 0.2 mL at 4°C in 100 mM sodium phosphate buffer pH 6. Aliquots of 0.5 μL were collected at 0.25, 0.5,

0.75, 1, 2, 4 and 24h and quantified by 280 nm absorption using a NanoDrop 2000 Spectrophotometer (Thermo Scientific, Waltham, USA) and the theoretical mass and extinction coefficient. The adsorbed protein was represented as a percentage and plotted against time.

8.5.4 Structural modelling of cellulases

The structures of *T. thermophilus* cellulases were computationally modeled using ColabFold. To incorporate substrates into our predicted model, we utilized the crystallographic structure of cellobiohydrolase I from *Trichoderma reesei*, TrCel7A (PDB: 4C4C), as a template. Additionally, we used the structure of cellobiohydrolase II from the same organism, TrCel6A (PDB: 1QK2), and performed structural alignments with PyMOL. The identification of loops was achieved through a protein alignment with representative cellulase sequences and by following established nomenclatures [97,111].

8.6 Optimization of cellulases mixture

We simultaneously tested 3 cellulases with CBM as a cocktail to study the synergistic response to different cellulosic substrates. To achieve this, it was used a mixture design experiment, called {q, m} Simplex-Lattice design, where each component or variable is a proportion that needs to sum 1 or 100%. Three (q) components (*Tth*Cel7A, *Tth*Cel6A, *Tth*Cel7B) and four (m+1) equal espaced levels (0, 0.333, 0.667 and 1) for this especific {3, 3} Simplex-Lattice design was employed. The resulting number of experimental points is defined by $(q + m - 1)! \,/\, ((m!\,(q-1)!)\,)$, giving a total of 10 runs represented in the next table:

Table 3 - Experimental runs describing the proportion of each component.

Component 1	Component 2	Component 3
1.000	0.000	0.000
0.000	1.000	0.000
0.000	0.000	1.000
0.667	0.333	0.000
0.333	0.667	0.000
0.667	0.000	0.333

(continued)

(Continuation)

Table 4 - Experimental runs describing the proportion of each component.

Component 1	Component 2	Component 3
0.333	0.000	0.667
0.000	0.667	0.333
0.000	0.333	0.667
0.333	0.333	0.333

Source: By the author

As we are maintaining the same volume in all reactions, the use of concentration units (μM) can be added arithmetically to achieve a 100% mixture. Thus, the optimization of BC degradation by *G. hansenii* involved maintaining a total dose of 6 μM of the cellulase mixture while varying the combination ratios, as outlined in Table 3. The reaction comprised a specific enzymatic mixture, one BC disc, a 100 mM sodium phosphate buffer at pH 6, in a final volume of 100 μL. After incubating for 20 hours at 37°C, 50 μL of the supernatant containing the released reducing sugars was mixed with 50 μL of DNS and incubated at 100°C for 5 minutes. The quantification was carried out by measuring the absorbance at 540 nm and comparing it to a glucose standard curve. This experiment was conducted in triplicates (n=3).

The same approach was employed to enhance the degradation of *E. coli* biofilms, with a fixed 100% fraction of the cellulase mixture at 1.5 μM. The degradation of 24-hour-old biofilms was quantified using CV staining, as described in section 8.7. A total of forty experimental runs were conducted (n = 4).

The independent variables, *Tth*Cel7A (X1), *Tth*Cel6A (X2), and *Tth*Cel7B (X3) and the response Y1 (concentration of reducing sugars or biofilm biomass eradication) was submeted to a regression analysis using the package software MATLAB 9.12.0 (The MathWorks Inc., Natick, Massachusetts, USA) and a special cubic model shown in Eq. (3).

$$E(Y1) = \sum_{i=1}^{q} \beta_i X_i + \sum_{i=1}^{q} \sum_{i<j}^{q} \beta_{ij} X_i X_j + \sum_{k=1}^{q} \sum_{j<k}^{q} \sum_{i<j}^{q} \beta_{ijk} X_i X_j X_k \qquad (3)$$

Or a full cubic model, represented in Eq (4)

$$E(Y1) = \sum_{i=1}^{q} \beta_i X_i + \sum_{i=1}^{q} \sum_{i<j}^{q} \beta_{ij} X_i X_j + \sum_{i=1}^{q} \sum_{i<j}^{q} \delta_{ij} X_i X_j \left(X_i - X_j\right) + \sum_{k=1}^{q} \sum_{j<k}^{q} \sum_{i<j}^{q} \beta_{ijk} X_i X_j X_k \qquad (4)$$

8.7 Biofilm eradication assay

A robust clinical biofilm-forming *E. coli* strain and the pathogenic model *E. coli* 042 were utilized in the subsequent experiments. For the eradication assay, an overnight bacterial culture was adjusted to an OD_{600} of 0.05 with fresh TSB medium. Subsequently, 100 µL of this suspension was added to a 96-well plate and allowed to grow under static conditions for 24 hours at 37°C. The biofilm was then washed twice with 150 µL of 0.9% NaCl, and 100 µL of a two-fold serial dilution of the optimized cellulase mixture in TSB broth was applied. After 20 hours of incubation at 37°C, the remaining biomass of the biofilm was washed again and quantified using crystal violet (CV) staining. Briefly, 105 µL of a 0.1% (w/v) CV solution was added and agitated for 30 minutes at room temperature. Following this, the biofilm was rinsed with ultrapure water and dried before destaining with 110 µL of 70% (v/v) ethanol for 30 minutes with gentle shaking. The absorbance at 595 nm (A_{595}) was recorded and the percentage of biofilm eradication was calculated using the equation (5):

$$\%\ Biofilm\ erradication = 100 - 100\ \times (Sample_{A595} - SC_{A595})/(GC_{A595} - SC_{A595}) \quad (5),$$

where SC_{A595} and GC_{A595} correspond to the measurements of the sterility control and the growth control, respectively.

8.8 Resazurin test

The percentage of metabolically active bacteria was determined by adding 20 µL of a 0.15 mg/mL resazurin (Sigma-Aldrich, St. Louis, USA) solution to 100 µL of the resuspended cells. This mixture was incubated at 37 °C for 2 h in a 96-well black plate in static conditions and the fluorescence was measured at the excitation/emission wavelengths of 550/590 nm, respectively, in an Infinite 200M PRO microplate reader (Tecan, Hombrechtikon, Switzerland). The percentage of active cells was calculated using the equation (2):

$$\%\ Planktonic\ viable\ cells = 100\ \times (Sample_{550/590} - SC_{550/590})/(GC_{550/590} - SC_{550/590}) \quad (6),$$

where $SC_{550/590}$ and $GC_{550/590}$ correspond to the fluorescence measurement of the sterility control and the growth control, respectively. The experiments were performed in triplicate.

8.9 MCBE test and synergism with antibiotics

The minimum concentration biofilm eradication dose of multiple antibiotics was determined. 24-old biofilm was produced under the described protocol in section 8.7. Then, serial dilutions (from 34 μg/mL to 0.125 μg/mL) of chloramphenicol, tetracycline and gentamicin in TSB medium were applied into the washed biofilms and incubated for 24 hours. After that, the supernatant was discarded and the remaining biofilm , and the cells embedded in its structure, were resuspended in 100 μL of 0.9% NaCl and bath sonicated for 10 min. Then the metabolic active bacteria were quantified as described in section, using the resazurin stain. The same entire proceeding was employed for the synergistic effect of the cellulase mix (1μM). This treatment was applied simultaneously with the antibiotics at concentration below the determined MCBE. All treatments were performed in triplicates.

8.10 Biofilm cellulose extraction and Congo red staining

Biofilms were cultured employing 150 mm Petri dishes to increase adherent surfaces, and for that, we used a total of 500 mL of liquid culture medium. After 24 hours, the supernatant was collected and centrifuged at 5000 x *g* for 10 minutes. Meanwhile, the adherent biofilms were solubilized using a 1% (v/v) Triton-X100 solution and then centrifuged under the same conditions. Both resulting pellets were combined and washed with a 0.9% NaCl solution. A solution containing 30 mL of 80% (v/v) acetic acid and 3 mL of concentrated nitric acid was added to the pellet. The mixture was then incubated at 100 °C for 30 minutes in a water bath. The hydrolyzed products were centrifuged at 10,000 x g for 30 minutes. Finally, the insoluble cellulose fraction pellet was retrieved, washed with ultrapure water, and dried for further studies. Biofilm as is and after purification were stained with Congo red at a final concentration of 80 μg/mL and incubated for 2 h at 37 °C. Unspecific binding was avoided by three sequential washes with 0.9% (w/v) NaCl. A red staining was visually inspected.

8.11 Confocal laser scanning microscopy

24h-old biofilms from *E. coli* 1 and 48-old biofilms from *E. coli* 042, were growth in a 24-well plate at a final volume of 0.5 mL as described previously. The treatment involved applying either 1μM of the optimized cellulase mixture or 1μM of the least effective treatment to each

biofilm. Then, the planktonic remaining bacteria were discarded, and the biofilms were rinsed twice with 0.9 % NaCl. 500 µL of White Calcofluor solution (10 µg/mL) was applied to the biofilm and dark incubated for 15 min. Then, the excess stain was washed twice with 0.9% NaCl solution. After that, 500 µL of FilmTracer™ SYPRO® Ruby biofilm matrix stain was applied to the biofilm and incubated at room temperature protected from light for 20 min. A final wash with 0.9% NaCl solution was performed. These samples were analyzed on a fluorescence confocal microscope (Zeiss LSM 780, Oberkochen, Germany).

The White Calcofluor fluorescence was excited at 405 nm, with emission detected at 447 nm. SYPRO® Ruby was excited at 450 nm, and its emission was captured at 610 nm. Subsequently, image analysis was performed utilizing ZEISS ZEN 3.8 software (Zeiss, Oberkochen, Germany)

8.12 Powder X-ray diffraction

X-ray diffraction (XRD) data were acquired from dried and ground cellulose obtained from *G. hansenii*, *E. coli* 1, and 042. The measurements were performed using a Rigaku Miniflex 600 X-ray diffractometer operating at 40 kV and 15 mA, with Cu Kα radiation (λ = 1.5406 Å). Detection covered the 2θ range from 5 to 50°, with a step interval of 0.05° and an exposure time of 15 seconds per step. The deconvolution process was carried out using PeakFit® 4.12 software. The crystallinity index (CrI) was determined following the next equation (7):

$$CrI = \frac{A_{crystal}}{A_{total}} \times 100 \quad (7)$$

$A_{crystal}$ represents the sum of deconvoluted crystalline band areas, while A_{total} denotes the total area under the diffractogram.

Chapter 9

Results and discussion

9.1 Expression and purification of cellulases

The filamentous fungi *T. thermophilus* has a diversity of glucosyl hydrolases as revealed by previous genomic analysis [50] . It is predicted six and three members for the GH7 and GH 6 families respectively, distributed in almost all *T.thermophilus* genome, except for the chromosomes 5 and 6 [50]. We studied three candidates that encompass the most relevant features of the cellulase family. Cellobiohydrolases active on the reducing end of cellulose (*Tth*Cel7A/CBHI), an endoglucanase (*Tth*Cel7B/Egla), and a nonreducing end-acting cellobiohydrolase (*Tth*Cel6A/CBHII) were cloned and expressed in an *Aspergillus nidulans* system (Figure 21a). Remarkably, our target proteins cover all CBM-bearing GH6/GH7 cellulases (with carbohydrate binding module) of *T. thermophilus* genome. Other predicted parameters showed weight range between 46 to 54 kDa and the mostly acidic nature of these enzymes (Figure 21b).

The recombinant cellulase production on *A.nidulans* expression system was successful (Figure 21c), obtaining pure enzymes with an average yield of 8.8 mg per liter of culture. All enzymes appeared as single bands with high molecular mass compared to the prediction: *Tth*Cel7A (66 kDa), *Tth*Cel7B (58 kDa) and *Tth*Cel6A (61 kDa). Since *A.nidulans* is capable of glycosylation of secreted proteins, this extra molecular bulk shifts the expected molecular weight [112] .

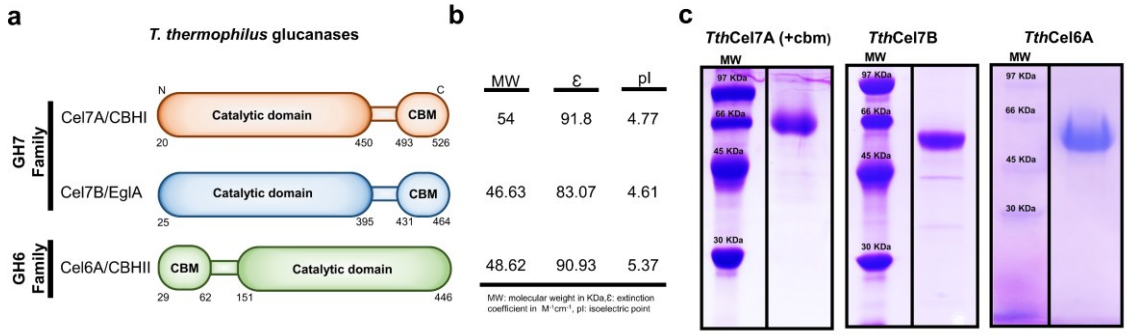

Figure 21 - Expression of cellulases from *T.thermophilus*.(a) Classification and description of cellulases following the CAZY and the CD database. (b) Molecular weight , extinction coefficient and isoelectric point predicted by ProtParam. (c) SDS-PAGE of purified cellulases.
Source: By the author

9.2 Biochemical characterization of cellulases

The studied fungal GH7 cellulases tend to have an optimal pH in the acidic range, while *Tth*Cel6A stands out with a neutral pH optimum (Figure 22a). Lowering the pH can make glycosidic bonds more susceptible to enzymatic cleavage and, the acidic residues (e.g., aspartate and glutamate) in the active site of glucanases are more likely to be protonated, which can enhance their ability to catalyze the hydrolysis of glycosidic bonds in cellulose. All glucanases exhibit a similar activity profile at high temperatures, with an optimum around 60 °C (Figure 22b). This aligns with the natural response of *T. thermophilus*, which thrives in conditions of growth set between 50-60 °C in acidic environment, and with previous works on native [111] and recombinant enzymes [113,114] produced and characterized from this organism.

A rapid kinetic binding experiment demonstrates the affinity of the cellulases for bacterial cellulose from *G. hansenii* (BC) discs (Figure 22c). *Tth*Cel7A reaches the highest bound fraction (80%), followed by *Tth*Cel6A (60%) and *Tth*Cel7B (50%). The binding is affected by the presence of the CBM domain which confers substrate binding location and specificity. CBMs from endoglucanases typically bind to amorphous or internal regions of cellulose and related polysaccharides; meanwhile the CBM from cellobiohydrolases bind to crystalline or exposed ends of cellulose chains [115] . Since BC is a polymer with high crystallinity [109], it is expected that *Tth*Cel7A exhibits the maximum value of adsorption.

Substrate preference analysis indicates that, among all cellulases, PASC is the favored substrate, except for *Tth*Cel7B, which exhibits higher efficiency in cleaving the CMC substrate. Initial trials with the BC substrate reveal that cellobiohydrolases possessing a CBM domain from the GH7/6 family demonstrate moderate activity on this particular substrate. Avicel cellulose, known for its recalcitrance, ranks as the least preferred substrate (Figure 22d). This response may be attributed to the inherent characteristics of these substrates. For instance, CMC is a water-soluble cellulose with multiple chemical substitutions (-CH2-COOH). As we will discuss in detail later, it can be hydrolyzed by enzymes with a tolerance for substituted cellulose through open and spacious pockets, resembling those found in endoglucanases. In contrast, PASC and BC substrates are insoluble, possessing a crystalline-like arrangement of cellulose chains, with BC exhibiting an even higher degree of crystallinity.

A detailed examination of BC substrate hydrolysis using the HPAEC system uncovers distinct patterns in the release of cellobiose (C2), cellotriose (C3), and glucose (C1) (Figure 22e). *Tth*Cel7A stands out by yielding the greatest proportion of C2 while completely lacking in C1 and exhibiting minimal C3 production. On the other hand, *Tth*Cel7B releases C2 to a

lesser extent along with a modest amount of C1. In contrast, *Tth*Cel6A generates significantly more C1 than C2.

The ratio of C1, C2, and C3 production has previously been proposed as a parameter for assessing the processivity of glucanases. Upon qualitative analysis of this model, it becomes evident that enzymes producing a higher proportion of C2 in comparison to C1 and C3 tend to exhibit greater processive activity, which means that successive hydrolysis of a chain of cellulose is performed without dissociation [97]. According to this definition, *Tth*Cel7A demonstrates the highest processive activity, followed by *Tth*Cel7B and *Tth*Cel6A. Notably, *Tth*Cel6A stands out for its notable production of glucose, an atypical characteristic for exoglucanases, previously observed in some endoglucanases [116]. To the best of our knowledge, this is the first time such behavior was observed in a cellobiohydrolase II enzyme.

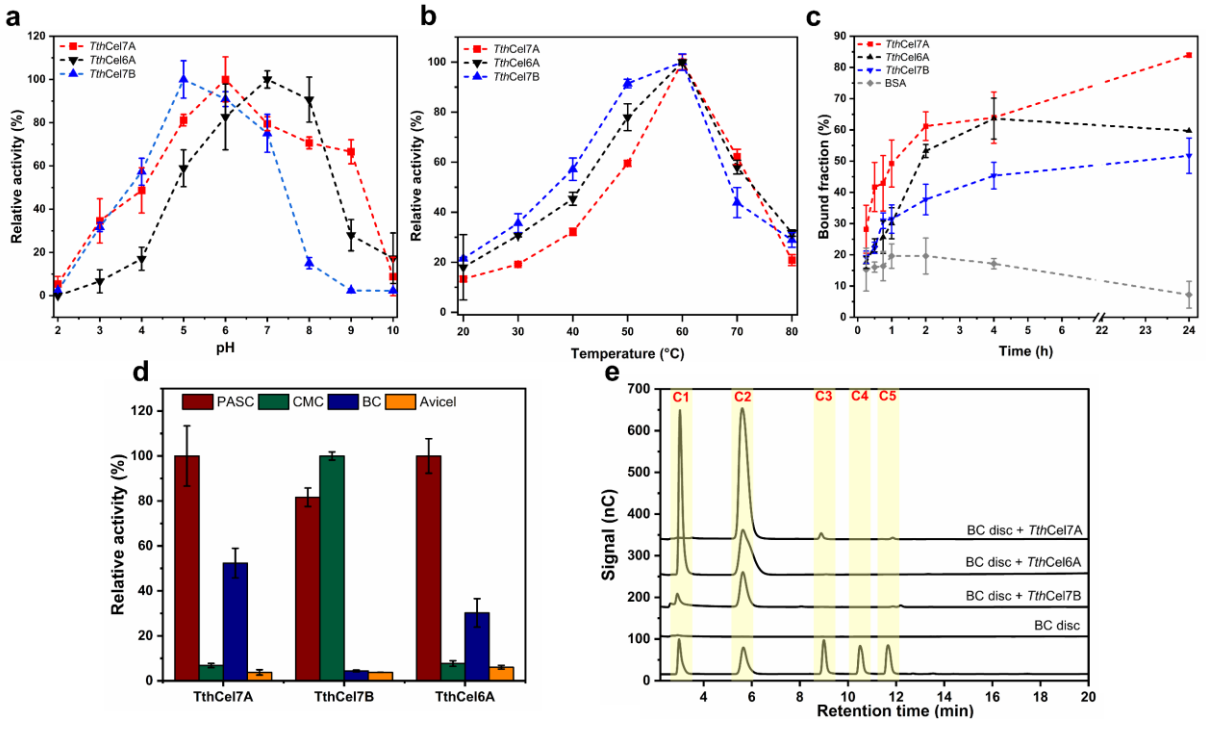

Figure 22 - Biochemical characterization of cellulases from *T. thermophilus*. Effects of pH and temperature on the enzymatic activity are demonstrated in panels (a) and (b), respectively. The binding kinetic of cellulases was evaluated on BC disc (c). Substrate preference was determined using different types of cellulosic substrates (d). Standard enzymatic reaction consisted of 100 mM sodium acetate buffer pH 5, 0.5% (w/v) PASC substrate and 0.1 µM of cellulase, incubated at 60°C for 30 min. Variation were applied for each type of characterization. For optimal pH, a citrate-phosphate-glycine buffer system was used; other commercial substrates like Avicel PH-101 and CMC low viscosity were used at 0.5% (w/v) and a suspension of BC at 0.2% (w/v). All assays were performed in triplicate (n=3) and bars refer to standard deviation. In (e), the identification of soluble products released by *T. thermophilus* cellulases is depicted. HPAEC-PAD analysis of the hydrolysis of BC discs was conducted using 1 µM of cellulase in 100 mM sodium phosphate buffer at pH 6, incubated at 37 °C for 24 hours.

Source: By the author

9.3 Structural characteristics of cellulases

The catalytic domain of the cellobiohydrolase is a mainly β-sheet class protein with Concanavalin A-like folding (Figure 23a). Some structural features like the catalytic triad Glu213/Asp215/Glu218 and Glu211/ Asp213/Glu216 are conserved among *Tth*Cel7A and *Tth*Cel7A(-cbm), respectively. Moreover, similar arrangement of loops A and B are surrounding and enclosing the substrate, as is commonly found in cellobiohydrolase tunnel-like structures. Loops A1 and B1 form the cellulose entrance; and A4 and B4, the region of product releasing [97]. Loops B3 play a role in recognition of crystalline substrate when its flexibility is confined in few conformational states,[117] with crucial interactions with loops A3 as reported in *Tr*Cel7A [118]. Previous crystallographic studies on native *Tth*Cel7A reveal a structure identical as predicted by our work using ColabFold approach [111].

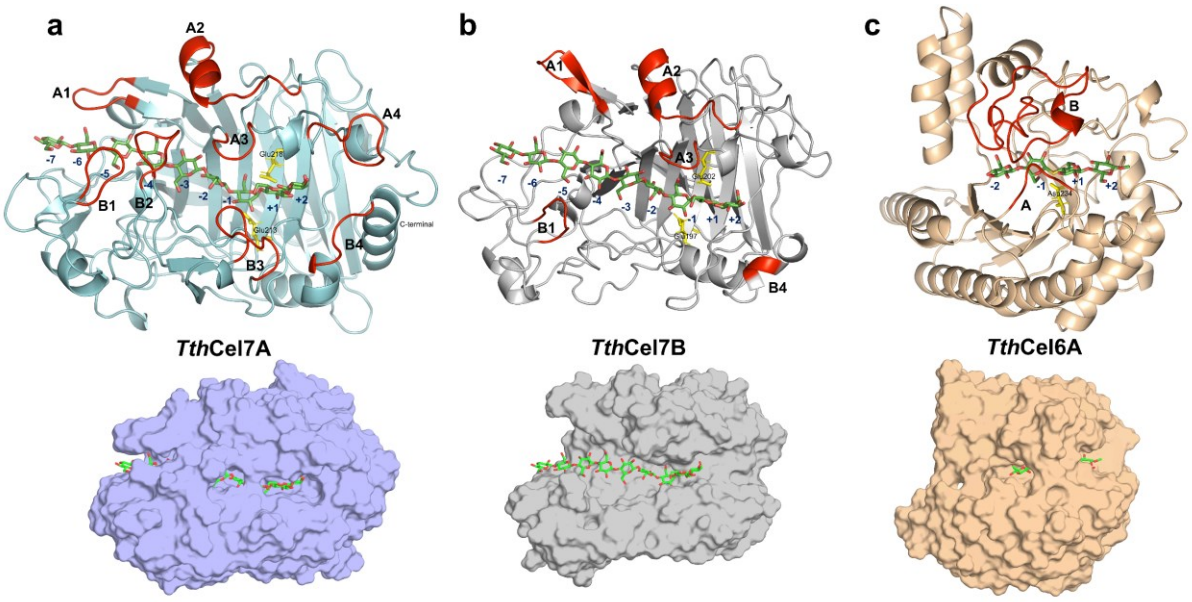

Figure 23 - Structure of *T.thermophilus* cellulases generated by ColabFold. Structure of *Tth*Cel7A (a),), *Tth*Cel7B (b) and *Tth*Cel6A (c), in cartoon representation. Loops are in colored in red and catalytic residues in yelow sticks. Substrate was docked, colored in cyan and marked following previous nomenclatures.
Source: By the author

From the side of *Tth*Cel7B endoglucanase, the central characteristic of this enzymes consists of a β-sandwich configuration, formed by the alignment of two anti-parallel β-sheets positioned in a face-to-face manner [119] (Figure 23b). This arrangement is also shared by the cellobiohydrolases. Additionally, the structure incorporates short helical segments and is predominantly composed of loop regions. These loops are arranged in a way that *Tth*Cel7B

exhibits a cleft-like substrate entrance. The catalytic triad of acidic aminoacids consist of Glu 197, Glu 199 and Asp202 , and they are located in between the region +1 and -1 , where the enzymatic cleavage will be carried out. The most noteworthy distinctions from cellobiohydrolases are the lack of loops A4, B2 and B3.

*Tth*Cel6A cellobiohydrolase structure is characterized by an architecture that is similar to an alpha/beta barrel (TIM barrel), with the distinction that the eight β-strand is replaced in the core with a long loop (loop B) that extend to the C-termini connecting the last α-helix (α8) (Figure 23c). It was proposed that a loop located between the second β-strand and third α-helix (loop A), in conjunction with loop B, are key determinants for the substrate recognition [97]. The putative catalytic residue of *Tth*Cel6A would be D234. This structure is very similar to the GH6 cellobiohydrolases from *T. reesei* [120] and *Thermochaetoides thermophila* [121].

9.4 Optimization of enzyme mixture

To investigate the synergistic effects of combining cellulases, a set of experiments was conducted using the Simplex-Lattice model. Previous works using this model [122–125] are focused on the degradation of plant biomass substrates and the enzymes loading at 100% are defined in units of mg/g of substrate. Since the experiments were carried out on cellulose samples from *G. hansenii*, *E. coli 1*, and *E. coli 042*, and the weight of substrate are incompatible to be measured , we modified these units in order to adapt the model to make it applicable to our system. For these reasons, the enzyme quantities used in these experiments were measured in μM units. Also, this unit choice allowed us to normalize the enzyme weights (in mg or μg) across different cellulases by considering the total number of molecules. All the experiments were performed at physiological temperature of 37°C for 20h and at different pH or culture mediums. Finally, the *Tth*Cel7A (-cbm) enzyme was excluded from these experiments because it exhibited a reduced capacity to bind to cellulose (BC) and showed a similar hydrolysis capability to that of its CMB-bearing counterpart when degrading bacterial biofilm.

9.4.1 Design mixture experiments for hydrolysis of BC discs.

After conducting a series of 10 experiments, in triplicates, with a 100% loading of 6 μM of cellulases, we observe values of reducing sugars range from 0.202 mg/mL to 1.577 mg/mL with specific enzyme combinations (Table 4). The data shows some symmetry in terms of

enzyme concentrations. For example, when *Tth*Cel7a and *Tth*Cel6a concentrations are swapped (2 μM and 4 μM), the reducing sugar values are very similar (1.577 mg/mL and 1.505 mg/mL) and belong to the highest product concentration. This suggests that *Tth*Cel7a and *Tth*Cel6a may have similar effects on reducing sugar production in this context.

Table 5 - The effect of the ternary cellulase mixture on the hydrolisis of *G. hansenii* BC.

TthCel7a (μM)	*Tth*Cel6a (μM)	*Tth*Cel7b (μM)	Reducing sugars (mg/mL) Observed values
6	0	0	0.520 ± 0.110
0	6	0	0.547 ± 0.082
0	0	6	0.202 ± 0.012
4	2	0	1.505 ± 0.133
2	4	0	1.577 ± 0.130
4	0	2	1.513 ± 0.169
2	0	4	1.467 ± 0.165
0	4	2	1.194 ± 0.059
0	2	4	1.130 ± 0.193
2	2	2	1.403 ± 0.176

Source: By the author

In order to get insight in a more statistical and quantitative way the analysis of our dataset, we conducted a regression analysis using a special cubic model (Table 5). This model presents the highest R-Squared (0.931, $P_{model} < 0.01$) and adjusted R-squared (0.908, $P_{model} < 0.01$) when compared to a quadratic and cubic model (data not shown).

Table 5 - Regression analysis of the special cubic model for optimizing reducing sugar production.

Factor	Coefficient	Standard error (SE)	p-Value	Model analysis
Cel7a	0.486	0.087	2.58E-05	Root Mean Squared Error: 0.155
Cel6a	0.551	0.086	4.98E-06	R-Squared: 0.931
Cel7b	0.233	0.086	0.013946	Adjusted R-Squared 0.908
Cel7a Cel6a	4.570	0.448	6.60E-09	F-statistic vs. zero model: 192
Cel7a Cel7b	5.112	0.446	1.07E-09	p-value = 1.34e-15
Cel6a Cel7b	3.466	0.399	7.52E-08	
Cel7a Cel6a Cel7b	-12.983	3.487	0.001555	

Source: By the author

The Cel7a , Cel6a and Cel7b coefficients displayed a positive effect on the production of reducing sugars. The binary combination of cellulases shows a robust synergism up to 10 times greater than when the enzymes are applied separately. A negative coefficient was observed for the term Cel7a Cel6a Cel7b, indicating an antagonistic mixture effect. It seems that the equal mixture of the three components did not increase the production of reducing

sugars as expected, despite its high production (1.403 ± 0.176 mg/mL). A plausible explanation could be cellobiose inhibition and the jamming effect. The latter causes competition for free binding sites and, consequently, crowding of cellulase molecules, leading to a decrease in the enzymatic hydrolysis rate [126].

All calculated coefficients of the factors were statistically significant ($P < 0.05$). Then, the final equation of reducing sugar production from BC in function of the amount of the cellulases is:

$$Reducing\ sugars(mg\ /\ mL) = 0.486 * \text{Cel7a} + 0.551 * \text{Cel6a} + 0.233 * \text{Cel7b} + 4.570 * \text{Cel7a} * \text{Cel6a} + 5.112 * \text{Cel7a} * \text{Cel7b} + 3.466 * \text{Cel6a} * \text{Cel7b} - 12.983 * \text{Cel7a} * \text{Cel6a} * \text{Cel7b}$$

Taking equation above and varying the amounts of *Tth*Cel7A, *Tth*Cel7B, and *Tth*Cel6A in the reaction, we generated a ternary contour diagram to visualize the production of reducing sugars (Figure 24a,b). The diagram reveals that the highest product yield (greater than 1.5 mg/mL) is in the central region between the *Tth*Cel7A and *Tth*Cel6A axes and extending towards the lower end of the *Tth*Cel7B vertex.

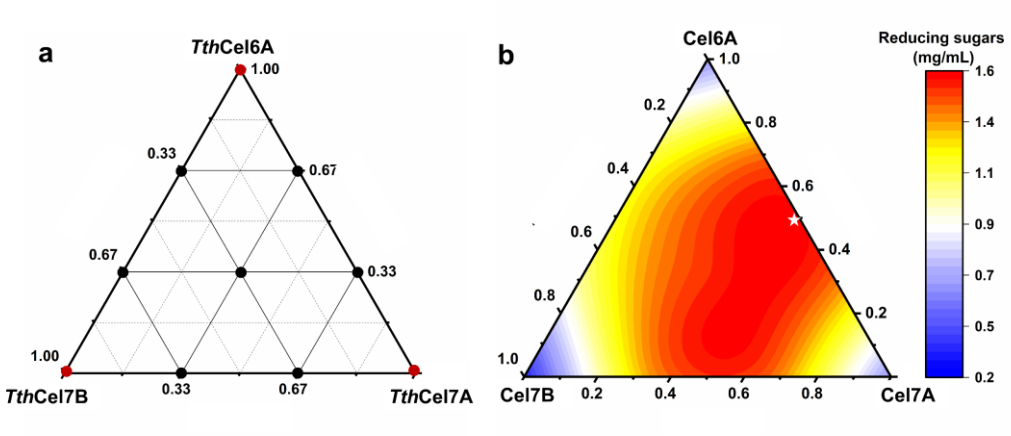

Figure 24 - Design mixture experiments for the hydrolysis of BC discs. (a) Configuration of experiment runs for a {3,3} Simplex-Lattice design.(b) Ternary contour plot of predicted reducing sugars concentration values from {3,3} Simplex-Lattice design, and the predicted optimal mixture (*Tth*Cel7A: 0.493, *Tth*Cel6A:0.507 and *Tth*Cel7B : 0.00, marked as a white star).
Source: By the author

To determine the optimal mixture of cellulases, we implemented a Python code to maximize the function response. The analysis indicated that an ideal composition consists of

49.3% *Tth*Cel7A and 50.7% *Tth*Cel6A, resulting in a predicted maximum reducing sugar yield of 1.66 mg/mL (Figure 24b). To validate this result, we used the optimized mixture in an experimental trial, and a value of 1.58 mg/mL was obtained, which is lower to the modeled data by 4.82 % of error (Figure 25a). This exo/exo synergism was previously reported using bacterial cellulose ribbons, Cel7A and Cel6a enzymes from *Humicola insolens* [127]. In this model is proposed an endo-initiated mechanism hydrolysis of *Hi*Cel6A acting on the opposite end of the cellulose chain where also a high processive Cel7A act [127]. The mode of action described is compatible with the highly successful degradation executed by our cellobiohydrolases, evidenced in the substantial thinning of the BC disc substrates.

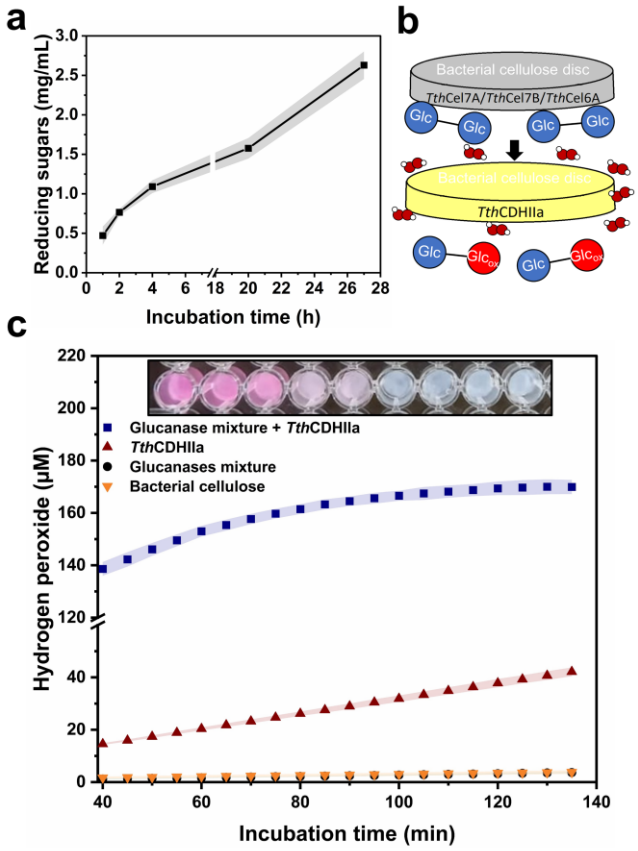

Figure 25 - Coupling of cellulases and *Tth*CDHIIa on BC Discs. (a) Production of reducing sugars over 24 hours using the optimized mixture of glucanases (3.5µM total).(b) Schematic representation of a BC disc embedded with glucanase and its coupling with another BC disc containing *Tth*CDHIIa, enabling the production of cellobionic acid and hydrogen peroxide using the previously generated C2. (c) Experimental coupling of both discs was analyzed using the Amplex Red test under semi-dry conditions. All experiments were performed in triplicate, and the shaded areas represent the standard deviation.
Source: By the author

To capitalize on the high production of reducing sugars and the cellulases' capacity to bind to the BC discs through the CBM domain, we have devised a method for generating a BC

hydrogel that continuously produces cellobiose (Figure 25b). Then *Tth*CDHIIa, which was previously studied in Part I, was immobilized onto BC discs and coupling it with our BC discs containing optimized cellulases . This approach enables us to continuously produce H_2O_2 without the need for external addition of cellobiose or glucose, achieving up to 170 μM which is higher that our previously reported quantity of 90 μM, using *Tth*CDHIIa with cellobiose (Figure 25c). Similar approaches using celluloses disc chemically synthesized have been reported [39].

9.4.2 Enzyme mixture design experiments for hydrolysis of biofilm of a pathogenic *E. coli* strain (EAEC 042)

Commensal and pathogenic *E. coli* produce biofilms with cellulosic nature [128,129]. Taking advantage of the effect of our cellulases, we used the enteroaggregative pathogenic *E. coli* 042 (EAEC) biofilm as a new target. The 100% enzyme loading was set to 1.5 μM, and a total of 40 experiments were performed (n = 4) for the 10 combinatorial conditions.

The raw data shows that *E. coli* 042 is less susceptible to our treatment with a maximum eradication percentage of 44.6% (Table 6, Figure 26a). Treatment with cellobiohydrolases *Tth*Cel7a and *Tth*Cel6a separately, produce almost no degradation on biofilm, with values of 3.1 and 2.6 % respectively.

In accordance with our methodology, we fitted our data to a full cubic model (R-Squared: 0.93, P_model < 0.01) to obtain coefficients for each factor (Table 7). The coefficients of the linear factors Cel7A and Cel6a have minimal contributions to the model and are also not statistically significant, with P-values of 0.489 and 0.738, respectively.

Table 6 - The effect of the ternary cellulase mixture on the eradication of *E. coli* 042 biofilm

*Tth*Cel7a (μM)	*Tth*Cel6a (μM)	*Tth*Cel7b (μM)	*E. coli* 042 biofilm eradication (%)
1.5	0.0	0.0	3.1 ± 3.2
0.0	1.5	0.0	2.6 ± 1.6
0.0	0.0	1.5	16.9 ± 1.6
1.0	0.5	0.0	34.6 ± 2.8
0.5	1.0	0.0	40.8 ± 4.3
1.0	0.0	0.5	29.3 ± 2.5
0.5	0.0	1.0	39.1 ± 5.1
0.0	1.0	0.5	30.5 ± 6.2
0.0	0.5	1.0	44.6 ± 3.1
0.5	0.5	0.5	31.2 ±10.0

Source: By the author

Table 7 - Regression analysis of the full cubic model for optimizing the eradication of *E. coli* 042

Factor	Coefficient	Standard error (SE)	p-Value	Model analysis
Cel7a	1.7	2.4	0.48928	Root Mean Squared Error: 4.84
Cel6a	0.8	2.4	0.73852	R-Squared: 0.93
Cel7b	16.9	2.4	2.1666e-07	Adjusted R-Squared 0.905
Cel7a Cel6a	158.3	12.2	7.2161e-13	F-statistic vs. zero model: 136
Cel7a Cel7b	112.1	10.9	1.1885e-10	p-value = 7.96e-20
Cel6a Cel7b	129.2	10.9	5.542e-12	
Cel7a Cel6a (-)	-27.0	29.3	0.3647	
Cel7a Cel7b (-)	-31.5	24.3	0.20661	
Cel6a Cel7b (-)	-59.3	24.3	0.022073	
Cel7a Cel6a Cel7b	-555.3	104.1	1.4001e-05	

Source: By the author

However, there is stronger synergism observed in the binary combinations; hence, the factor Cel7a Cel6a possesses a significant coefficient of 158.3. This behavior is also evident in the other mixtures. All coefficients associated with the δ parameters of the model, despite their highly negative values, do not make a statistically relevant contribution to the fitting. The reduced equation that describes the impact of cellulase proportions on the eradication of *E. coli* 042 biofilm is:

$$E.coli\ 042\ \text{biofilm eradication}\ (\%) = 16.9 * \text{Cel7b} + 158.3 * \text{Cel7a} * \text{Cel6a} + 112.1 * \text{Cel7a} * \text{Cel7b} + 129.2 * \text{Cel6a} * \text{Cel7b} - 555.3 * \text{Cel7a} * \text{Cel6a} * \text{Cel7b}$$

The ternary contour plot reveals a region with higher eradication (>36.1%) concentrated in the Cel7B and Cel6A axes (Figure 26b). The specific combination of cellulases that maximizes the degradation of *E. coli* 042 biofilm, achieving up to 41.3% (predicted), consists of 0% *Tth*Cel7A, 56.5% *Tth*Cel7B, and 43.5% *Tth*Cel6A. In a dose-response experiment using this newly optimized mixture, it is found that the half-maximal effective concentration (EC_{50}) is approximately 0.63 μM (Figure 26c). When employing the same concentration as used in the mixture design experiment (1.5 μM), a biofilm biomass growth of 54.1% or a 45.9% level of eradication is observed. This experimental value is 11.1% higher than the predicted value, which is in close agreement with our adjusted R-squared for the model (0.905). Furthermore, at higher concentrations of this *Tth*Cel7B/*Tth*Cel6A synergistic mixture (6μM), the biofilm did not exhibit any further degradation, retaining approximately 46.5% of its biomass (equivalent to 53.5% eradication).

To better comprehend the impact of our cellulases on the structure of *E. coli* 042 biofilm, we conducted a confocal laser scanning microscopy (CLSM) experiment (Fig. 26d). Upon initial examination of the growth control, it became evident that the biofilm matrix is highly heterogeneous. There were isolated regions where carbohydrates and proteins were co-localized, but the micrographs also revealed numerous structures consisting solely of a protein matrix.

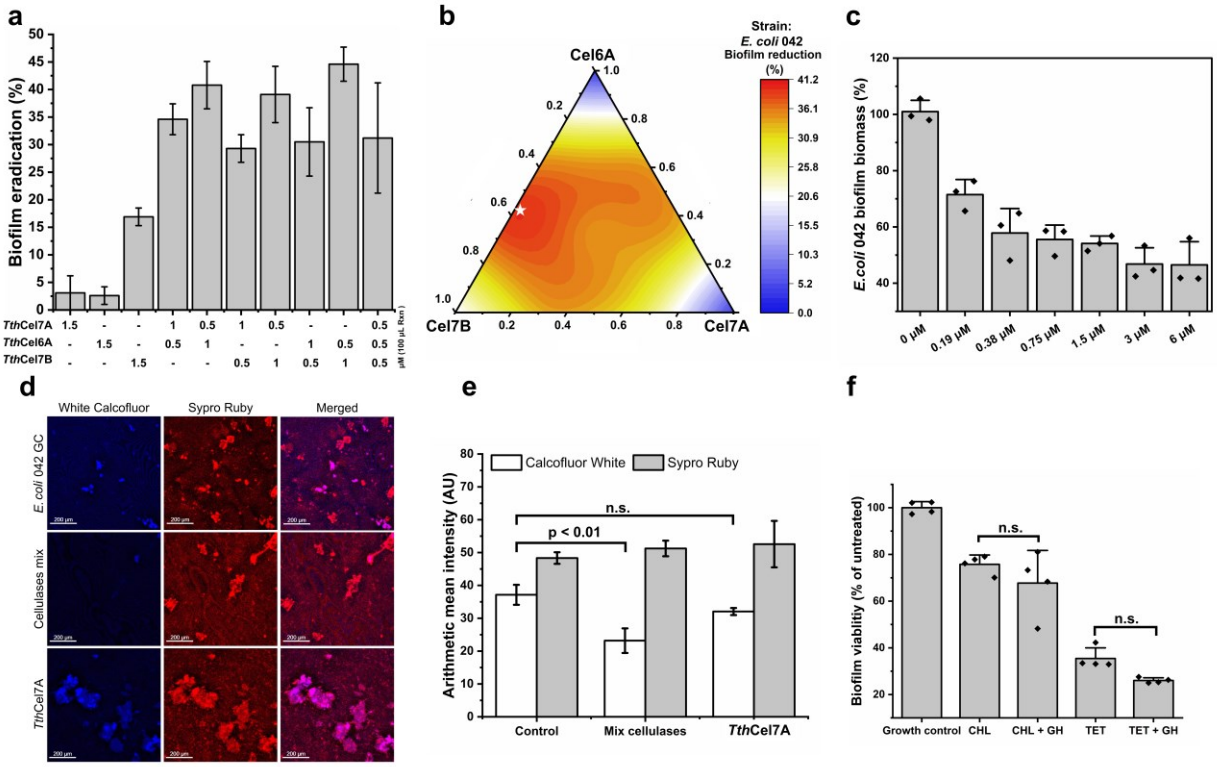

Figure 26 - Design mixture experiments for the hydrolysis of a pathogenic *E. coli* 042 biofilm. (a) The effect of the ternary cellulase mixture on the degradation of *E. coli 042* biofilm upon incubation at 37°C for 20h (b) Ternary contour plot of predicted biofilm eradication values from a {3,3} Simplex-Lattice design, with the optimal response located at *Tth*Cel7B: 0.565 and *Tth*Cel6A: 0.435.(c) Dose-response experiment using a log2 dilution of the optimized cellulase. The experiments were conducted using 24-hour-old biofilms, where cellulases were applied after dilution in fresh TSB medium for 20 hours at 37 °C. Biofilm biomass determination was achieved through CV staining. Each experiment was replicated three times (n=3). (d) CLSM analysis of *E. coli* 042 biofilm under treatment with the optimized cellulase mixture (1 µM) and the least effective treatment, *Tth*Cel7A (1 µM). The protein matrix is visualized in red, while carbohydrates appear in blue following staining with SYPRO Ruby and Calcofluor White, respectively. (e) Analysis of the arithmetic mean intensity of representative micrographs (n=4). (f) Biofilm viability test of *E. coli* 042 biofilms co-treated with cellulases and chloramphenicol (CHL) or tetracycline (TET). Bars represent the standard deviation.

Source: By the author

In contrast, the application of 1 µM of optimized treatment clearly exhibited degradation of the carbohydrate polymers while leaving the protein matrix unaffected. Consequently, the protein matrix not only proved to be an abundant structure in *E. coli* 042 biofilm, but also

exhibited remarkable stability, showing minimal interaction with the carbohydrate matrix. This observation elucidates why our treatment achieved only a 53.5% level of hydrolysis, as the remaining portion is mainly attributed to the protein structure or possibly other EPS. The treatment with 1 μM *Tth*Cel7A exhibited no hydrolysis, as confirmed by the CV-staining test, which showed only a 3.1% eradication rate. Due to the high heterogeneity of this biofilm, visual analysis presented difficulties. Therefore, we recorded the mean intensity of fluorescence for each channel (Fig. 4e). We found a significant difference ($p < 0.01$) between the growth control (37.1 a.u.) and the optimized cellulase treatment (23.1 a.u.), but no significant difference for the *Tth*Cel7A treatment (32 a.u.). Although the intensities on the Calcofluor White and SYPRO Ruby channels in the growth control were not significantly different, a noticeable trend towards a more proteinaceous biofilm was observed. All these characteristics are reflected in the absence of synergism of the cellulase mixture with antibiotics (chloramphenicol and tetracycline) in the reduction of biofilm viability (Fig. 26f).

9.4.2 Enzyme mixture design experiments for hydrolysis of a clinical *E. coli* biofilm (*E. coli 1*)

We applied the previous approach for degradation of stablished biofilms of a non-multi-drug resistance clinical *E. coli* strain denominated here as *E. coli* 1.

From the raw data we can see the effectiveness of the enzyme combinations at eradicating *E. coli* 1 biofilms (Table 8). The percentages range from approximately 76.1% to 94.1% degradation. It appears that higher concentrations of *Tth*Cel7b (1.5 μM) tend to result in higher biofilm eradication percentages. The presence of *Tth*Cel7a and *Tth*Cel6a also contributes to biofilm eradication, but their individual effects are less clear, as the percentages vary across different combinations.

The non-linear regression, using a full-cubic model, presents good R-squared (0.975, $P_{model} < 0.01$) and adjusted R-squared (0.967, $P_{model} < 0.01$) (Table 9). The linear coefficients show the high effect of the cellulases when applied individually, with Cel7B (92.9) being the maximum, followed by Cel7A (84.2) and Cel6A (76.1). In all binary mixtures, a synergistic effect is observed, with all coefficients being positive. The δ parameters are statistically significant ($P < 0.05$) and have values that contribute to the fitting of the model. Additionally, we found a strong negative interaction of the three cellulases (-124.4 coefficient) with this type of substrate.

Table 8 - The effect of the ternary cellulase mixture on the eradication of *E. coli* 1 biofilm

*Tth*Cel7a (μM)	*Tth*Cel6a (μM)	*Tth*Cel7b (μM)	*E. coli* 1 biofilm eradication (%)
1.5	0.0	0.0	84.2 ± 1.7
0.0	1.5	0.0	76.1 ± 0.7
0.0	0.0	1.5	92.9 ± 0.3
1.0	0.5	0.0	89.8 ± 0.8
0.5	1.0	0.0	89.3 ± 0.5
1.0	0.0	0.5	94.1 ± 0.5
0.5	0.0	1.0	92.7 ± 0.6
0.0	1.0	0.5	90.7 ± 0.4
0.0	0.5	1.0	90.4 ± 0.8
0.5	0.5	0.5	89.8 ± 0.8

Source: By the author

Table 9 - Regression analysis of the full cubic model for optimizing the eradication of *E. coli* 1 biofilm.

Factor	Coefficient	Standard error (SE)	p-Value	Model analysis
E. coli 1				
Cel7a	84.2	0.4	3.6717e-47	Root Mean Squared Error: 0.93
Cel6a	76.1	0.4	7.6038e-46	R-Squared: 0.975
Cel7b	92.9	0.4	1.96e-48	Adjusted R-Squared 0.967
Cel7a Cel6a	42.1	2.0	5.8752e-19	F-statistic vs. zero model: 3.68e+04
Cel7a Cel7b	21.6	2.0	2.1799e-11	p-value = 1.83e-58
Cel6a Cel7b	27.2	2.0	7.3288e-14	
Cel7a Cel6a (-)	-14.9	4.7	0.0033411	
Cel7a Cel7b (-)	28.9	4.7	8.5115e-07	
Cel6a Cel7b (-)	39.6	4.7	1.8882e-09	
Cel7a Cel6a Cel7b	-124.4	15.2	3.8869e-09	

Source: By the author

The following is the final equation derived from the model above:

$$E.coli\ 1\ biofilm\ erradication = 84.2 * Cel7a + 76.1 * Cel6a + 92.9 * Cel7b + 42.1 * Cel7a * Cel6a + 21.6 * Cel7a * Cel7b + 27.2 * Cel6a * Cel7b - 14.9 * Cel7a * Cel6a * (Cel7a - Cel6a) + 28.9 * Cel7a * Cel7b * (Cel7a - Cel7b) + 39.6 * Cel6a * Cel7b * (Cel6a - Cel7b) - 124.4 * Cel7a * Cel6a * Cel7b$$

Using the described approach, we created a ternary contour plot based on this equation. Visually, we observed a shift in the proportion of cellulases leading to significant biofilm degradation (Figure 27a). There is a distinct region with a high percentage of degradation situated close to the midpoint between the Cel7B and Cel7A axes, and at the lower end of the Cel6A vertex, where degradation exceeds 91.7%. The cellulase proportions that maximize the

output of the model (predicted 94.3 % of eradication) were found to be 59.6% for *Tth*Cel7A, 40.4% for *Tth*Cel7B, and 0% for *Tth*Cel6A.

The over-night incubation of the optimized mixture diluted on fresh TSB medium and applied to a 24h-old biofilm of *E. coli* 1, showed a dose-dependent activity, with an EC_{50} of approximately 0.086 µM (Figure 27b). It is worth emphasizing that increasing the concentration beyond 2 µM did not result in complete degradation of the biofilm biomass. At treatment concentrations ranging from 1 to 2 µM, which is close to the concentration used in the mixture design experiment (1.5 µM), we observe a biofilm biomass of approximately 16%. In other words, there is an 84% degradation, which is 10.6% lower than the predicted eradication value.

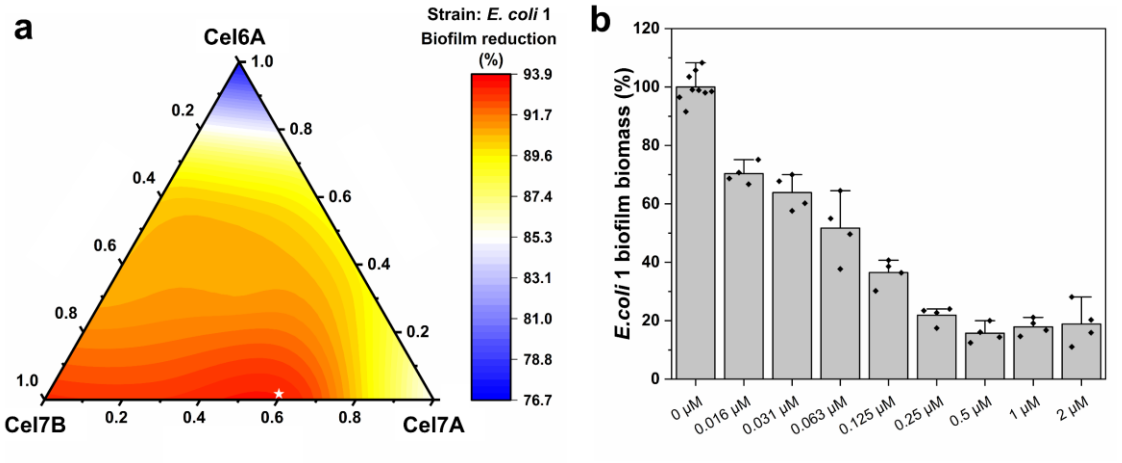

Figure 27 - Design mixture experiments for the hydrolysis of a clinical *E. coli* biofilm. (a) Ternary contour plot of predicted biofilm eradication values from a {3,3} Simplex-Lattice design, with the predicted optimal mixture (*Tth*Cel7A: 0.596 and *Tth*Cel7B: 0.404, marked as a white star). (b) Dose response experiment using a log2-dilution of the optimized cellulase mixture. All of experiments were performed on 24-old biofilms and applying *T.thermophilus* cellulases diluted in fresh TSB medium for 20h at 37°C. The test employed for determination of biofilm biomass was CV-stainng. Experiments were performed in quadruplicates (n=4) , excepts for the control, and the bars represent the standard deviation.
Source: By the author

To complement our eradication essay, which is based on CV staining commonly used as a screening test, we conducted a CLSM experiment. In this test, Calcofluor White fluorescent dye was used to label carbohydrate polymers, including cellulose, and SyproRuby was used for protein staining. The 3D volume images reveal that the 24-hour-old *E. coli* 1 biofilm, without any treatment, exhibits a robust and heterogeneous structure of carbohydrate and protein matrix (Figure 28). This colocalization is clearly evident in the merged micrograph channels. The

thickness of the biofilm is about 235 μm, considering the highest point of the z-stack measurements.

When treated with the optimized cellulase mixture, a significant reduction in the carbohydrate signal is achieved. Surprisingly, the protein matrix signal is also slightly diminished, possibly due to a strong interaction between these two types of biofilm matrix components. Even when applying the least effective cellulase, *Tth*Cel6A, the biofilm is still degraded, reducing the thickness to 138 μm while maintaining the heterogeneity observed in the control experiment. This result is consistent with the previously conducted CV staining, which achieved a 76.1% eradication rate.

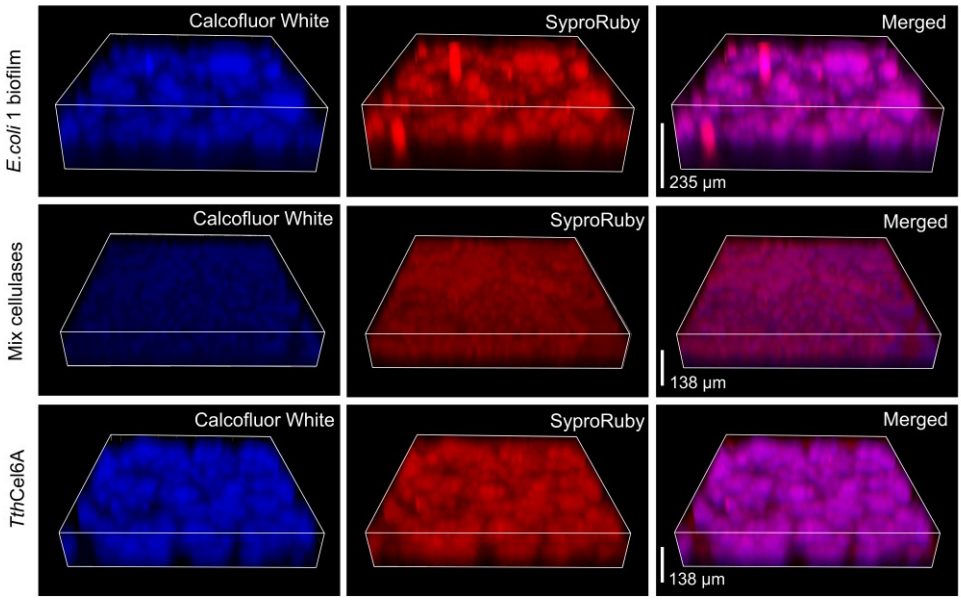

Figure 28 - Confocal laser scanning microscopy (CLSM) analysis of *E. coli* 1 biofilm. Untreated biofilms used as controls. The effect of the optimized mixture of cellulases (1μM) and *Tth*Cel6A(1μM) on the biofilm architecture is illustrated. Protein matrix in red and carbohydrate in blue after staining with SyproRuby and Calcofluor White, respectively.
Source: By the author

Also, to demonstrate the effectiveness of our cellulase mixture in degrading the carbohydrate component of the *E. coli* 1 biofilm, we conducted a synergism experiment using three different antibiotics. The MBEC values for tetracycline, gentamicin, and chloramphenicol were concentrations above 4, 4, and 8 μg/mL, respectively. In all cases, at very little concentration of antibiotics, it is exhibited greater efficacy in reducing biofilm viability when incubated with the cellulases (Figure 29). It's important to note that our resazurin test calculates relative viability rather than absolute viability, which allows for a higher number of parallel experiments. Additionally, the specificity of the test can measure metabolically active bacteria

that cannot be cultured, which explains why, with both treatments, we did not achieve a 0% biofilm viability. Furthermore, recalcitrant cells may still be embedded in the remaining biofilm after cellulase treatment.

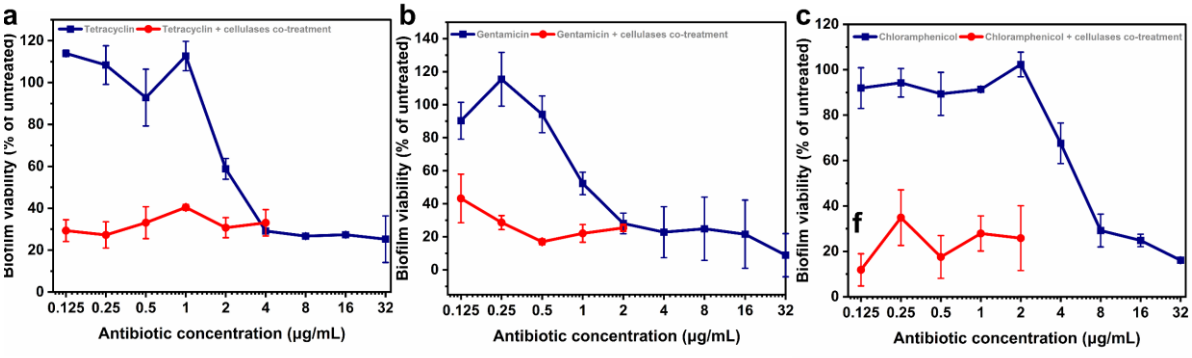

Figure 29 - Cellulase cotreatment effect with different antibiotics. Tetracycline (a), gentamicin (b) and chloramphenicol (c) antibiotics used at concentrations between 0.125 and 32 µg/mL (blue line) and in cotreatment with 1µM of optimized cellulase (red line). All measurement were performed with the resazurin test in triplicates (n=3) and bars represent standard deviation.
Source: By the author

9.5 Biofilm characterization

The switch to the optimal mixture of *T. thermophilus* cellulases against the described cellulosic structures demonstrates a common use of endoglucanase in both *E. coli* 1 and 042 strain eradication tests. This indicates the prevalence of an amorphous cellulosic structure in biofilms. As previously mentioned, the *E. coli* cellulose secretion system (Bcs type II) produces pEtN cellulose, which is naturally amorphous [130].

To experimentally demonstrate this, we isolated the cellulose fraction from the studied biofilms. A preliminary Congo red stain indicated the presence of carbohydrates both before and after acidic purification, with a relatively higher concentration in the *E. coli* 1 biofilm (Figure 30a). The dried, purified cellulose was subjected to X-ray powder diffraction (XRD) analysis, which also included dried and ground BC and carboxymethyl cellulose (CMC) (Figure 30b). The cellulose from *G. hansenii* displayed an XRD pattern with two major peaks at approximately 22.47° and 14.41° 2θ angles, corresponding to the previously reported cellulose profile [109] (Figure 30b). In contrast, both *E. coli* biofilms exhibited broad peaks spanning angles around 18° and 24°, indicative of an amorphous structure. Surprisingly, both patterns have a high resemblance with the CMC diffractogram.

We conducted a deconvolution analysis of the data to separate the peaks in the X-ray diffractograms. This approach allowed us to determine the crystallinity index (CrI) for each isolated cellulose (Figure 30b). It confirmed that the CrI for *G. hansenii* cellulose was higher at 72% compared to *E. coli* biofilms and CMC. A slight difference in CrI was observed between the cellulose from clinical *E. coli* 1 biofilm (53.27%) , the pathogenic model *E. coli* 042 biofilm (49.86%) and CMC substrate (46.12%), with the latter being the more amorphous substrate. The explanation for this difference could be the existence of more chemical substitutions in the cellulose structure (carboxymethyl and pEtN groups), hindering its packing into an ordered cellulose polymer.

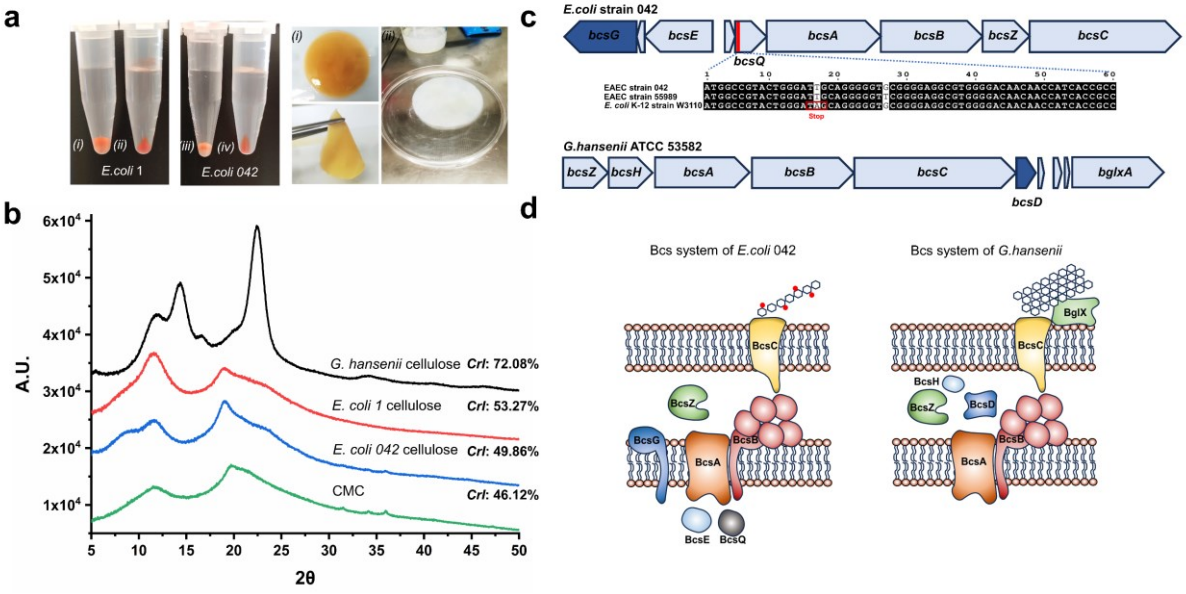

Figure 30 - Characterization of cellulose from bacterial biofilms. (a) Congo red staining of *E. coli* 042 and 1, before (i,iii) and after (ii, iv) cellulose extraction; and *G. hansenii* production of cellulose biofilm before (i) and after (ii) the treatment with 0.1 M NaOH (right panel). (b) XDR pattern obtained from the cellulose purified from *G. hansenii*, *E. coli* 1 and 042 and carboxymethyl cellulose (CMC). (c) Bcs operon arrangement of *E. coli* 042 (accession: PRJEA40647) and *G. hansenii* (PRJEB10804), with distinctive genes highlighted in blue. Alignment of the 5' flanking region (highlighted in red) of *E. coli* 042 *bcsQ* gene with *E. coli* strain 55989 (PRJNA33413) and *E. coli* K-12 (PRJNA16351). (d) Diagram illustrating the organization of proteins involved in cellulose secretion in *E. coli* 042 and *G. hansenii* based on previous works.[94,133]

Source: By the author

From the reported genomic data of *E. coli* 042 [131] and *G. hansenii* [132], we analyzed and illustrated the bacterial cellulose operon of both models (Figure 30c,d). BcsG in *E. coli* is fundamental for the addition of pEtN on cellulose chain, and BcsQ is a key cytoplasmatic factor [94,133]. Previous studies showed that a premature termination codon mutation on bcsQ results in *E. coli* strains lacking the capacity for cellulose synthesis, such as *E. coli* K-12 [134]. On the contrary, the absence of this mutation leads to the formation of robust cellulosic biofilms, like

those produced by *E. coli* strain 55989 [134] and the *E. coli* 042 reported here, which possesses an intact bcsQ gene (Figure 30c). *G. hansenni* have up to three operons for cellulose synthesis [132]. Graphically illustrated is operon I, emphasizing BcsD, the factor responsible for crystalline arrangement of cellulose fibrils [94,133](Figure 30c).

Simplex lattice design experiments using cellulases have been reported for optimizing biomass hydrolysis [122–125]. Here, for the first time, individual recombinant glucanases were used under this model to optimize the hydrolysis of non-canonical substrates. The results on optimizing the hydrolysis of BC , strictly a type of bacterial biofilm, reveal and exo/exo synergism as described before [127]. The hydrolysis of *E. coli* biofilms switches to exo/endo synergistic action of glucanases. However, there are differences between the *E. coli* 1 and 042 patterns of degradation, showing the diversity of the biofilm response. *E. coli* 1 is more susceptible to our optimized treatment with a 6-fold lower EC_{50} compared to *E. coli* 042. The cellulase and antimicrobial co-treatment reveals the difficulty in treating a strain with multiple antibiotic resistance like *E. coli* 042, which has genes encoding resistance to chloramphenicol, tetracycline, streptomycin, spectinomycin and sulfonamide [131].

The treatment of *E. coli* biofilms with cellulases has been previously reported, with variations in growth conditions and enzymatic application. For instance, the enteropathogenic *E. coli* O157:H7 biofilm, grown in BHI medium for 24 hours, was exposed to 20 mg/mL of a commercial cellulase from *Trichoderma viridae* (Cellulase R-10) for 1 hour in a 10-fold diluted medium, resulting in a degradation of 29.3% [135]. In contrast to these findings, we achieved a 50% degradation of established biofilms from *E. coli* 1 and *E. coli* 042, using 3.2 μg/mL and 18 μg/mL of cellulases (expressed previously in μM units), respectively. It is important to highlight that we conducted a 20-hour enzyme incubation under the same culture conditions, using TSB as the dilution medium. This approach helped us avoid suboptimal growth conditions, which are more likely to render biofilms more vulnerable to treatments.

Another study showed the treatment of a uropathogenic *E. coli* strain 536 with an unknown commercial cellulase (13.8 U/mL) resulted in a reduction of the aggregative index by up to 75%. In this case, a 3-hour incubation was performed on an aggregative model, which is a variant of the biofilm model, using the culture medium RPMI 1640 [136]. Isolated cellulose from a mutant *E. coli* MG1655 was degraded with a *T. reesei* cocktail (5 mg/mL) during a 16-hour incubation to confirm the polysaccharide nature of the biofilm, by another research group[137].

Cellulases were already employed to degrade different cellulosic biofilms, such as those found in *Mycobacterium bovis* bacille Calmette-Guérin, resulting in a degradation rate of 70.6% when using 1.024 mg/mL of an unidentified cellulase [138]. Studies conducted on *M. tuberculosis*

biofilms revealed the efficacy of treating infected human lung tissue with a 5 mg/mL *T. viridae* cellulose cocktail. Additionally, nebulization with 30 U (less than 3 mg) of the same cocktail in a mice model demonstrated a reduction in cellulose signals in a CLSM experiment, consequently reducing the lung area involved in the pathology [108].

The identical cocktail and concentration were also employed to treat *Mycobacterium intracellulare* biofilms associated with catheter implants in a mice model [139]. A comprehensive study involving 12 different biofilms treated with various enzymes indicated that *Enterobacter cancerogenus* was the only biofilm eradicated, at approximately 50%, following the application of 1 mg/mL of the *T. viridae* cellulase cocktail[140].

Additional examples are provided for various biofilms, including *B. cereus* biofilm [141], mono- and dual-species biofilms of *P. aeruginosa* [142], *S. aureus* biofilms in a wound model [143,144], *Salmonella* variants [145,146], and *Enterococcus faecalis* [147].

From all the cited works, it is evident that a high concentration (ranging from 1 to 30 mg/mL) of various cocktails of fungal cellulases from different strains, such as *T. viridiidae* (marketed as Cellulase R-10)[108,135,139,140,146], *T. reesei* (marketed as Celluclast)[137,147–149], and *A. niger* [142–144], has been used for biofilm eradication. These mixtures are primarily formulated for the hydrolysis of plant cellulose and typically consist of cellobiohydrolases, endoglucanases, and glucosidases in varying proportions. In fact, an analysis of the Celluclast cocktail reveals a predominant composition of hemicellulases (40%), followed by cellulases (30%) [125].

Chapter 10

Conclusions

In Part II of this study, cellulases from *T. thermophilus* were successfully produced and subjected to biochemical characterization, revealing general features such as their optimal activity at an acidic pH and high temperature for hydrolysis. Additionally, the utilization of substrates in terms of catalytic hydrolysis and binding is described and linked to their three-dimensional predicted structure.

The implementation of a simplex design mixture model has provided a robust method for optimizing the proportion of our cellulases capable of hydrolyzing different bacterial cellulose biofilms. Despite the differing responses of both *E. coli* samples toward the same set of enzymes, endoglucanase *Tth*Cel7B is proposed here as a key enzyme for the eradication of cellulosic biofilms. Since this EPS is highly amorphous and possesses crystalline properties close to CMC (Figure 30b), we propose this last substrate as a model that mimics the cellulosic biofilm. Indeed, TthCel7B exhibits high CMCase activity (Figure 22d), making CMC a good starting point for screening new biofilm eradicators. Further studies on new endoglucanases as potential biofilm treatment could be found in the same Bcs operon, where genes like BcsZ (Figure 30c,d) produce GH8 endoglucanases highly active on CMC [150]. Searching for enzymes with tolerance to other chemical modifications like acetylation would expand specific treatment options against Pseudomonal and Clostridial targets.

PART III

General conclusions and perspectives

The present study introduces four new antibiofilm agents derived from the enzymatic machinery of the fungal microorganism *T. thermophilus*. These carbohydrate-active enzymes (CAZymes) encompass two primary approaches for hydrolyzing or modifying cellulosic substrates: the redox and bond breakage methods. Cellobiohydrolase (*Tth*CDHIIa) exhibits broad substrate recognition, enabling the oxidation of various mono- and oligosaccharides while generating H_2O_2. These versatile characteristics positioned *Tth*CDHIIa as a potential candidate for antimicrobial and antibiofilm applications, including both eradication and inhibition of *S. aureus* biofilm.

On the other hand, selecting the appropriate cellulase through a mixture designed experiment enhances the biofilm hydrolysis rate. *Tth*Cel7B is proposed as a key enzyme targeting chemically modified cellulose in *E. coli* biofilms, while *Tth*Cel7A is well-suited for degrading crystalline biofilms, such as those produced by *G. hansenii* (BC). The action of *Tth*Cel7A generates cellobiose, which was integrated into a BC disc embedded with *Tth*CDHIIa, enabling continuous H_2O_2 production.

The quest for new treatments against pathogenic biofilms is of utmost urgency, especially since recent reports have described life-threatening infections associated with the production of robust cellulose-based biofilms[107,108]. Despite previous use of cellulases in research, there is no documented implementation of specific enzymatic cocktails to address this health issue, as many of these cocktails are primarily designed for biomass treatment.

Future endeavors include the characterization of bacterial CAZymes, including enzymes encoded by biofilm-forming microorganisms in their auto-dispersal late phase. Additionally, exploring other sources such as phages, which naturally target bacteria and potentially degrade biofilms, is essential. Moreover, a more detailed characterization of the polysaccharide structure and distribution within biofilm EPS represents a challenging yet impactful next step.

REFERENCES

1 HARREITHER, W. *et al*. Catalytic properties and classification of cellobiose dehydrogenases from ascomycetes. **Applied and Environmental Microbiology**, v. 77, n. 5, p. 1804–1815, 2011. DOI:10.1128/AEM.02052-10.

2 CAMERON, M. D.; AUST, S. D. Cellobiose dehydrogenase–an extracellular fungal flavocytochrome. **Enzyme and Microbial Technology**, v. 28, n. 2–3, p. 129–138, 2001. DOI:10.1016/S0141-0229(00)00307-0.

3 SCHEIBLBRANDNER, S.; LUDWIG, R. Cellobiose dehydrogenase: bioelectrochemical insights and applications. **Bioelectrochemistry**, v. 131, p. 107345, 2020. DOI: 10.1016/j.bioelechem.2019.107345.

4 HALLBERG, B. M. *et al*. Crystal structure of the flavoprotein domain of the extracellular flavocytochrome cellobiose dehydrogenase. **Journal of Molecular Biology**, v. 315, n. 3, p. 421–434, 2002. DOI:10.1006/jmbi.2001.5246.

5 TAN, T. C. *et al*. Structural basis for cellobiose dehydrogenase action during oxidative cellulose degradation. **Nature Communications**, v. 6, n. 1, p. 7542, 2015. DOI:10.1038/ncomms8542.

6 COURTADE, G. *et al*. Interactions of a fungal lytic polysaccharide monooxygenase with β-glucan substrates and cellobiose dehydrogenase. **Proceedings of the National Academy of Sciences**, v. 113, n. 21, p. 5922–5927, 2016. DOI:10.1073/pnas.1602566113.

7 KADEK, A. *et al*. Interdomain electron transfer in cellobiose dehydrogenase is governed by surface electrostatics. **Biochimica et Biophysica Acta (BBA)** - general subjects, v. 1861, n. 2, p. 157–167, 2017. DOI: 10.1016/j.bbagen.2016.11.016.

8 LAURENT, C. V. F. P. *et al*. Interaction between cellobiose dehydrogenase and lytic polysaccharide monooxygenase. **Biochemistry**, v. 58, n. 9, p. 1226–1235, 2019. DOI: 10.1021/acs.biochem.8b01178.

9 CANTAREL, B. L. *et al*. The carbohydrate-active enzymes database (CAZy): an expert resource for glycogenomics. **Nucleic Acids Research**, v. 37, p. D233–D238, 2009. DOI: 10.1093/nar/gkn663

10 LEVASSEUR, A. *et al*. Expansion of the enzymatic repertoire of the CAZy database to integrate auxiliary redox enzymes. **Biotechnology for Biofuels**, v. 6, n. 1, p. 41, 2013. DOI: 10.1186/1754-6834-6-41.

11 SÜTZL, L. *et al*. The GMC superfamily of oxidoreductases revisited: analysis and evolution of fungal GMC oxidoreductases. **Biotechnology for Biofuels**, v. 12, n. 1, p. 118, 2019. DOI:10.1186/s13068-019-1457-0.

12 STOICA, L. *et al*. Biosensor based on cellobiose dehydrogenase for detection of catecholamines. **Analytical Chemistry**, v. 76, n. 16, p. 4690–4696, 2004. DOI:10.1021/ac049582j.

13 TASCA, F. *et al*. A third-generation glucose biosensor based on cellobiose dehydrogenase from Corynascus thermophilus and single-walled carbon nanotubes. **Analyst**, v. 136, n. 10, p. 2033–2036, 2011. DOI:10.1039/C0AN00311E.

14 YAKOVLEVA, M. *et al*. A novel combined thermometric and amperometric biosensor for lactose determination based on immobilised cellobiose dehydrogenase. **Biosensors and Bioelectronics**, v. 31, n. 1, p. 251–256, 2012. DOI: 10.1016/j.bios.2011.10.027.

15 SHARMA, A.; SINGH, G.; ARYA, S. K. Biofuel cell nanodevices. **International Journal of Hydrogen Energy**, v. 46, n. 4, p. 3270–3288, 2021. DOI: 10.1016/j.ijhydene.2020.02.164

16 TASCA, F. *et al*. Highly efficient and versatile anodes for biofuel cells based on cellobiose dehydrogenase from Myriococcum thermophilum. **Journal of Physical Chemistry C**, v. 112, n. 35, p. 13668–13673, 2008. DOI:10.1021/jp805092m.

17 YANG J. *et al*. Production of lactobionic acid using an immobilized cellobiose dehydrogenase/laccase system on magnetic chitosan spheres. **Process Biochemistry**, v. 100, p. 1–9, 2021. DOI: 10.1016/j.procbio.2020.09.024.

18 BEY, M. *et al*. Heterologous expression of Pycnoporus cinnabarinus cellobiose dehydrogenase in Pichia pastoris and involvement in saccharification processes. **Microbial Cell Factories**, v. 10, n. 1, p. 113, 2011. DOI:10.1186/1475-2859-10-113.

19 PHILLIPS, C. M. *et al*. Cellobiose dehydrogenase and a copper-dependent polysaccharide monooxygenase potentiate cellulose degradation by neurospora crassa. **ACS Chemical Biology**, v. 6, n. 12, p. 1399–1406, 2011. DOI:10.1021/cb200351y.

20 WANG, M.; LU, X. Exploring the synergy between cellobiose dehydrogenase from Phanerochaete chrysosporium and cellulase from trichoderma reesei. **Frontiers in Microbiology**, v. 7, n. 620, 2016. DOI:10.3389/fmicb.2016.00620.

21 FLEMMING, H. C. *et al*. The biofilm matrix: multitasking in a shared space. **Nature Reviews Microbiology**, v. 21, n. 2, p. 70–86, 2023. DOI:10.1038/s41579-022-00791-0.

22 FLEMMING, H. C. *et al*. Biofilms: an emergent form of bacterial life. **Nature Reviews Microbiology**, v. 14, n. 9, p. 563–575, 2016. DOI:10.1038/nrmicro.2016.94.

23 FLEMMING, H. C.; WUERTZ, S. Bacteria and archaea on Earth and their abundance in biofilms. **Nature Reviews Microbiology**, v. 17, n. 4, p. 247–260, 2019. DOI:10.1038/s41579-019-0158-9.

24 MARK WELCH, J. L. *et al*. Biogeography of a human oral microbiome at the micron scale. **Proceedings of the National Academy of Sciences**, v. 113, n. 6, p. E791–E800, 2016. DOI:10.1073/pnas.1522149113.

25 BRANDWEIN, M.; STEINBERG, D.; MESHNER, S. Microbial biofilms and the human skin microbiome. **npj Biofilms and Microbiomes**, v. 2, n. 1, p. 3, 2016. DOI:10.1038/s41522-016-0004-z.

26 DE VOS, W. M. Microbial biofilms and the human intestinal microbiome. **npj Biofilms and Microbiomes**, v. 1, n. 1, p. 15005, 2015. DOI: 10.1038/npjbiofilms.2015.5.

27 CIOFU, O. *et al*. Tolerance and resistance of microbial biofilms. **Nature Reviews Microbiology**, v. 20, n. 10, p. 621–635, 2022. DOI: 10.1038/s41579-022-00682-4.

28 PETROVA, O. E.; SAUER, K. Sticky situations: key components that control bacterial surface attachment. **Journal of Bacteriology**, v. 194, n. 10, p. 2413–2425, 2012. DOI:10.1128/JB.00003-12.

29 RUMBAUGH, K.P.; SAUER, K. Biofilm dispersion. **Nature Reviews Microbiology**, v. 18, n. 10, p. 571–586, 2020. DOI:10.1038/s41579-020-0385-0.

30 KOO, H. *et al*. Targeting microbial biofilms: current and prospective therapeutic strategies. **Nature Reviews Microbiology**, v. 15, n. 12, p. 740–755, 2017. DOI:10.1038/nrmicro.2017.99.

31 LIMOLI, D. H.; JONES, C. J. WOZNIAK, D. J. Bacterial extracellular polysaccharides in biofilm formation and function. **Microbiology Spectrum**, v. 3, n. 3, 2015. DOI: 10.1128/microbiolspec.MB-0011-2014.

32 NGUYEN, H. T. T.; NGUYEN, T. H.; OTTO, M. The staphylococcal exopolysaccharide PIA – biosynthesis and role in biofilm formation, colonization, and infection. **Computational and Structural Biotechnology Journal**, v. 18, p. 3324–3334, 2020. DOI: 10.1016/j.csbj.2020.10.027.

33 MA, L. Z. *et al*. Regulation of biofilm exopolysaccharide biosynthesis and degradation in Pseudomonas aeruginosa. **Annual Review of Microbiology**, v. 76, n. 1, p. 413–433, 2022. DOI: 10.1146/annurev-micro-041320-111355.

34 LE MAUFF, F. *et al*. The Pel polysaccharide is predominantly composed of a dimeric repeat of α-1,4 linked galactosamine and N-acetylgalactosamine. **Communications Biology**, v. 5, n. 1, p. 502, 2022. DOI:10.1038/s42003-022-03453-2.

35 KARYGIANNI, L. *et al*. Biofilm matrixome: extracellular components in structured microbial communities. **Trends in Microbiology**, v. 28, n. 8, p. 668–681, 2020. DOI: 10.1016/j.tim.2020.03.016.

36 MONTANARO, L. *et al*. Extracellular DNA in biofilms. **International Journal of Artificial Organs**, v. 34, n. 9, p. 824–831, 2011. DOI: 10.5301/ijao.5000051.

37 HEDE, K. Antibiotic resistance: an infectious arms race. **Nature**, v. 509, n. 7498, p. S2–S3, 2014. DOI: 10.1038/509S2a.

38 HØIBY, N. *et al*. Antibiotic resistance of bacterial biofilms. **International Journal of Antimicrobial Agents**, v. 35, n. 4, p. 322–332, 2010. DOI: 10.1016/j.ijantimicag.2009.12.011

39 CALIFANO, D. *et al*. Multienzyme cellulose films as sustainable and self-degradable hydrogen peroxide-producing material. **Biomacromolecules**, v. 21, n. 12, p. 5315–5322, 2020. DOI: 10.1021/acs.biomac.0c01393.

40 NYANHONGO, G. S.; THALLINGER, B.; GUEBITZ, G. M. Cellobiose dehydrogenase-based biomedical applications. **Process Biochemistry**, v. 59, p. 37–45, 2017. DOI: 10.1016/j.procbio.2017.02.023.

41 SULEJ, J. *et al*. Antimicrobial and antioxidative potential of free and immobilised cellobiose dehydrogenase isolated from wood degrading fungi. **Fungal Biology**, v. 123, n. 12, p. 875–886, 2019. DOI: 10.1016/j.funbio.2019.09.007.

42 TEGL, G. *et al*. Antimicrobial cellobiose dehydrogenase-chitosan particles. **ACS Applied Materials & Interfaces**, v. 8, n. 1, p. 967–973, 2016. DOI: 10.1021/acsami.5b10801.

43 THALLINGER, B. *et al*. Preventing microbial colonisation of catheters: antimicrobial and antibiofilm activities of cellobiose dehydrogenase. **International Journal of Antimicrobial Agents**, v. 44, n. 5, p. 402–408, 2014. DOI: 10.1016/j.ijantimicag.2014.06.016

44 THALLINGER, B. *et al*. Cellobiose dehydrogenase functionalized urinary catheter as novel antibiofilm system. **Journal of Biomedical Materials Research Part B**: applied biomaterials, v. 104, n. 7, p. 1448–1456, 2016. DOI: 10.1002/jbm.b.33491.

45 NYANHONGO, G. S. *et al*. Synthesis of multifunctional bioresponsive polymers for the management of chronic wounds. **Journal of Biomedical Materials Research Part B**: applied biomaterials, v. 101B, n. 5, p. 882–891, 2013. DOI: 10.1002/jbm.b.32893.

46 SAMANIEGO, L. V. B. *et al*. Staphylococcus aureus microbial biofilms degradation using cellobiose dehydrogenase from Thermothelomyces thermophilus M77. **International Journal of Biological Macromolecules**, v. 247, p. 125822, 2023. DOI: 10.1016/j.ijbiomac.2023.125822.

47 BHAT, K. M.; MAHESHWARI, R. Sporotrichum thermophile growth, cellulose degradation, and cellulase activity. **Applied and Environmental Microbiology**, v. 53, n. 9, p. 2175–2182, 1987. DOI: 10.1128/aem.53.9.2175-2182.1987.

48 SUBRAMANIAM, S. S.; NAGALLA, S. R.; RENGANATHAN, V. Cloning and characterization of a thermostable cellobiose dehydrogenase from sporotrichum thermophile. **Archives of Biochemistry and Biophysics**, v. 365, n. 2, p. 223–230, 1999. DOI: 10.1006/abbi.1999.1152.

49 VU, V. V. *et al*. A family of starch-active polysaccharide monooxygenases. **Proceedings of the National Academy of Sciences**, v. 111, n. 38, p. 13822–13827, 2014. DOI: 10.1073/pnas.1408090111.

50 BERKA, R. M. *et al*. Comparative genomic analysis of the thermophilic biomass-degrading fungi Myceliophthora thermophila and Thielavia terrestris. **Nature Biotechnology**, v. 29, n. 10, p. 922–927, 2011. DOI: 10.1038/nbt.1976.

51. MIRDITA, M. *et al*. ColabFold: making protein folding accessible to all. **Nature Methods**, v. 19, n. 6, p. 679–682, 2022. DOI:10.1038/s41592-022-01488-1

52 HANEY, E. F.; TRIMBLE, M. J.; HANCOCK, R. E. W. Microtiter plate assays to assess antibiofilm activity against bacteria. **Nature Protocols**, v. 16, n. 5, p. 2615–2632, 2021. DOI: 10.1038/s41596-021-00515-3.

53 CRUZ, C. D.; SHAH, S.; TAMMELA, P. Defining conditions for biofilm inhibition and eradication assays for Gram-positive clinical reference strains. **BMC Microbiology**, v. 18, n. 1, p. 173, 2018. DOI: 10.1186/s12866-018-1321-6.

54 CHIBA, A. *et al*. A refined technique for extraction of extracellular matrices from bacterial biofilms and its applicability. **Microbial Biotechnology**, v. 8, n. 3, p. 392–403, 2015. DOI: 10.1111/1751-7915.12155.

55 GIOVANNETTI, R. The use of spectrophotometry UV-Vis for the study of porphyrins. *In*: UDIN, J. (ed). **Macro to nano spectroscopy**. Croatia: InTech, 2012. p. 87-108. DOI: 10.5772/38797.

56 ROTSAERT, F. A. J. *et al*. Biophysical and structural analysis of a novel heme b iron ligation in the flavocytochrome cellobiose dehydrogenase. **Journal of Biological Chemistry**, v. 278, n. 35, p. 33224–33231, 2003. DOI: 10.1074/jbc.M302653200.

57 SCHULZ, C. *et al*. Enhancement of enzymatic activity and catalytic current of cellobiose dehydrogenase by calcium ions. **Electrochemistry Communications**, v. 17, n. 1, p. 71–74, 2012. DOI: 10.1016/j.elecom.2012.01.031.

58 SULEJ, J. *et al*. Characterization of cellobiose dehydrogenase and its FAD-domain from the ligninolytic basidiomycete Pycnoporus sanguineus. **Enzyme and Microbial Technology**, v. 53, n. 6–7, p. 427–437, 2013. DOI: 10.1016/j.enzmictec.2013.09.007.

59 SULEJ, J. *et al*. Characterization of cellobiose dehydrogenase from a biotechnologically important cerrena unicolor strain. **Applied Biochemistry and Biotechnology**, v. 176, n. 6, p. 1638–1658, 2015. DOI:10.1007/s12010-015-1667-2.

60 PRICELIUS, S. *et al*. Substrate specificity of Myriococcum thermophilum cellobiose dehydrogenase on mono-, oligo-, and polysaccharides related to in situ production of H2O2. **Applied Microbiology and Biotechnology**, v. 85, n. 1, p. 75–83, 2009. DOI: 10.1007/s00253-009-2062-0.

61 LI, S.; SCHÖNEICH, C.; BORCHARDT, R. T. Chemical instability of protein pharmaceuticals: mechanisms of oxidation and strategies for stabilization. **Biotechnology and Bioengineering**, v. 48, n. 5, p. 490–500, 1995. DOI: 10.1002/bit.260480511.

62 BALAŽ, A. M. *et al*. Semi-rational design of cellobiose dehydrogenase for increased stability in the presence of peroxide. **Molecular Diversity**, v. 24, n. 3, p. 593–601, 2020. DOI: 10.1007/s11030-019-09965-0.

63 FLITSCH, A. *et al*. Cellulose oxidation and bleaching processes based on recombinant Myriococcum thermophilum cellobiose dehydrogenase. **Enzyme and Microbial Technology**, v. 52, n. 1, p. 60–67, 2013. DOI: 10.1016/j.enzmictec.2012.10.007.

64 HARREITHER, W. *et al*. Investigation of the pH-dependent electron transfer mechanism of ascomycetous class II cellobiose dehydrogenases on electrodes. **Langmuir**, v. 28, n. 16, p. 6714–6723, 2012. DOI: 10.1021/la3005486.

65 LANGSTON, J. A. *et al*. Cloning, expression, and characterization of a cellobiose dehydrogenase from Thielavia terrestris induced under cellulose growth conditions. **Biochimica et Biophysica Acta (BBA)** - proteins and proteomics, v. 1824, n. 6, p. 802–812, 2012. DOI: 10.1016/j.bbapap.2012.03.009.

66 SYGMUND, C. *et al*. Characterization of the two neurospora crassa cellobiose dehydrogenases and their connection to oxidative cellulose degradation. **Applied and Environmental Microbiology**, v. 78, n. 17, p. 6161–6171, 2012. DOI: 10.1128/AEM.01503-12

67 HARADA, H. *et al*. Interdomain flip-flop motion visualized in flavocytochrome cellobiose dehydrogenase using high-speed atomic force microscopy during catalysis. **Chemical Science**, v. 8, n. 9, p. 6561–6565, 2017. DOI: 10.1039/C7SC01672G.

68 ZHANG, R.; FAN, Z.; KASUGA, T. Expression of cellobiose dehydrogenase from Neurospora crassa in Pichia pastoris and its purification and characterization. **Protein Expression and Purification**, v. 75, n. 1, p. 63–69, 2011. DOI: 10.1016/j.pep.2010.08.003.

69 FERRARI, A. R. *et al*. Discovery of a Xylooligosaccharide oxidase from Myceliophthora thermophila C1. **Journal of Biological Chemistry**, v. 291, n. 45, p. 23709–23718, 2016. DOI: 10.1074/jbc.M116.741173.

70 VUONG, T. V. *et al*. Xylo- and cello-oligosaccharide oxidation by gluco-oligosaccharide oxidase from Sarocladium strictumand variants with reduced substrate inhibition. **Biotechnology for Biofuels**, v. 6, n. 1, p. 148, 2013. DOI: 10.1186/1754-6834-6-148.

71 HADDAD MOMENI, M. *et al*. Discovery of fungal oligosaccharide-oxidising flavo-enzymes with previously unknown substrates, redox-activity profiles and interplay with LPMOs. **Nature Communications**, v. 12, n. 1, p. 2132, 2021. DOI: 10.1038/s41467-021-22372-0.

72 KUJAWA, M. *et al*. Structural basis for substrate binding and regioselective oxidation of monosaccharides at C3 by pyranose 2-oxidase. **Journal of Biological Chemistry**, v. 281, n. 46, p. 35104–35115, 2006. DOI: 10.1074/jbc.M604718200.

73 REFFUVEILLE, F. *et al*. Staphylococcus aureus biofilms and their impact on the medical field. *In*: ENANY, S.; CROTTY E. L. (ed.) **The rise of virulence and antibiotic resistance in Staphylococcus aureus**. Croatia: InTech, 2017. p. 187. DOI: 10.5772/66380

74 LISTER, J. L.; HORSWILL, A. R. Staphylococcus aureus biofilms: recent developments in biofilm dispersal. **Frontiers in Cellular and Infection Microbiology**, v. 4, n. 178, 2014. DOI: 10.3389/fcimb.2014.00178.

75 ZHENG, Y. *et al*. Colonization of medical devices by staphylococci. **Environmental Microbiology**, v. 20, n. 9, p. 3141–3153, 2018. DOI: 10.1111/1462-2920.14129.

76 WEINRICK, B. *et al*. Effect of mild acid on gene expression in Staphylococcus aureus. **Journal of Bacteriology**, v. 186, n. 24, p. 8407–8423, 2004. DOI: 10.1128/JB.186.24.8407-8423.2004.

77 RODRIGUEZ, A. V.; NADRA, M. C. M. Effect of pH and hydrogen peroxide produced by Lactobacillus hilgardii on Pediococcus pentosaceus growth. **FEMS Microbiology Letters**, v. 128, n. 1, p. 59–62, 1995. DOI: 10.1111/j.1574-6968.1995.tb07500.x.

78 PRESTERL, E. *et al*. Effects of alcohols, povidone-iodine and hydrogen peroxide on biofilms of Staphylococcus epidermidis. **Journal of Antimicrobial Chemotherapy**, v. 60, n. 2, p. 417–420, 2007. DOI: 10.1093/jac/dkm221.

79 CHRISTENSEN, B. E. *et al*. Biofilm removal by low concentrations of hydrogen peroxide. **Biofouling**, v. 2, n. 2, p. 165–175, 1990. DOI: 10.1080/08927019009378142.

80 IZANO, E.A. *et al*. Differential roles of poly- N-acetylglucosamine surface polysaccharide and extracellular DNA in Staphylococcus aureus and Staphylococcus epidermidis biofilms. **Applied and Environmental Microbiology**, v. 74, n. 2, p. 470–476, 2008. DOI: 10.1128/AEM.02073-07.

81 ARCHER, N. K. *et al*. Staphylococcus aureus biofilms. **Virulence**, v. 2, n. 5, p. 445–459, 2011. DOI: 10.4161/viru.2.5.17724.

82 HILTUNEN, A. K. *et al*. Structural and functional dynamics of Staphylococcus aureus biofilms and biofilm matrix proteins on different clinical materials. **Microorganisms**, v. 7, n. 12, p. 584, 2019. DOI: 10.3390/microorganisms7120584.

83 GÖKÇEN, A.; VILCINSKAS, A.; WIESNER, J. Methods to identify enzymes that degrade the main extracellular polysaccharide component of Staphylococcus epidermidis biofilms. **Virulence**, v. 4, n. 3, p. 260–270, 2013. DOI: 10.4161/viru.23560.

84 DUAN, J.; AVCI, F. Y.; KASPER, D. L. Microbial carbohydrate depolymerization by antigen-presenting cells: deamination prior to presentation by the MHCII pathway. **Proceedings of the National Academy of Sciences**, v. 105, n. 13, p. 5183–5188, 2008. DOI: 10.1073/pnas.0800974105.

85 CHANG, K. L. B.; TAI, M. C.; CHENG, F. H. Kinetics and products of the degradation of chitosan by hydrogen peroxide. **Journal of Agricultural and Food Chemistry**, v. 49, n. 10, p. 4845–4851, 2001. DOI: 10.1021/jf001469g.

86 MARQUES, S. C. *et al*. Formation of biofilms by Staphylococcus aureus on stainless steel and glass surfaces and its resistance to some selected chemical sanitizers. **Brazilian Journal of Microbiology**, v. 38, n. 3, p. 538–543, 2007. DOI: 10.1590/S1517-83822007000300029.

87 GANESHNARAYAN, K. *et al*. Poly- N-Acetylglucosamine matrix polysaccharide impedes fluid convection and transport of the cationic surfactant cetylpyridinium chloride through bacterial biofilms. **Applied and Environmental Microbiology**, v. 75, n. 5, p. 1308–1314, 2009. DOI: 10.1128/AEM.01900-08.

88 CAMPOCCIA, D.; MONTANARO, L.; ARCIOLA, C. R. Extracellular DNA (eDNA). a major ubiquitous element of the bacterial biofilm architecture. **International Journal of Molecular Sciences**, v. 22, n. 16, p. 9100, 2021. DOI: 10.3390/ijms22169100.

89 DADDI OUBEKKA, S. *et al*. Correlative time-resolved fluorescence microscopy to assess antibiotic diffusion-reaction in biofilms. **Antimicrobial Agents and Chemotherapy**, v. 56, n. 6, p. 3349–3358, 2012. DOI: 10.1128/AAC.00216-12

90 TAN, Y. *et al*. Co-immobilization of cellobiose dehydrogenase and deoxyribonuclease I on chitosan nanoparticles against fungal/bacterial polymicrobial biofilms targeting both biofilm matrix and microorganisms. **Materials Science and Engineering C**, v. 108, p. 110499, 2020. DOI: 10.1016/j.msec.2019.110499

91 GONZALEZ MORENO, M.; TRAMPUZ, A.; DI LUCA, M. Synergistic antibiotic activity against planktonic and biofilm-embedded Streptococcus agalactiae, Streptococcus pyogenes and Streptococcus oralis. **Journal of Antimicrobial Chemotherapy**, v. 72, n. 11, p. 3085–3092, 2017. DOI: 10.1093/jac/dkx265.

92 FANAEI PIRLAR, R. *et al*. Combinatorial effects of antibiotics and enzymes against dual-species Staphylococcus aureus and Pseudomonas aeruginosa biofilms in the wound-like medium. **PLOS ONE**, v. 15, n. 6, p. e0235093, 2020. DOI: 10.1371/journal.pone.0235093.

93 MCDONNELL, G. The use of hydrogen peroxide for disinfection and sterilization applications. *In*: RAPPOPORT, Z. (ed.) **PATAI'S chemistry of functional groups**. New York: John Wiley & Sons, 2014. p. 1–34. DOI: 10.1002/9780470682531.pat0885

94 ABIDI, W. *et al*. Weaving of bacterial cellulose by the Bcs secretion systems. **FEMS Microbiology Reviews**, v. 46, n. 2, 2022. DOI:10.1093/femsre/fuab051.

95 SAJITH, S. *et al*. An overview on fungal cellulases with an industrial perspective. **Journal of Nutrition & Food Sciences**, v. 06, n. 1, 2016. DOI:10.4172/2155-9600.1000461.

96 SINGH, A. *et al*. An overview on the recent developments in fungal cellulase production and their industrial applications. **Bioresource Technology Reports**, v. 14, p. 100652, 2021. DOI: 10.1016/j.biteb.2021.100652.

97 PAYNE, C. M. *et al*. Fungal cellulases. **Chemical Reviews**, v. 115, n. 3, p. 1308–1448, 2015. DOI: 10.1021/cr500351c.

98 KNOTT, B. C. *et al*. The mechanism of cellulose hydrolysis by a two-step, retaining cellobiohydrolase elucidated by structural and transition path sampling studies. **Journal of the American Chemical Society**, v. 136, n. 1, p. 321–329, 2014. DOI: 10.1021/ja410291u.

99 MAYES, H. B. *et al*. Who's on base? Revealing the catalytic mechanism of inverting family 6 glycoside hydrolases. **Chemical Science**, v. 7, n. 9, p. 5955–5968, 2016. DOI: 10.1039/C6SC00571C.

100 KUHAD, R. C.; GUPTA, R.; SINGH, A. Microbial cellulases and their industrial applications. **Enzyme Research**, v. 2011, n. 1, p. 1–10, 2011. DOI: 10.4061/2011/280696.

101 BAR-ON, Y. M.; PHILLIPS, R.; MILO, R. The biomass distribution on Earth. **Proceedings of the National Academy of Sciences**, v. 115, n. 25, p. 6506–6511, 2018. DOI: 10.1073/pnas.1711842115.

102 LITTLE, A. *et al*. Revised phylogeny of the cellulose synthase gene superfamily: insights into cell wall evolution. **Plant Physiology**, v. 177, n. 3, p. 1124–1141, 2018. DOI: 10.1104/pp.17.01718.

103 SCOTT, W. *et al*. Identification of the Clostridial cellulose synthase and characterization of the cognate glycosyl hydrolase, CcsZ. **PLOS ONE**, v. 15, n. 12, p. e0242686, 2020. DOI: 10.1371/journal.pone.0242686.

104 ELLERMANN, M.; SARTOR, R. B. Intestinal bacterial biofilms modulate mucosal immune responses. **Journal of Immunological Sciences**, v. 2, n. 2, p. 13–18, 2018

105 TYRIKOS-ERGAS, T. *et al*. Synthetic phosphoethanolamine-modified oligosaccharides reveal the importance of glycan length and substitution in biofilm-inspired assemblies. **Nature Communications**, v. 13, n. 1, p. 3954, 2022. DOI: 10.1038/s41467-022-31633-5.

106 HOLLENBECK, E. C. *et al*. Phosphoethanolamine cellulose enhances curli-mediated adhesion of uropathogenic Escherichia coli to bladder epithelial cells. **Proceedings of the National Academy of Sciences**, v. 115, n. 40, p. 10106–10111, 2018. DOI: 10.1073/pnas.1801564115.

107 TRIVEDI, A. *et al*. Thiol reductive stress induces cellulose-anchored biofilm formation in Mycobacterium tuberculosis. **Nature Communications**, v. 7, n. 1, p. 11392, 2016. DOI: 10.1038/ncomms11392.

108 CHAKRABORTY, P. *et al*. Biofilm formation in the lung contributes to virulence and drug tolerance of Mycobacterium tuberculosis. **Nature Communications**, v. 12, n. 1, p. 1606, 2021. DOI: 10.1038/s41467-021-21748-6.

109 COSTA, A. F. S. *et al*. Production of bacterial cellulose by gluconacetobacter hansenii using corn steep liquor as nutrient sources. **Frontiers in Microbiology**, v. 8, 2017. DOI: 10.3389/fmicb.2017.02027.

110 MILLER, G. L. Use of dinitrosalicylic acid reagent for determination of reducing sugar. **Analytical Chemistry**, v. 31, n. 3, p. 426–428, 1959. DOI: 10.1021/ac60147a030

111 KADOWAKI, M. A. S. *et al*. Biochemical and structural insights into a thermostable cellobiohydrolase from Myceliophthora thermophila. **FEBS Journal**, v. 285, n. 3, p. 559–579, 2018. DOI: 10.1111/febs.14356.

112 SEGATO, F. *et al*. High-yield secretion of multiple client proteins in Aspergillus. **Enzyme and Microbial Technology**, v. 51, n. 2, p. 100–106, 2012. DOI: 10.1016/j.enzmictec.2012.04.008.

113 YANG, J. *et al*. Modulation of the catalytic activity and thermostability of a thermostable GH7 endoglucanase by engineering the key loop B3. **International Journal of Biological Macromolecules**, v. 248, p. 125945, 2023. DOI: 10.1016/j.ijbiomac.2023.125945.

114 DADWAL, A.; SHARMA, S.; SATYANARAYANA, T. Recombinant cellobiohydrolase of Myceliophthora thermophila: characterization and applicability in cellulose saccharification. **AMB Express**, v. 11, n. 1, p. 148, 2021. DOI: 10.1186/s13568-021-01311-8.

115 BLAKE, A. W. *et al*. Understanding the biological rationale for the diversity of cellulose-directed carbohydrate-binding modules in prokaryotic enzymes. **Journal of Biological Chemistry**, v. 281, n. 39, p. 29321–29329, 2006. DOI: 10.1074/jbc.M605903200.

116 ORABY, H. *et al*. Enhanced conversion of plant biomass into glucose using transgenic rice-produced endoglucanase for cellulosic ethanol. **Transgenic Research**, v. 16, n. 6, p. 739–749, 2007. DOI : 10.1007/s11248-006-9064-9

117 SILVEIRA, R. L.; SKAF, M. S. Molecular dynamics simulations of family 7 cellobiohydrolase mutants aimed at reducing product inhibition. **Journal of Physical Chemistry B**, v. 119, n. 29, p. 9295–9303, 2015. DOI: 10.1021/jp509911m.

118 BODENHEIMER, A. M.; MEILLEUR, F. Crystal structures of wild-type Trichoderma reesei Cel7A catalytic domain in open and closed states. **FEBS Letters**, v. 590, n. 23, p. 4429–4438, 2016. DOI: 10.1002/1873-3468.12464.

119 KLEYWEGT, G. J. *et al*. The crystal structure of the catalytic core domain of endoglucanase I from Trichoderma reesei at 3.6 Å resolution, and a comparison with related enzymes 1 1Edited by K.Nagai. **Journal of Molecular Biology**, v. 272, n. 3, p. 383–397, 1997. DOI: 10.1006/jmbi.1997.1243.

120 ROUVINEN, J. *et al*. Three-dimensional structure of cellobiohydrolase II from Trichoderma reesei. **Science**, v. 249, n. 4967, p. 380–386, 1990. DOI: 10.1126/science.2377893.

121 THOMPSON, A. J. *et al*. Structure of the catalytic core module of the Chaetomium thermophilum family GH6 cellobiohydrolase Cel6A. **Acta Crystallographica Section D:** biological crystallography, v. 68, n. 8, p. 875–882, 2012. DOI: 10.1107/S0907444912016496.

122 LAOTHANACHAREON, T. *et al*. Synergistic action of recombinant accessory hemicellulolytic and pectinolytic enzymes to Trichoderma reesei cellulase on rice straw degradation. **Bioresource Technology**, v. 198, p. 682–690, 2015. DOI: 10.1016/j.biortech.2015.09.053.

123 INOUE, H. *et al*. Identification and characterization of core cellulolytic enzymes from Talaromyces cellulolyticus (formerly Acremonium cellulolyticus) critical for hydrolysis of lignocellulosic biomass. **Biotechnology for Biofuels**, v. 7, n. 1, p. 151, 2014. DOI: 10.1186/s13068-014-0151-5

124 BUNTERNGSOOK, B. *et al*. Optimization of a minimal synergistic enzyme system for hydrolysis of raw cassava pulp. **RSC Advances**, v. 7, n. 76, p. 48444–48453, 2017. DOI: 10.1039/C7RA08472B.

125 SUWANNARANGSEE, S. *et al*. Optimization of synergistic biomass-degrading enzyme systems for efficient rice straw hydrolysis using an experimental mixture design. **Bioresource Technology**, v. 119, p. 252–261, 2012. DOI: 10.1016/j.biortech.2012.05.098.

126 BOMMARIUS, A. S. *et al*. Cellulase kinetics as a function of cellulose pretreatment. **Metabolic Engineering**, v. 10, n. 6, p. 370–381, 2008. DOI: 10.1016/j.ymben.2008.06.008.

127 BOISSET, C. *et al*. Imaging the enzymatic digestion of bacterial cellulose ribbons reveals the endo character of the cellobiohydrolase Cel6A from Humicola insolens and its mode of synergy with cellobiohydrolase Cel7A. **Applied and Environmental Microbiology**, v. 66, n. 4, p. 1444–1452, 2000. DOI: 10.1128/AEM.66.4.1444-1452.2000.

128 ZOGAJ, X. *et al*. The multicellular morphotypes of *Salmonella typhimurium* and *Escherichia coli* produce cellulose as the second component of the extracellular matrix. **Molecular Microbiology**, v. 39, n. 6, p. 1452–1463, 2001. DOI: 10.1046/j.1365-2958.2001.02337.x

129 BOKRANZ, W. *et al*. Expression of cellulose and curli fimbriae by Escherichia coli isolated from the gastrointestinal tract. **Journal of Medical Microbiology**, v. 54, n. 12, p. 1171–1182, 2005. DOI: 10.1099/jmm.0.46064-0

130 THONGSOMBOON, W. *et al*. Phosphoethanolamine cellulose: a naturally produced chemically modified cellulose. **Science**, v. 359, n. 6373, p. 334–338, 2018. DOI: 10.1126/science.aao4096

131 CHAUDHURI, R. R. *et al*. Complete genome sequence and comparative metabolic profiling of the prototypical enteroaggregative Escherichia coli strain 042. **PLoS ONE**, v. 5, n. 1, p. e8801, 2010. DOI: 10.1371/journal.pone.0008801

132 FLOREA, M. *et al*. Genome sequence and plasmid transformation of the model high-yield bacterial cellulose producer Gluconacetobacter hansenii ATCC 53582. **Scientific Reports**, v. 6, n. 1, p. 23635, 2016. DOI: 10.1038/srep23635

133 RÖMLING, U.; GALPERIN, M. Y. Bacterial cellulose biosynthesis: diversity of operons, subunits, products, and functions. **Trends in Microbiology**, v. 23, n. 9, p. 545–557, 2015. DOI: 10.1016/j.tim.2015.05.005

134 SERRA, D. O.; RICHTER, A. M.; HENGGE, R. Cellulose as an architectural element in spatially structured Escherichia coli biofilms. **Journal of Bacteriology**, v. 195, n. 24, p. 5540–5554, 2013. DOI: 10.1128/JB.00946-13

135 LIM, E. S. *et al*. Bio-enzymes for inhibition and elimination of Escherichia coli O157:H7 biofilm and their synergistic effect with sodium hypochlorite. **Scientific Reports**, v. 9, n. 1, p. 9920, 2019. DOI: 10.1038/s41598-019-46363-w.

136 ROWE, M. C.; WITHERS, H. L.; SWIFT, S. Uropathogenic Escherichia coli forms biofilm aggregates under iron restriction that disperse upon the supply of iron. **FEMS Microbiology Letters**, v. 307, n. 1, p. 102–109, 2010. DOI: 10.1111/j.1574-6968.2010.01968.x.

137 GUALDI, L. *et al*. Cellulose modulates biofilm formation by counteracting curli-mediated colonization of solid surfaces in Escherichia coli. **Microbiology**, v. 154, n. 7, p. 2017–2024, 2008. DOI: 10.1099/mic.0.2008/018093-0.

138 ZHANG, Z. *et al.* Synergistic antibacterial effects of ultrasound combined nanoparticles encapsulated with cellulase and levofloxacin on Bacillus Calmette-Guérin biofilms. **Frontiers in Microbiology**, v. 14, 2023. DOI: 10.3389/fmicb.2023.1108064.

139 YAMAMOTO, K.; TSUJIMURA, Y.; ATO, M. Catheter-associated Mycobacterium intracellulare biofilm infection in C3HeB/FeJ mice. **Scientific Reports**, v. 13, n. 1, p. 17148, 2023. DOI: 10.1038/s41598-023-44403-0.

140 KIM, M. J.; LIM, E. S.; KIM, J. S. Enzymatic inactivation of pathogenic and nonpathogenic bacteria in biofilms in combination with chlorine. **Journal of Food Protection**, v. 82, n. 4, p. 605–614, 2019. DOI: 10.4315/0362-028X.JFP-18-244.

141 LIM, E. S. *et al*. Strain variation in Bacillus cereus biofilms and their susceptibility to extracellular matrix-degrading enzymes. **PLOS ONE**, v. 16, n. 6, p. e0245708, 2021. DOI: 10.1371/journal.pone.0245708.

142 KAMALI, E. *et al*. In vitro activities of cellulase and ceftazidime, alone and in combination against Pseudomonas aeruginosa biofilms. **BMC Microbiology**, v. 21, n. 1, p. 347, 2021. DOI: 10.1186/s12866-021-02411-y.

143 REDMAN, W. K.; WELCH, G. S.; RUMBAUGH, K. P. Differential efficacy of glycoside hydrolases to disperse biofilms. **Frontiers in Cellular and Infection Microbiology**, v. 10, 2020. DOI: 10.3389/fcimb.2020.00379.

144 FLEMING, D.; CHAHIN, L.; RUMBAUGH, K. Glycoside hydrolases degrade polymicrobial bacterial biofilms in wounds. **Antimicrobial Agents and Chemotherapy**, v. 61, n. 2, 2017. DOI: 10.1128/AAC.01998-16.

145 ZHANG, X. *et al*. Sub-inhibitory concentrations of cefotaxime treatment enhances biofilm formation of monophasic Salmonella Typhimurium variant strain SH16SP46. **FEMS Microbiology Letters**, v. 369, n. 1, 2022. DOI: 10.1093/femsle/fnac092.

146 WANG, H. *et al*. Removal of Salmonella biofilm formed under meat processing environment by surfactant in combination with bio-enzyme. **LWT - Food Science and Technology**, v. 66, p. 298–304, 2016. DOI: 10.1016/j.lwt.2015.10.049.

147 VELÁZQUEZ-MORENO, S. *et al*. Use of a cellulase from Trichoderma reesei as an adjuvant for Enterococcus faecalis biofilm disruption in combination with antibiotics as an alternative treatment in secondary endodontic infection. **Pharmaceutics**, v. 15, n. 3, p. 1010, 2023. DOI: 10.3390/pharmaceutics15031010.

148 LI, J. *et al*. Impact of different enzymes on biofilm formation and mussel settlement. **Scientific Reports**, v. 12, n. 1, p. 4685, 2022. DOI: 10.1038/s41598-022-08530-4.

149 LEROY, C. *et al*. Effects of commercial enzymes on the adhesion of a marine biofilm-forming bacterium. **Biofouling**, v. 24, n. 1, p. 11–22, 2008. DOI: 10.1080/08927010701784912.

150 PANG, J. *et al*. Identification and characterization of an Endo-glucanase secreted from cellulolytic Escherichia coli ZH-4. **BMC Biotechnology**, v. 19, n. 1, p. 63, 2019. DOI: 10.1186/s12896-019-0556-0

Annex

Published article.

SAMANIEGO, L. V. B. *et al*. Staphylococcus aureus microbial biofilms degradation using cellobiose dehydrogenase from *Thermothelomyces thermophilus* M77. **International Journal of Biological Macromolecules**, v. 247, p. 125822, 2023. DOI:10.1016/j.ijbiomac.2023.125822

Article in preparation.

SAMANIEGO, L. V. B. *et al*. Cloning, expression and biochemical characterization of exo- and endo-glucanases from *Thermothelomyces thermophilus* and their applications as antibiofilm agents